Master's Thesis

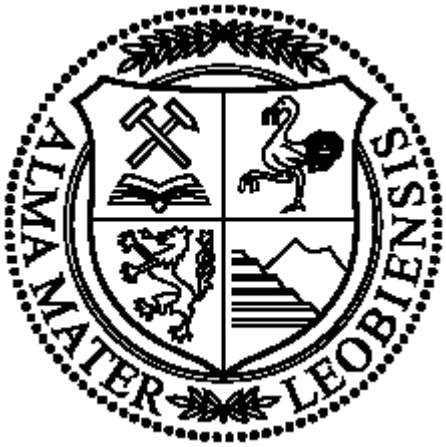

3D thermal modeling and hydrocarbon potential of the Mura-Zala Basin, Slovenia

by

David Hagenbuchner

Supervisor:

Univ.-Prof. Mag.rer.nat. Dr.mont. Reinhard Sachsenhofer

EIDESSTATTLICHE ERKLÄRUNG

Ich erkläre an Eides statt, dass ich die vorliegende Masterarbeit selbständig und ohne fremde Hilfe verfasst, andere als die angegebenen Quellen und Hilfsmittel nicht benutzt und die den benutzten Quellen wörtlich und inhaltlich entnommenen Stellen als solche erkenntlich gemacht habe.

AFFIDAVIT

I declare in lieu of oath, that I wrote this thesis and performed the associated research myself, using only literature cited in this volume.

_____ _____

Datum Unterschrift

Contents

Appreciations

I want to thank the Montanuniversitaet Leoben as a whole, for allowing me the outstanding opportunity to pursue this great path of education.

Specifically, I want to thank Mr. Univ.-Prof. Mag.rer.nat. Dr.mont. Reinhard Sachsenhofer, who offered to be my supervisor for this thesis, for his time, support, knowledge and personal effort he put into making this thesis possible, which I am particularly grateful for.

Further, I want to thank Mrs. Assoz. Prof. Dipl.-Ing. Dr.mont. Doris Groß, for her expertise in basin modelling in Petrel and her patience with me regarding the software licenses I used to confiscate while working on the models.

A special thank you goes also to Mr. Miloš Markič and Mr. Dejan Šram, who provided me with the model, which is the very basis of this thesis as well as lots of important and valuable information thanks to their deep knowledge of the area, and who were always available if I needed their help. I also want to thank the rest of the team of the Geološki zavod Slovenije, for all the information they kindly provided.

Finally, I want to thank a dear colleague, Mr. Dipl. Ing. Wolfgang Schaffar, who is a wandering Petrel encyclopaedia, full-blood petroleum geoscientist and a great friend.

Abstract

The Mura-Zala Basin is situated on the western margin of the Pannonian Basin and is the most prospective area for hydrocarbon exploration in Slovenia. Multiple source rock studies have been carried out in the area and 1D and 2D numerical models of the thermal evolution of the basin were established in the past. Together with a newly available 3D geometric model of the Mura-Zala Basin, the available data was integrated, refined and combined in a 3D petroleum system model. This allows evaluation of the thermal history in the 3D space. Two hydrocarbon generation scenarios with different source rock distributions and kinetic data sets were conducted.

In Karpatian and Early Badenian times, strongly elevated heat flow in the north (between Maribor and Gora Radgona) and the south-east of the basin (Lendava area) probably led to an early hydrocarbon generation phase at these locations. Heat flow decreased until Sarmatian time and stayed at values between 50 and 80 mW/m² until today. A second, major stage of hydrocarbon generation started about 8 Ma ago due to deep burial and generation continued at least until the post-Pontian basin inversion. The youngest formation that became mature is the turbiditic sequence of the Lendava Formation (Pannonian). The structure defining the most important oil and gas field in Slovenia, the Petisovci-Dolina field, only formed during post-Pontian basin inversion. Modeling of hydrocarbon accumulations shows, that the known hydrocarbon deposits cannot be charged from the known Miocene source rocks alone. Therefore, the model favours the idea of an additional pre-Miocene source rock. Alternatively, a far superior source rock may be present in the Miocene succession, which was not drilled so far.

Kurzfassung

Das Mura-Zala Becken befindet sich am westlichen Rand des Pannonischen Beckens und ist das bedeutendste Gebiet für Kohlenwasserstoffexploration in Slowenien. Muttergesteine in diesem Gebiet wurden bereits im Rahmen mehrerer Studien untersucht. Ebenso wurden 1D und 2D numerische Modelle der thermischen Geschichte durchgeführt. Gemeinsam mit einem seit kurzem verfügbarem geometrischen 3D Modell des Mura-Zala Beckens, wurden die vorhandenen Daten aufbereitet, zusammengeführt und in ein 3D Petroleum Systems Model umgewandelt. Dies erlaubt eine Evaluierung der thermischen Geschichte im dreidimensionalen Raum. Zwei Szenarien mit unterschiedlicher Muttergesteinsverteilung und unterschiedlichen Muttergesteinskinetiken wurden simuliert um die Kohlenwasserstoffgenese, -migration und -akkumulation zu berechnen.

Im Karpat und im frühen Baden, führte stark erhöhter Wärmefluss im nördlichen (zwischen Maribor und Gora Radgona) und südöstlichen Teil des Beckens (Bereich Lendava) zur einer ersten, frühen Phase der Generierung von Kohlenwasserstoffe in diesen Bereichen. Der Wärmefluss nahm daraufhin bis ins Sarmat ab und pendelte sich bei Werten zwischen 50 und 80 mW/m² ein, wo sie bis heute verblieben. Eine zweite Phase der Kohlenwasserstoffgenerierung begann vor rund 8 Millionen Jahren durch tiefe Versenkung und endete frühestens durch eine post-miozäne Beckeninversion. Die Struktur, welche für die wichtigste Kohlenwasserstofflagerstätte, das Petisovci-Dolina Feld, verantwortlich ist, wurde erst während dieser Beckeninversion gebildet. Die jüngsten Sedimente, welche das Ölfenster erreicht haben, waren die turbiditischen Schichten der Lendava-Formation (Pannonium). Das Modellieren der Kohlenwasserstoffakkumulationen zeigt, dass die bekannten Lagerstätten mit den bekannten Muttergesteinen nicht gefüllt werden können. Dies deutet auf ein zusätzliches, prä-miozänes Muttergestein hin. Alternativ könnte allerdings auch ein weit besseres Muttergestein in den miozänen Abfolgen vorhanden sein, welches allerdings bisher noch nicht erbohrt wurde.

1 Introduction

The Mura-Zala Basin in Slovenia is situated on the western margin of the Pannonian Basin System (Figure 1) and is the most prospective area for hydrocarbon exploration in Slovenia (Markič et al., 2016). It extends into four different countries: Slovenia, Hungary, Croatia and a small part of Austria.

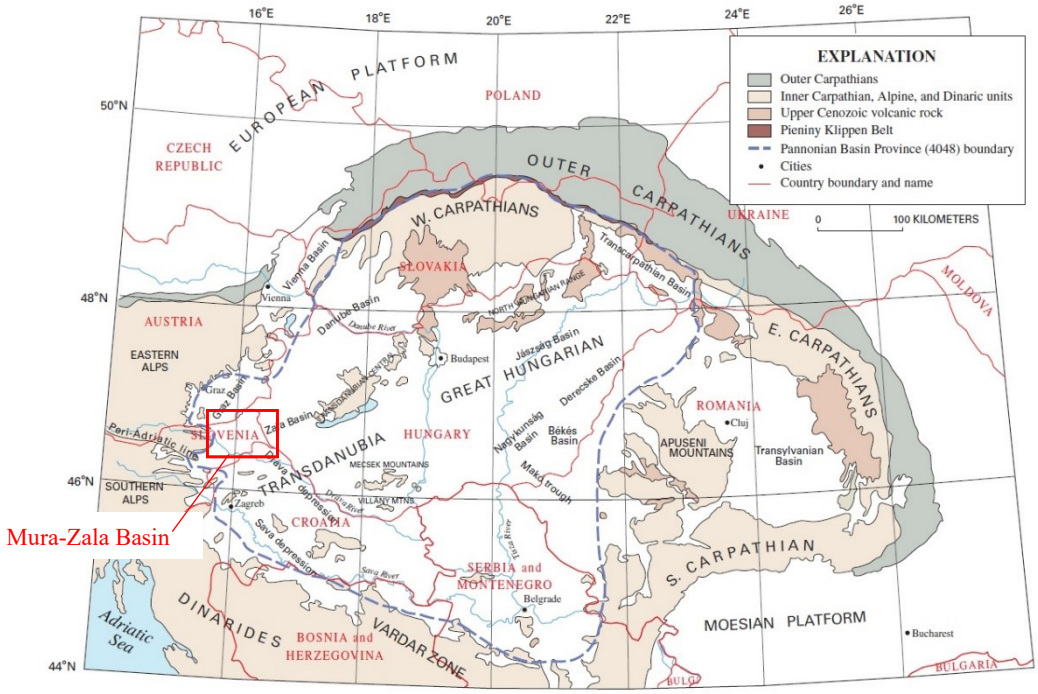

Figure 1 - Index map showing the main geographic and tectonic units of the Alpine Foldbelt and the Alpine-Carpathian-Dinaric-Mountains and outlining the extent of the Pannonian Basin System. (After Horváth, 1985b; Dolton, 2006)

The Pannonian Basin is considered to be a Tertiary back-arc basin, formed through the Carpathian orogeny (Jelen & Rifelj, 2005; Horváth et al., 2015). It contains several Neogene basins, on top of a complexly deformed and faulted set of Mesozoic, Paleozoic and Precambrian basement rocks, which are part of the Inner Carpathian fold belt (Šram et al., 2015). The basin spans over a variety of Central European countries and is under investigation for its geopotentials, especially hydrocarbons and geothermal development (e.g. Cloetingh et al., 2010; Limberger et al., 2014; Horváth et al., 2015), due to its generally high geothermal gradient and heat flow density (Lenkey et al., 2002).

The Mura-Zala Basin plays an important role in the oil and gas industry of Slovenia, Hungary and Croatia and has a long history in exploration and production (e.g. Pleničar, 1954; Bader, 1976; Djurasek, 1988; Mioč & Žnidarčič, 1996; Lučić et al., 2001; Dolton, 2006; Kurevija & Vulin, 2011; Markič, 2013). Studies conducted by Sachsenhofer et al. (1998, 2001) and Hasenhüttl et al. (2001) have shown that the basin has a rather complicated heat flow history, making predictions for hydrocarbon generation relatively tricky. A 3D geological model of the Slovenian part of the basin was recently established by Šram et al. (2015). The model includes the latest information on the geological structures in NE Slovenia and contains nine lithostratigraphic units and their boundaries. Large parts of the basin were also investigated according to their hydrocarbon potential, regarding source rock quality and maturity (Sachsenhofer et al. 1998, 2001; Hasenhüttl et al., 2001) using 1D and 2D thermal modelling techniques.

Based on these previous papers, the goal of this thesis is to combine the newly available 3D structural data with maturity data and data on source rock quality. The resulting 3D petroleum systems model of the basin is used for the evaluation of its hydrocarbon potential. Based on paleo heat flow distributions the timing and spatial extent of hydrocarbon generation within the basin is assessed and the locations of possible accumulations are determined. A comparison between the model results and the known present day accumulations and their volumes can then be used to make assumptions about the source rock(s) and eventual undiscovered accumulations.

2 Geological Overview

2.1 Structural evolution

The Alpine-Mediterranean region was a convergence zone enclosed by the African and Eurasian Plate in Late Cretaceous and Cenozoic time. In this general compressional setting, extensional basins have developed since the Oligocene. The description of the structural evolution follows mainly Horváth et al. (2015).

The Pannonian Basin is located in eastern Central Europe and an integral part of the Alpine orogenic system. It is surrounded by the Alpine, Dinaric and Carpathian mountain ranges (Figure 1). The basin is superimposed on the Alcapa and Tisza-Dacia plates, which derive from different paleogeographic positions of the Alpine orogenic system (Figure 2; Schmid et al., 2008). The formation of this extensional basin was accompanied by intensive calc-alkaline magmatism, including silicic volcanism during the Early to Middle Miocene. Subsequently, high heat flow and temperature gradients occurred in the Pannonian region (Horváth et al., 2006).

The structural evolution of the Pannonian Basin System can be subdivided into seven phases; (i) Cretaceous nappe forming, (ii) Late Cretaceous basin evolution and structural exhumation, (iii) Late Oligocene to Early Miocene strike-slip faulting and thrusting, (iv) late Early Miocene rifting, (v) late Sarmatian strike-slip deformation, (vi) Late Miocene post-rift subsidence and (vii) structural inversion from the latest Miocene to Quatenary (Fodor et al., 2011). Their development is discussed in more detail below.

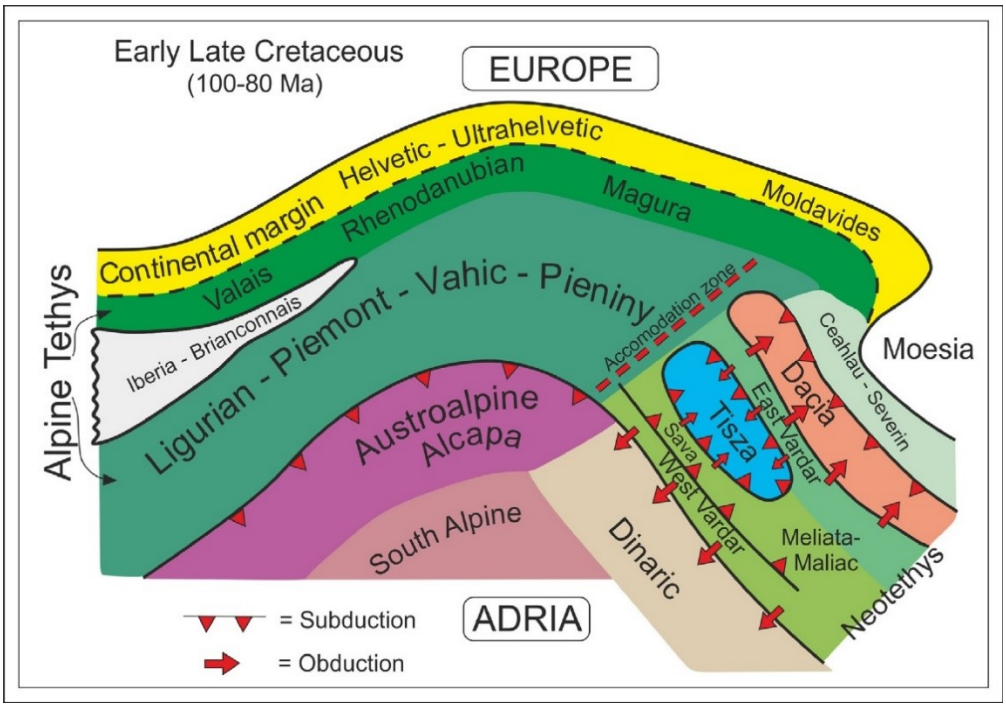

Figure 2 – Schematic paleogeography of the Alpine-Mediterranean region in the early Late Cretaceous (mainly after Csontos and Vörös, 2004; Schmid et al., 2008; Handy et al., 2010)

Two different oceanic realms existed between the European and Adriatic blocks; the Neotethys and the younger Alpine Tethys (Figure 2). In the late Paleozoic, the Neotethys developed through rifting of the northern margin of Gondwana and the following closure of the Paleotethys (Stampfli & Borel, 2002). The Meliata-Maliac ocean opened in the Late Triassic and was surrounded by a large shelf region where extensive carbonate platforms developed on the shallow shelfs and the slopes. Contemporaneously, ocean pelagic limestones were deposited in the Neotethys (Haas et al, 1995). The Eastern and Western Vardar oceans are also branches of the Neotethys (Schmid et al., 2008), spreading between Tisza and Europe and the Dinaric margin of Adria and Europe, respectively. At the beginning of the Jurassic, Dacia was separated from Europe through the spreading of the Ceahlau-Severin ocean, which is considered a part of the Alpine Tethys. Closing of this system began during the Late Jurassic. The Eastern Vardar and Ceahlau-Severin ocean were completely closed by Late Cretaceous time due to ongoing convergence (i), (ii). The West Vardar ocean was fully subducted below Tisza and Dacia in the Early Eocene. During Eocene and Oligocene times, large scale thrusting took place as the continental collision in the Dinarides peaked (Tomlijenovic et al., 2008; Ustaszewski et al., 2010).

The rifting process that gave birth to the Central Atlantic ocean also created the Alpine Tethys (Stampfli & Borel, 2002). Its southern part (Ligurian-Piemont-Vahic-Pieniny) developed during the Jurassic, while the northern branch (Valais-Rhenodanubian-Magura) formed in the Early Cretaceous, separating the Iberia-Brianconnais Block from Europe. The closure of the Alpine Tethys is separated into three stages; first the subduction of the Ligurian ocean in the mid Cretaceous, followed by the rest of the southern branch during Mid to Late Cretaceous until Eocene times and completed by the subduction of the northern branch and the Brianconnais terrain (Handy et. al., 2010). The continental collision started in the middle Eocene in the Central and Eastern Alps (Schmid et al., 2013). From the Middle to Late Eocene,

the continental collision of the Alps and Dinarides was accompanied by delamination of the mantle lithosphere and its roll-back.

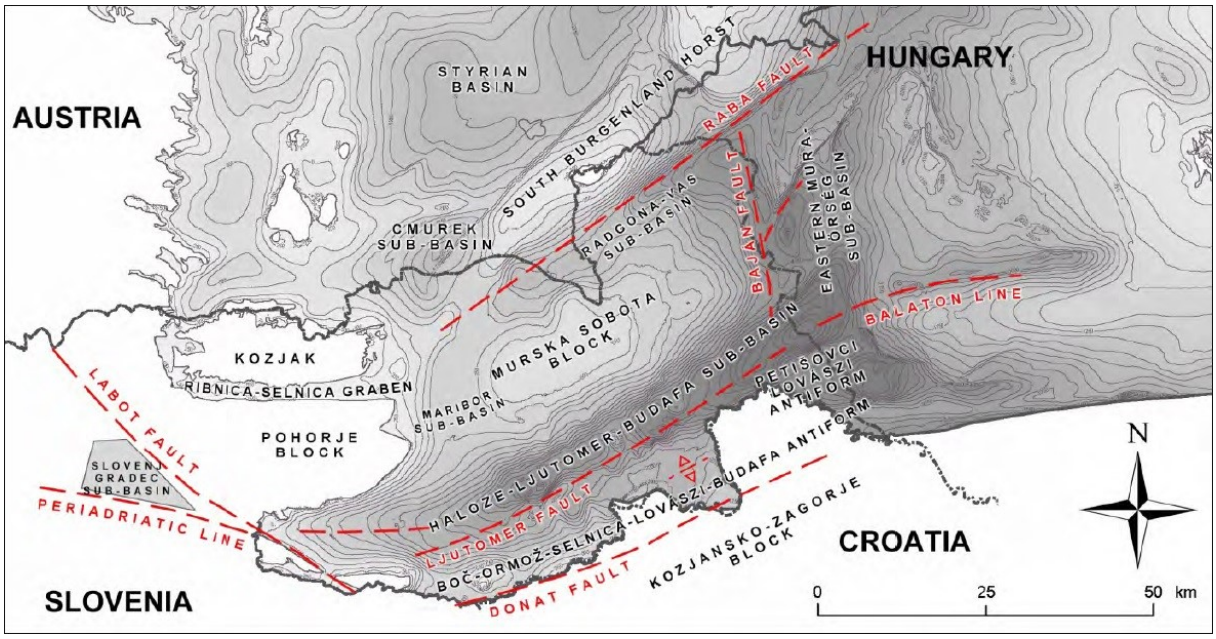

Figure 3 - Contour map of the pre-Neogene basement with major tectonic features (adapted from reports of Jelen et al., 2006, Maros et al., 2012)

The Pannonian Basin saw the start of its formation in the Early Miocene, around 21 Ma ago. The main structural pattern developed during Karpatian to Sarmatian times (iv), where the rift extension culminated (Posser, 1993; Horvath et al., 2006) and reactivated detachment faults (v) formed during the Cretaceous (Fodor et al., 2011). The extension can be dated thermochronologically due to studies of the exhumed metamorphic rocks of the Tauern Window and similar behavior of the Rechnitz Window, all showing slow exhumation rates between 30 Ma and around 20 Ma, sharply increasing afterwards until finally ceasing at around 14 Ma. This is in good agreement with the main rifting phase of the Alcapa terrane (Scharf et al., 2013; Dunkl et al., 1998; Fodor et al., 2008) and the emplacement of the Pohorje Pluton (for location of the Pohorje Block see Figure 3), which is dated to 18.6 Ma (Fodor et al., 2008). Continuous delamination and roll-back of the central and southern Dinaric slab probably controlled the extension in the south-eastern part of the basin as well as the Vardar zone and further to the south (Matenco & Radivojevic, 2012). This is relatable to the counterclockwise rotation of the Alcapa and clockwise rotation of the Tisza-Dacia terranes in the Pannonian Basin, followed by eventual ceasing of the extension. Recent studies suggest an opposite rotation of the terranes with differential rotations within the terranes and distinctive phases of rotational events, peaking between 18 Ma and 10 Ma. (Marton & Fodor, 2003; Marton et al., 2007; Van Hinsbergen et al., 2008; Tomljenovic et al., 2008; Ustaszweski et al., 2008). In the Slovenian part of the basin, the Late Oligocene to Early Miocene strike-slip faulting and thrusting (iii) led to the formation of the Murska Sobota extensional Block (Figure 3) (sensu Jelen & Rifelj, 2010), which is bound by strike-slip grabens in the north (Radgona-Vas sub-basin) and the much deeper Ptuj-Ljutomer-Budafa half-graben in the south (Figure 3). The following and partly simultaneous rifting caused gravitational subsidence (vi) of the Murska Sobota Block (Fodor et al., 2011).

The counterclockwise rotation of Adria created a stress field change at the margins of the Pannonian Basin (vii) leading to a compressional setting and structural inversion during the Pliocene and Quaternary (Horváth & Cloething, 1996; Grenerczy et al., 2005; Bada et al., 2007). This event led to the folds that are dominating the southern part of the Mura-Zala Basin (Fodor et al., 2011), which are the most important trap forming structures in the basin (Boc-Ormoz-Selnica-Lovaszi-Budafa-Antiform, Figure 3). They are supposedly connected to the Sava Folds in the west (Dank, 1962) and the folds in the Haloze area. The folding already commenced during Pannonian sedimentation (Uhrin et al., 2009), which implies that the structural inversion already started 7.5 Ma ago, although during its initial stages the regional post-rift subsidence compensated for the structural uplift. Neotectonics probably affected the Murska Sobota Block by rotating it counterclockwise and tilting it to the north as it was demonstrated in similar fashion for the Haloze area (Marton et al., 2002).

2.2 Basin Structure

The Mura-Zala Basin is separated from the Styrian Basin by the South Burgenland Swell. It is characterized by several WSW-ENE trending, fault-bounded troughs and basement highs (e.g. Hasenhüttl et al., 2001). Their locations are indicated in Figure 3, where the northernmost structural element is the above mentioned South Burgenland Swell bordered by the Raba Fault, followed southwards by the Radgona-Vas sub-basin, the Murska-Sobota Block, and the Haloze-Ljutomer-Budafa sub-basin, which is bordered to the south by the Ljutomer Fault. The Haloze-Ljutomer-Budafa sub-basin is the deepest trough in the basin with up to 5000 m of Neogene sediment infill (Figure 4). To the south-east of the Murska-Sobota Block, the Maribor sub-basin is located. The Boc-Ormoz-Selnica-Lovaszi-Budafa anticline extends south to the Ljutomer Fault and splits eastwards into a double-anticline, which hosts Slovenia´s most important hydrocarbon accumulations. The Donat Fault borders this anticline to the south.

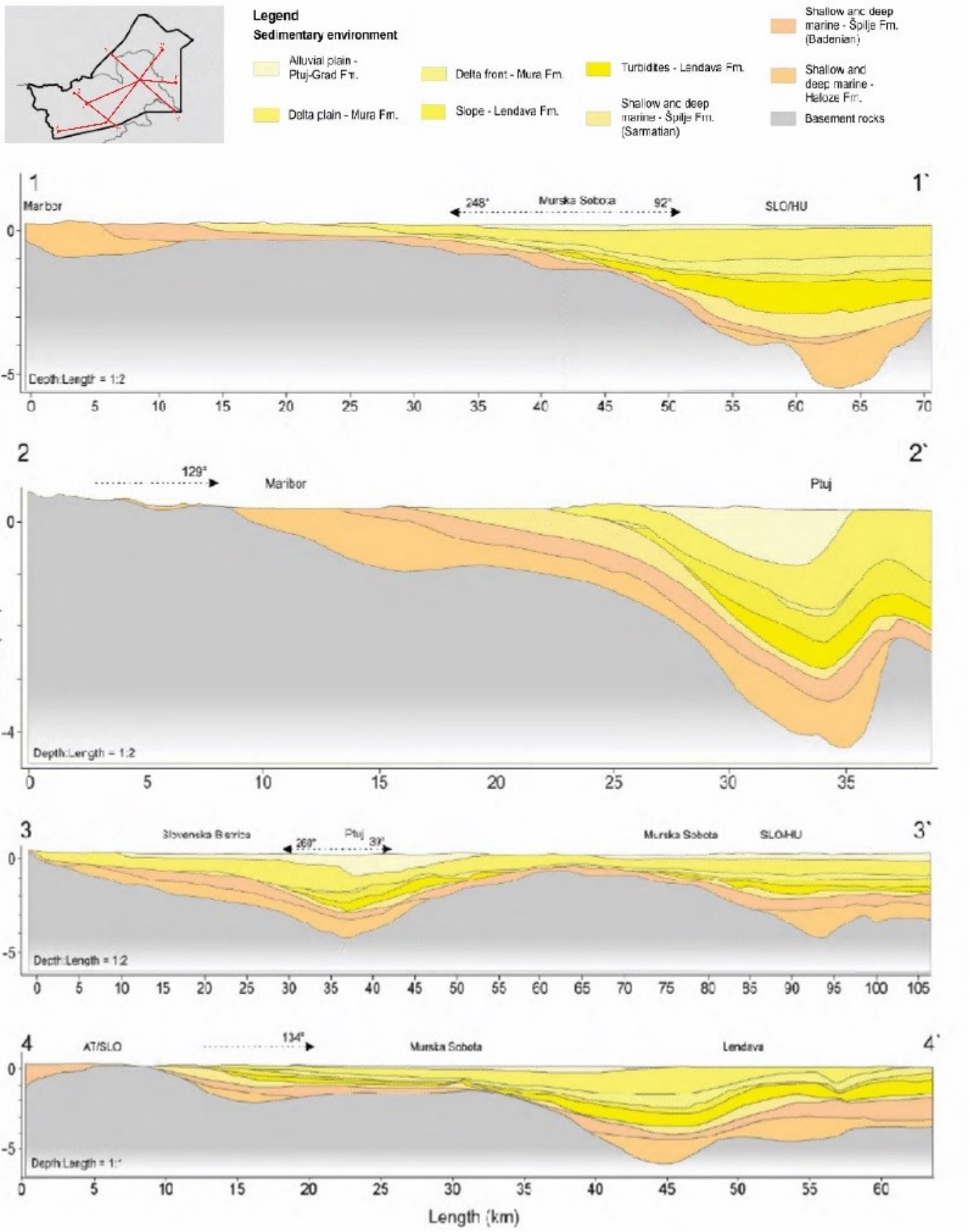

Figure 4 - Cros sections through the study area, with structural elements indicated (Šram et al., 2015)

2.3 Stratigraphy of the Neogene basin fill

This section describes the Slovenian part of the Pannonian Basin, starting with the Karpatian as first sedimentary infill on top of mainly pre-Mesozoic basement rocks. The description follows mainly Fodor et al. (2011).

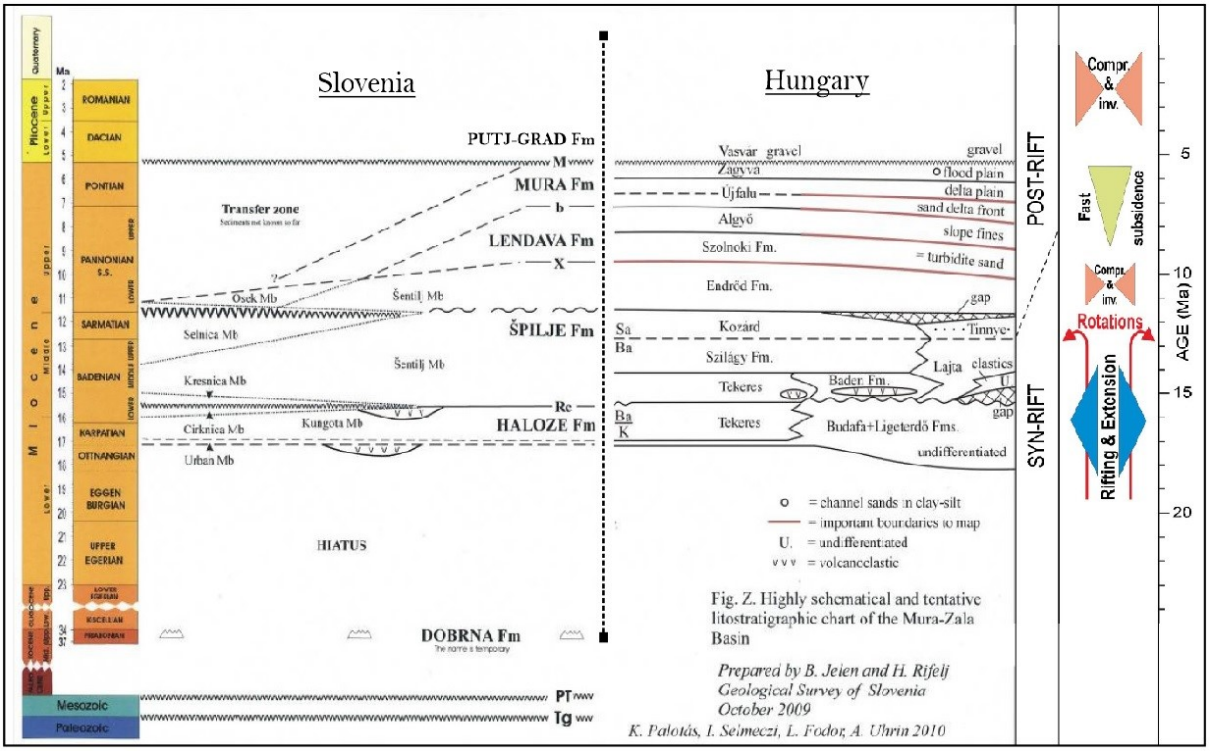

Figure 5 - Stratigrahic chart correlating the hungarian and slovenian units of the Miocene (Fodor et al., 2011) with the different stages of tectonic development on the right (after Horváth et al., 2015)

2.3.1 Haloze Formation – Upper Ottnagian to Lower Badenian

Upper Ottnangian and Karpatian to lowermost Badenian synrift deposits in the Mura-Zala Basin belong to the Haloze Formation (Jelen & Rifelj, 2005c, 2006). It represents the sedimentary infill of the "core complex" stage, the initial infill onto Pre-Cenozoic basement, enabled through noticeable subsidence along the ENE trending Donat transtensional fault system (Figure 3) and the Raba extensional corridor (Jelen & Rifelj, 2003, 2004, 2005a).

The Haloze Formation consists of sandstone, conglomerate, muddy breccia, conglomerate and oyster banks in the Karpatian, representing the lower part of the Haloze Formation in the Maribor sub-basin. The Haloze – Ljutomer – Budafa sub-basin is filled with sandy and silty marl, alternations of sandy marl, silty marl and sandstone representing the Karpatian and Lower Badenian parts of the Haloze Formation. Early Badenian tuff deposits as well as conglomerates are also present. The uppermost part belongs to the Lower Badenian and comprises alterations of sandstone, sand, sandy marl and conglomerate.

The Mura-Zala Basin received turbiditic sediments from the Karpatian to the Early Pontian (Jelen & Rifelj, 2001, 2003). Haloze deposits are found in the Maribor and the Haloze – Ljutomer – Budafa sub-basins, but are missing on the Murska Sobota Block. This can be

explained by non-deposition or subsequent erosion. The Haloze Formation is up to 1300 m thick.

2.3.2 Spilje Formation

2.3.2.1 Spilje Formation – Badenian

Tectonic uplift and a eustatic sea level drop at the Karpatian/Badenian boundary led to an erosional unconformity in the shallow parts of the basin and to deposition of coarse-grained fan deposits in the deeper parts, while the most distal parts became "starved basins" (Fodor et al., 2011). After the uplift and sea level drop, rapid subsidence occurred (second part of the first syn-rift phase) and was accompanied by an Early Badenian transgression (Jelen & Rifelj, 2001, 2004, 2005a, b). The Lower Badenian onlaps onto the Pre-Tertiary basement of the relatively uplifted blocks. Deepwater conditions were established and mud rich turbidites and hemipelagic mud began to cover the deepest parts of the basin. The sedimentation pattern was then abruptly changed to sand rich turbidites, due to an extensional collapse paired with the onset of compressional tectonics in the Alps (Massari et al., 1986). In the distal parts, this change is reflected by a progradation in the Upper Badenian, while the deepest parts of the sub-basins represent a falling stage system track. In the shallow parts of the basin, an unconformity appears close to the Badenian/Sarmatian boundary during the low stand system track and in the deeper parts of the basins, the sequence boundary moves towards the sand rich turbidite fans (Fodor et al., 2011).

2.3.2.2 Spilje Formation – Sarmatian

The transgressive system tract deposited heterolitic siliciclatics and carbonates in the shallow parts of the Mura-Zala Basin during Early Sarmatian time. The deeper parts continued to undergo turbiditic sedimentation (Fodor et al., 2012).

The collision of the Alcapa Block with the eastern European lithospheric platform in the Late Sarmatian, resulted in a weak kinematic inversion in the Mura-Zala Basin, leading to inversion of certain structures (e.g. Pecarovci, Dankovci – found in the Radgona-Vas sub-basin) and subsequently increasing coarse-grained sedimentation (Sadnikar, 1993, Gosar, 2005). By the end of the Sarmatian, the Maribor sub basin as well as the western parts of the Radgona-Vas and Haloze-Ljutomer-Budafa sub-basins were filled up and acted as by-pass zones for sediments afterwards.

2.3.2.3 Spilje Formation – Pannonian

The base of the Pannonian is characterized by a major transgressive event, leading to carbonate mudstone deposition over wide and previously exposed areas in the eastern and southern part of the Murska Sobota Block (Djurasek 1988) and onlapping unconformably onto Sarmatian strata in shallower parts (Sadnikar 1993). This marl is considered the uppermost part of the Spilje Formation.

2.3.3 Lendava Formation – Pannonian

After the transgression, infill from the now emerging mountainous areas around started, represented by sandy turbidites, which reach their maximum thickness in the Haloze-Ljutomer-Budafa sub-basin. Those are defined as the lowermost part of the Lendava Formation. The upper part is made up of fine grade slope deposits with infrequent small-scale sand bodies (Fodor et al., 2011). The slopes are mainly north-south striking. The Lendava Formation as described here is only developed in the deeper parts of the basin due to insufficient relief below the prograding delta in the north-western part of the Mural-Zala Basin, however in areas along

the Croatian border, thick outcrops of the turbidite and slope deposits of the Lendava Formation can be found.

2.3.4 Mura Formation – Pannonian

The Mura Formation can be divided into delta front and delta plain deposits. The delta front is characterized by silt and coarsening upwards sand bodies, while the delta plain deposits are represented by fine grained sedimentation, including fining upwards and coarsening upwards sand bodies, as well as coal beds and rare gravel beds.

The absence of the "slope" facies beneath the Mura Formation in the northwestern part of the Mura-Zala Basin marks the transition between the basin and the marginal/terrestrial environment. This is reflected in the increased grain size and the regional distribution of different lithologies. Whereas the Haloze-Ljutomer-Budafa sub-basin in the west is filled with up to 60% of coarse grained material, the Hungarian part of the same facies usually contains less than 50% coarse grained material (Fodor et al., 2011).

2.3.5 Ptuj-Grad Formation – Pliocene

The Ptuj-Grad Formation consists of an alteration of gravely sand, silty sand, sandy and clayey gravel, gravely silt, clayey silt and silty clay in the southwestern part of the basin. East of the Mura River, an alteration of sand, gravely sand, sandy and silty clay, clayey and sandy gravel, basaltic tuff, tuffite and basalt belongs to the Ptuj-Grad Formation (Fodor et al., 2011).

Some characteristics of the formations, which are considered in the model, are summarized in Table 1 according to Maros et al. (2012). Quaternary deposits were not distinguished (Šram et al., 2015).

Table 1 - Miocene formations and their properties

Formation	Lithological description (after JELEN & RIFELJ, 2011)	Distinguishing criteria of borehole logs	Average sand content	Sedimentary environment	Time period	Porosity
Ptuj-Grad Fm.	alternation of gravel, sandy, silty and clayey gravel, sand, gravely and silty sand, silt, sandy and silty clay, basaltic tuff, tuffite and basalt, isolated coal occurrences	specific lithology and paleontological determination, superposition	15%	alluvial plain	Latest Pannonian to Pliocene	10%
Mura Fm.	alternation of silty clay, clay, silt, gravely, sandy and clayey silt, sand, silty and gravely sand, sandy gravel and coal	specific lithology and paleontological determination, alternation of fining- and coarsening- upward sand bodies from geophysical borehole logs, coal occurrences	50%	delta plain	earliest Pannonian to Late Pontian	10%
	alternation of sand/ sandstone, silt, marl, clayey marl, clay, marly, sandy and silty clay, coal	specific lithology and paleontological determination, thick, coarsening-upward sand bodies from geophysical borehole logs, coal occurrences	70%	delta front		12-14%
Lendava Fm.	sandy silt, marly clay, occasional sand bodies	superposition and the presence of approx. 200 m thick uniform silt horizon without distinct stratification	5%	slope	Early Pontian	5%
	alternation of sand/ sandstone, silt, sandy, silty and clayey marl, clay	specific lithology and paleontological determination, sand bodies with occasional gravel, predominately non-graded from geophysical borehole logs	30% (turbidites 50%, silt 5%)	deep lacustrine turbiditic	Late Pannonian	7% (turbidites 10%, silt 5%)
Špilje Fm.	alternation of sand, sandstone, sandy and silty marlstone, silt, siltstone, marly and silty clay, conglomerate, locally sandy algal and oolitic limestone, dolomite, coal	specific lithology and paleontological determination	50%	Sarmatian shallow (and deep) marine, fluvial, terrestrial	Mid Badenian to Early Pannonian	7%
	alternation of silty and clayey marl, sandstone, locally algal limestone, conglomerate, dolomite, coal	specific lithology and paleontological determination	30%, shallow areas more permeable	Badenian shallow (and deep) marine	Early Badenian to Sarmatian	5%
Haloze Fm.	alternation of sandy and silty marl, sandstone, conglomerate, muddy breccia, oyster banks, tuff	specific lithology and paleontological determination	30%	shallow (and deep) marine, terrestrial	Karpatian to Early Badenian	5%
pre-Neogene rocks	Metamorphic and carbonate rocks, marl, sand/sandstone, conglomerate	/	/	metamorphic, marine, brackish, lacustrine	Paleozoic to Oligocene	/

2.4 Oil and gas in Slovenia

Slovenia is virtually entirely dependent on imported gas with negligible domestic production. It can only account for about 10% of its gas demand (PMC, 2006). The Petisovci-Dolina area near Lendava is the only prosperous area for hydrocarbon exploitation in Slovenia so far. It is currently under development by the British company "Ascent Resources", who recently conducted a 3D seismic survey in the Petisovci area and drilled two new wells (Figure 6). For this reason, a special focus has also been put on the properties of that area in this thesis. In the remaining area of the Mura-Zala Basin, 41 wells have been drilled in the 1950s and 16 more since then, but commercial production could not be established anywhere else but in the Petisovci-Dolina field (Markič et al., 2016). Reservoirs in the Upper Miocene strata of the Petisovci-Dolina field used to have considerable economic value in the 1950's with production of up to $23*10^6$ m³ of oil per year, while deeper layers became more valuable later on. The deeper reservoir horizons are usually "tight gas" reservoirs, requiring hydraulic stimulation for production.

There are abnormally high vitrinite reflectance values found in Badenian and older sediments in the Lendava/Petisovci area, but especially in the Somat/Radkersburg area. This is probably caused by magmatic activity, which is well known in the Styrian Basin and south of the Ornmoz-Selinca anticline and occurred during Early Miocene times (6.2.3.1).

The source rock found in the Mura-Zala Basin is varying in quality (Hasenhüttl et al., 2001). Karpatian marls and silty marls in the Somat area contain between 0.8% and about 3% TOC, classified mainly as type II kerogen, while they have a lower TOC of about 1.3% and type III kerogen in the Ljutomer Trough. Badenian source rocks mostly contain less than 0.5% TOC and their HI stays below 200, while brackish Sarmatian sediments show a TOC of up to 1.35% and generally higher HI values, reaching up to 350 mg HC/g TOC. Upper Miocene rocks contain coaly sediments with a HI of about 100 mg HC/g TOC and high TOC values in the range of 5% (Hasenhüttl et al., 2001). Summarized it can be concluded that the source rock potential of Neogene sediments in the Mura-Zala Basin is overall fair, but not excellent in any part of the basin.

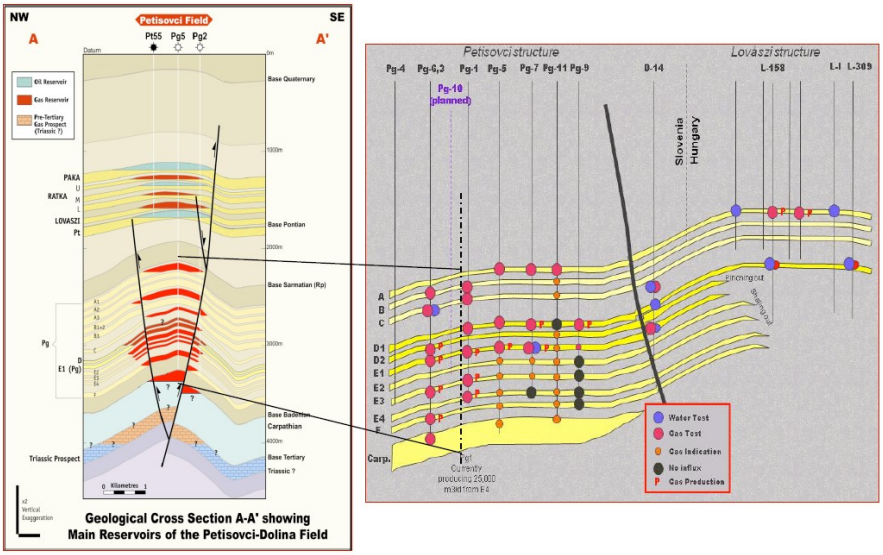

Figure 6 – Cross sections through the Petisovci and Lovaszi structures

3 Dataset

Datasets used for the petroleum systems model are presented in this section.

3.1 3D – regional geological model of the Mura-Zala Basin

The 3D structural model of the Mura-Zala Basin, built and kindly provided by Dejan Šram (2015), provides the basis of the model produced in this thesis. It was built through harmonization of preexisting models, reinterpretation of 145 borehole logs and using the 3D numerical model software JewelSuite© (Figure 7). It contains nine stratigraphic horizons, defined throughout the Mura-Zala Basin (Figure 8).

The data for the model was compiled using four different sources;

- Published geological surface maps (Mioč & Marković, 1998; Jelen & Rifelj, 2011),
- Models from previous studies of the area (Lapanje et al., 2007, Fodor et al., 2011, Maros et al., 2012, Rman, 2013),
- Digital surface map (CIAT, 2004)
- Borehole lithological logs

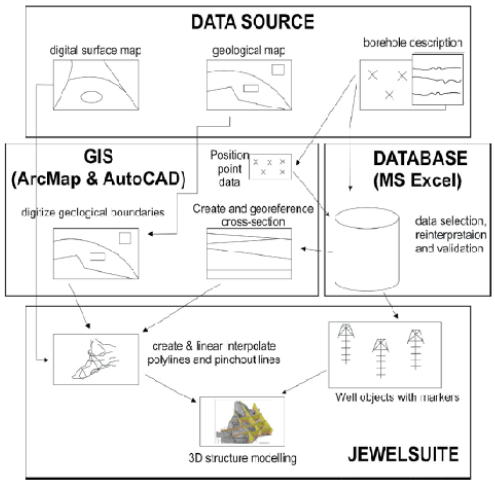

Figure 7 - Methodology for producing a 3D geological model (after Kaufmann & Martin, 2008)

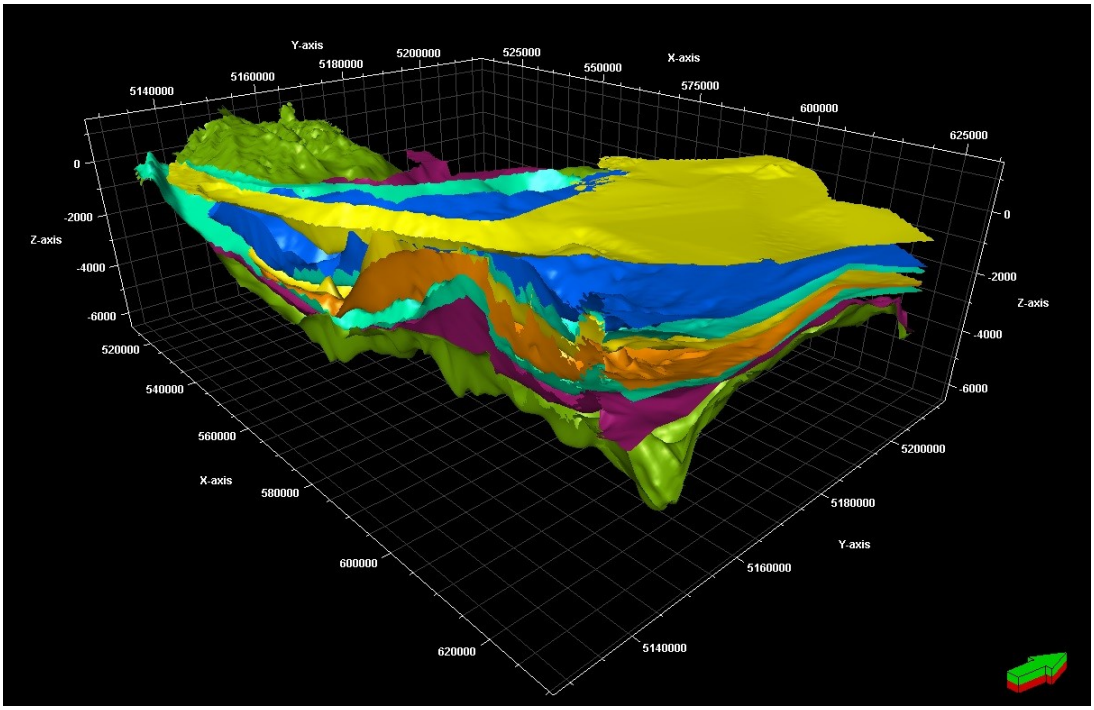

Figure 8 – Lithostratigraphic horizons as triangle meshes, directly exported from JewelSuite by Sram (2015)

3.2 Structural basement map

Since the 3D model from Šram (2015; section 3.1) extends exactly to the Slovenian border, the relevant geological structures in Austria, Hungary and Croatia had to be added. The structural map of the "pre-Tertiary basement in the Mura-Depression" (Durasek & Simon, 1994) was used for this purpose. This map also includes discovered and potential oil and gas objects in the basin.

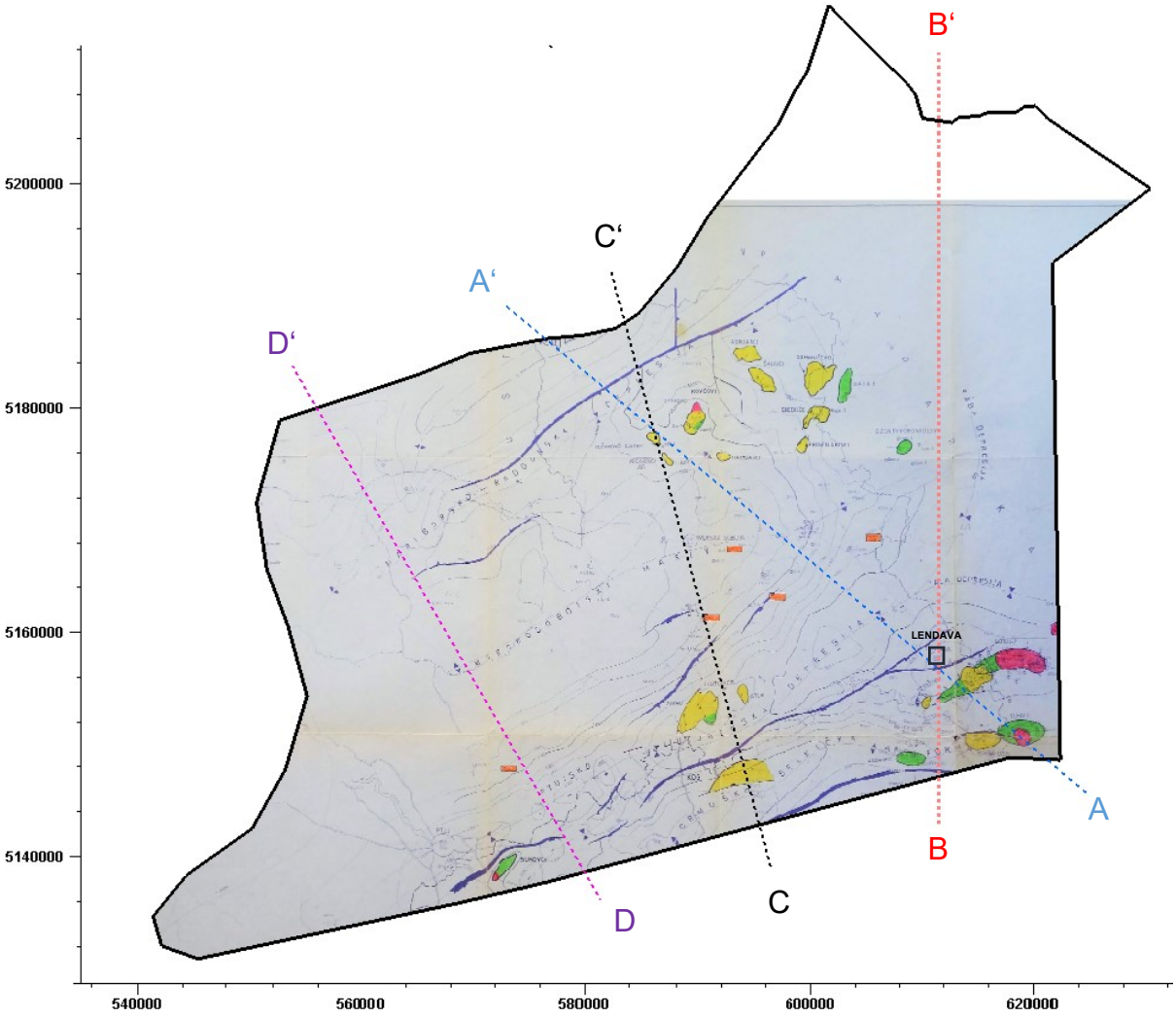

Figure 9 - Structural basement map of the Mura-Zala Basin, cut along the model borders. The locations of the profiles A-A', B-B', C-C' and D-D' are indicated (Durasek & Simon, 1994).

3.3 Well data

Sachsenhofer et al. (2001) and Hasenhüttl et al. (2001) investigated the hydrocarbon potential and thermal history of the Mura-Zala Basin. These authors provided a wealth of analytical data for a high number of samples from 16 wells. The following data are used in this thesis:

- Total organic carbon (TOC) [%]
- Hydrogen Index (HI) [mg HC/g TOC]
- Vitrinite Reflectance (%Rr)
- Hopane and sterane isomerization ratios
- S1 + S2 values (Rock Eval pyrolysis)

A visual presentation of the available information on TOC contents, hydrogen index and hopane and sterane isomerization is given in Figure 10 and Figure 11. A complete table including vitrinite reflectance data can be found in Appendix 1.

The TOC content measures the amount of organic carbon in the sediment as mass percent, it is a proxy for the organic material, which is potentially available for hydrocarbon generation.

The hydrogen index (HI) is an indicator for the amount of total organic carbon that can actually be transformed into hydrocarbons. Moreover, the hydrogen index is used for the classification of kerogen types.

Vitrinite reflectance (%Rr) is the most reliable and most widely used parameter to measure source rock maturity. Typically, source rocks get mature at about 0.6% Rr (oil window) and enter the gas window at 1.3 %Rr.

Hopane and sterane isomerization also measure the source rock maturity, where the 17β(H), 21β(H) stereochemistry changes to 17α(H), 21β(H) with increasing maturity for hopanes while reaching its equilibrium at around 0.6 and the isomerization at C-20 causes the 20S/(20S +20R) ratio to rise from 0 to about 0.5 with increasing maturity for steranes. However, they are only useful in a narrow range from immature to the beginning of the oil window, where they are very specific, but reach their equilibrium there (~0.65%Rr for hopane, ~0.85%Rr for sterane) and cannot provide information on higher maturity (Peters et al., 2007).

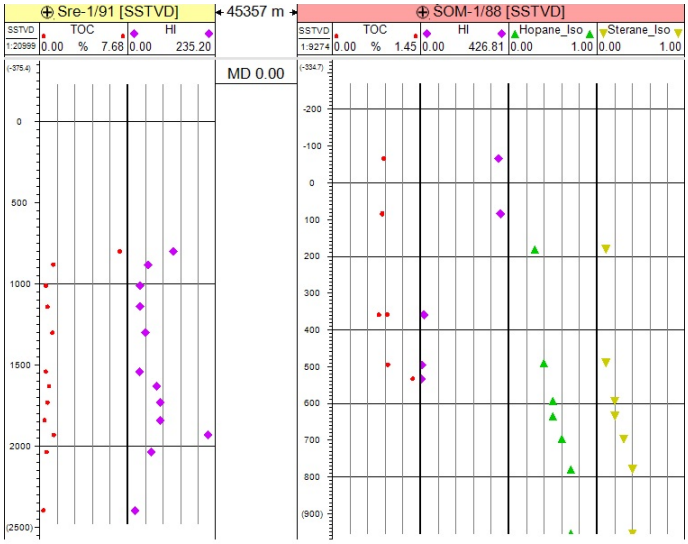

Figure 10 – Depth plot of TOC, HI, sterane isomerization and hopane isomerization.

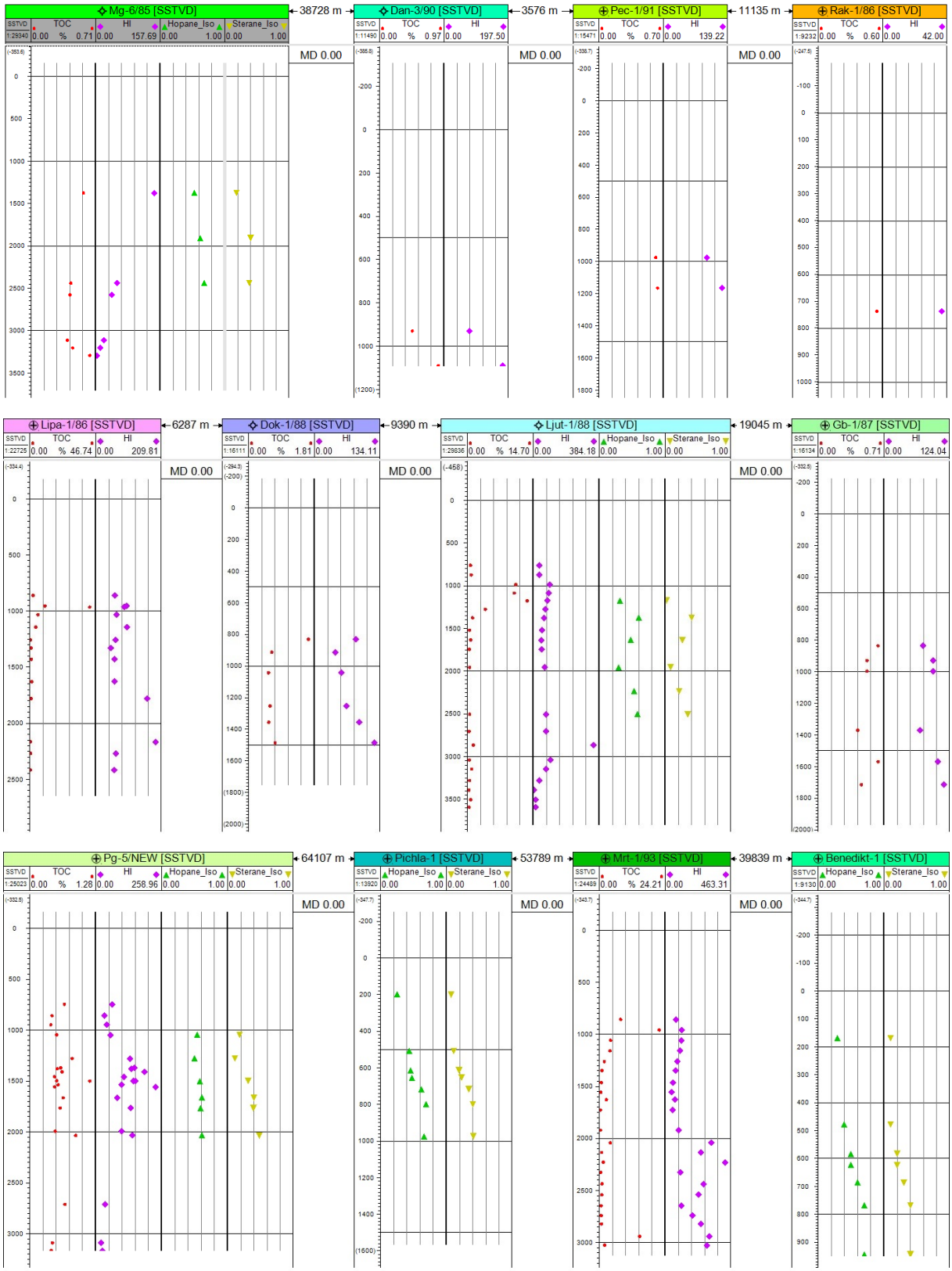

Figure 11 - Depth plot of TOC, HI, sterane isomerization and hopane isomerization

3.4 Seismic profiles and schematic cross sections

For the enhancement of the quality regarding the structures in the most important hydrocarbon province in Slovenia, the Petisovci-Lovaszi area, published seismic profiles and schematic cross sections by Ascent (2011) and Toth & Tari (2014) have been used.

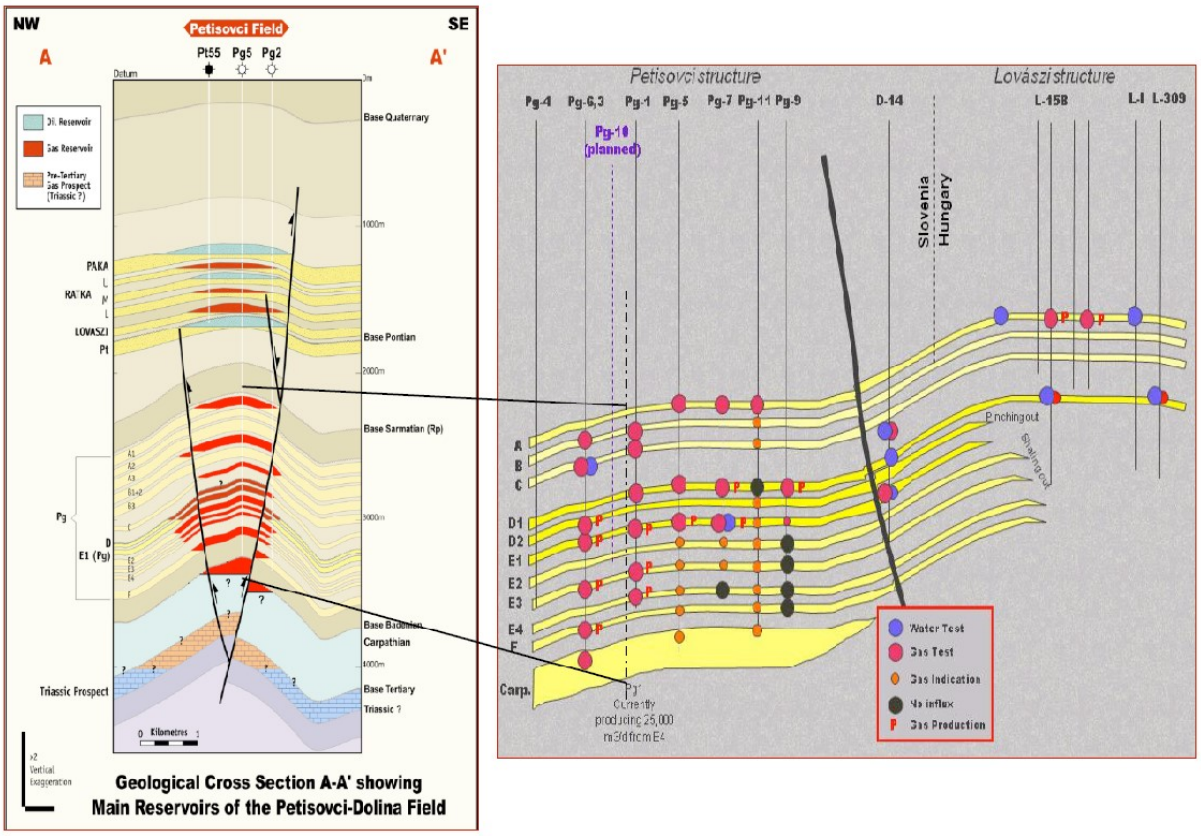

Figure 12 - Schematic cross-sections through the Petišovci field (Ascent, 2011)

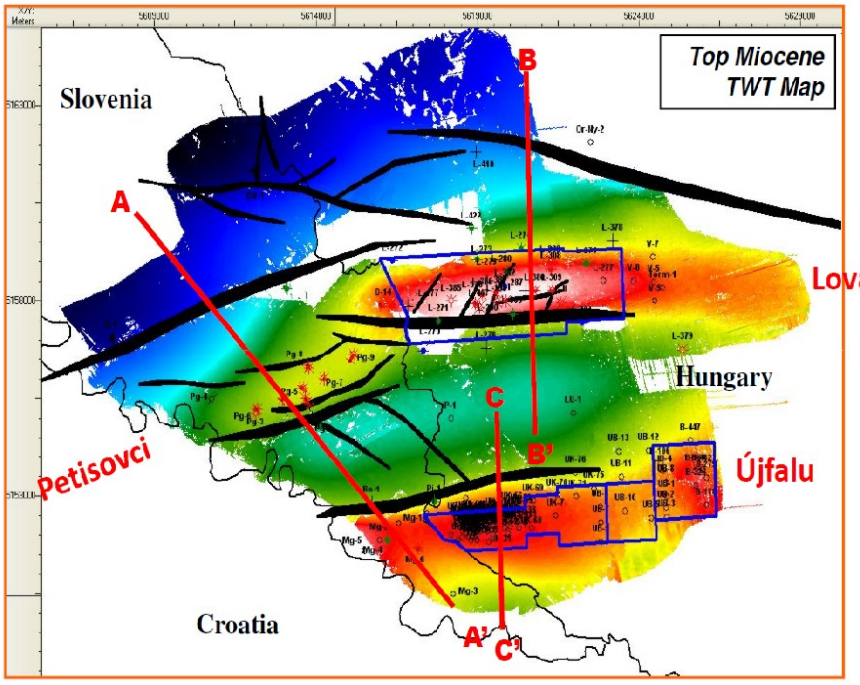

Figure 13 - Locations of the seismic cross sections A-A', B-B' and C-C' shown in figures 13-15 (Toth & Tari, 2014).

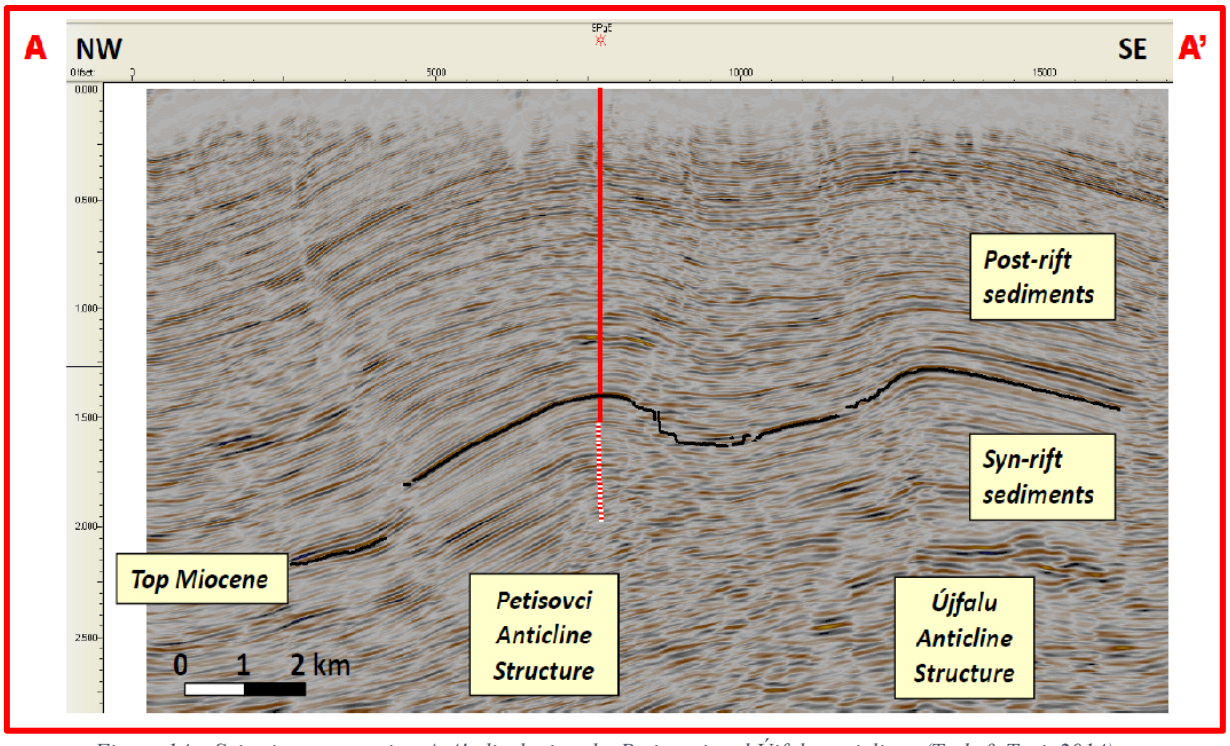

Figure 14 – Seismic cross section A-A', displaying the Petisovci and Újfalu anticlines (Toth & Tari, 2014).

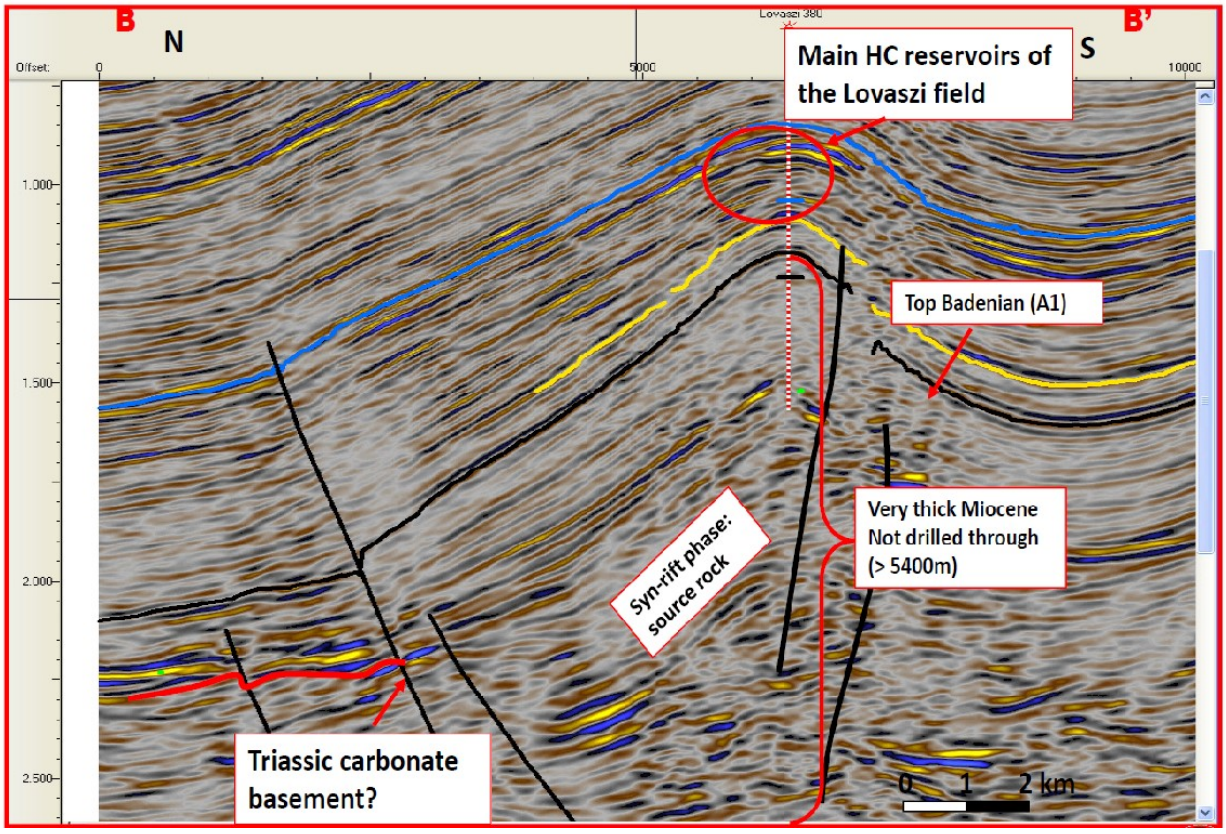

Figure 15 - Seismic cross section B-B', displaying the structure entrapping the Lovászi field (Toth & Tari, 2014).

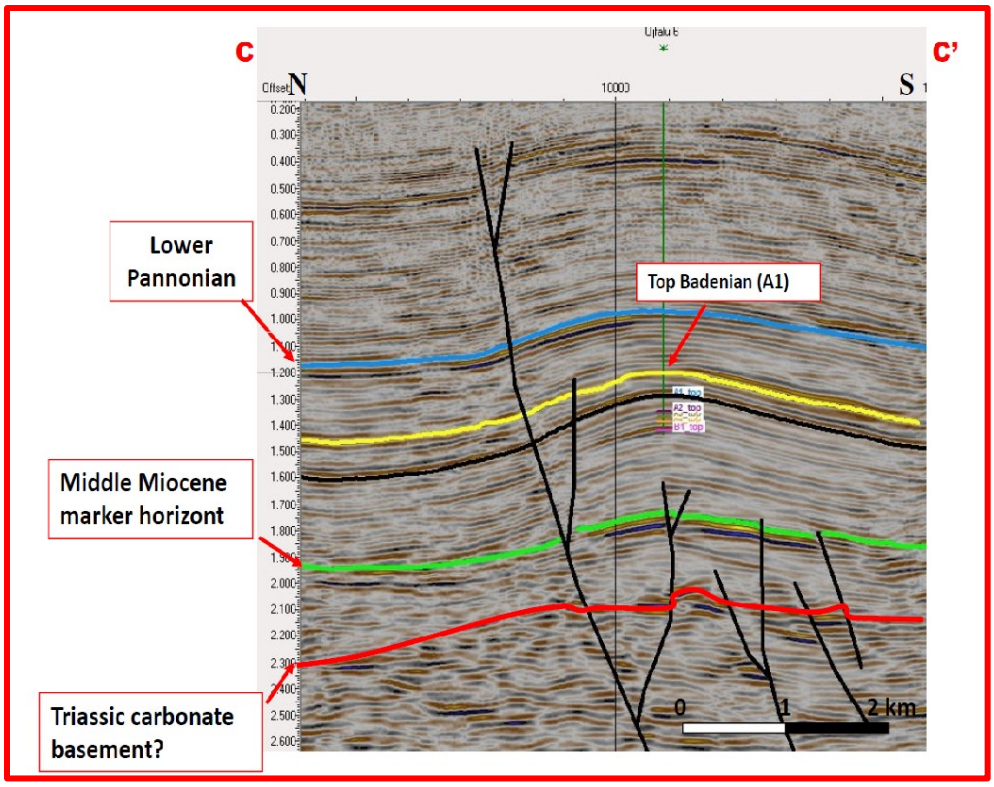

Figure 16 - Seismic cross section C-C', showing the Budafa-Anticline, which hosts the Budafa and Ujfalu oil and gas fields (Toth & Tari, 2014).

4 Model building process

4.1 1D Modelling and Calibration

For the determination of the boundary conditions (heat flow, paleo water depth, surface water interface temperature) as input parameters for a first approach of the 3D modelling process, 1D models have to be set up. The 1D models were built and simulated entirely in Petrel 2015 software (Figure 17).

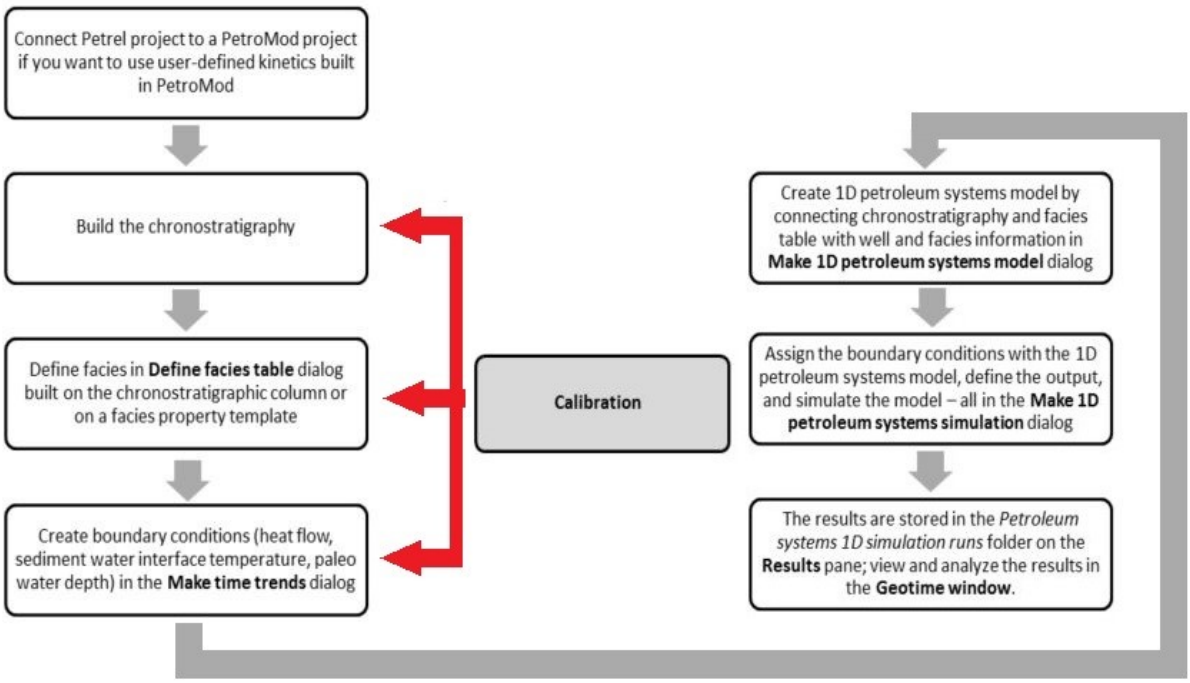

Figure 17 - Workflow for the construction, calibration and simulation of a 1D Petroleum System Model (Schlumberger, 2015)

To construct a 1D model, a chronostratigraphic table and a facies (lithostratigraphic) table had to be defined (Figure 18). To increase the resolution of the facies model, the Lendava Formation (Turbidites) and the Spilje Formation (Sarmat) have been further subdivided into two (Lendava Turbidites (80%), Lendava Turbidites (20%)) and three (Spilje – Sarmat 1, Spilje – Sarmat 2, Spilje – Sarmat 3) different lithostratigraphic units, respectively.

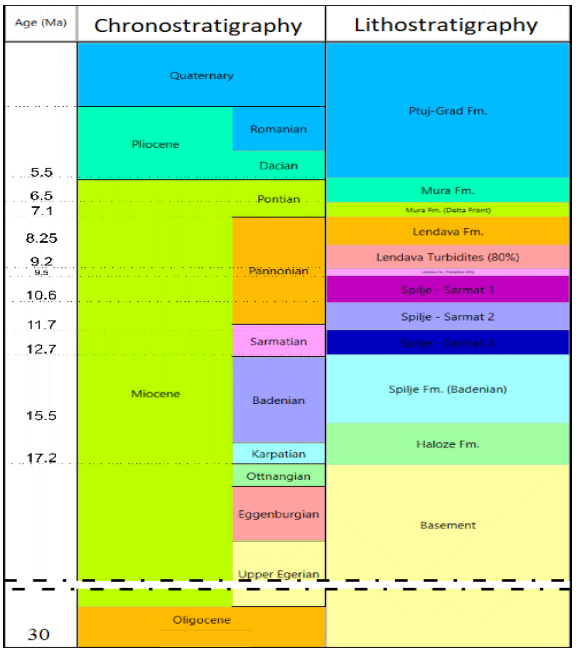

Figure 18 – Chrono-/Lithostratigraphy as used in the model

Detailed lithostratigraphic information was available for the wells Mg-6, Pg-5, Gb-1, Radk-2, Som-1, Bndkt-1, Pchl-1, Rak-1, Ljut-1 and Sre-1. For the other wells, an average lithology was created for every formation, based on a combination of typical well logs (Figure 19), published lithology descriptions and the information from the above wells with detailed lithology description. To keep the model simple, six different standard lithology types provided by Petrel have been used for the model (Figure 20), which have been mixed in different proportions to meet the expected requirements regarding petrophysical parameters (e.g. compaction properties, permeability, thermal conductivity, radiogenic heat generation). The composition of the formations as used in the model is shown in Table 2.

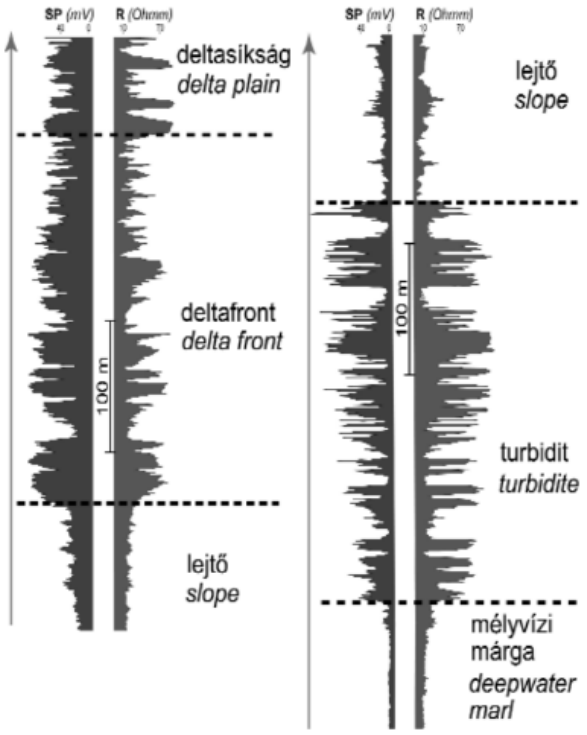

Figure 19 - Typical well-logs for characteristic clastic lithofacies of the Pannonian sequence, used for the estimation of average lithology content (Fodor et al., 2011)

Facies	Code	Color	Lithology group	Lithology	Petroleum system element
Sand	0		Clastic sedim	Sandstone (arkose, typical	Reservoir Rock
Conglomerat	1		Clastic sedim	Conglomerate (typical)	none
Silt	2		Clastic sedim	Siltstone (organic lean)	none
Shale	3		Clastic sedim	Shale (typical)	Source Rock
Marl	4		Carbonate ro	Marl	Source Rock
Basement	5		Igneous rocks	Granite (150 Ma old)	

Figure 20 - Petrel standard lithology types used

Since the 3D model uses only those six basic lithologies, rather than the very specific ones for the different well locations, all wells were simulated with the average lithology composition shown in Table 2. The difference in the results for this assumption compared to those obtained with the detailed lithologies is discussed later in the section “Sensitivity analysis”.

The first dataset of boundary conditions (heat flow, paleo water depth) was taken from publications of Sachsenhofer et al. (2001) and Hasenhüttl et al. (2001). The assumptions for

paleo water depths were kept throughout the whole modelling process, whereas heat flows were recalibrated to fit the vitrinite reflection data under the updated conditions.

Table 2 - Lithological composition of different stratigraphic units used in the model.

	Time of deposition [Ma]		Lithology [%]				
Formation	until	from	Sand	Conglomerate	Silt	Shale	Marl
Ptuj-Grad	0	5.5	15	75	5	5	0
Mura (Delta Plain)	5.5	6.5	50	5	5	40	0
Mura (Delta Front)	6.5	7.1	70	5	5	20	0
Lendava (Slope)	7.1	8.25	5	0	80	10	5
Levanda (Turbidites, 80%)	8.25	9.2	40	0	40	20	0
Levanda (Turbidites, 20%)	9.2	9.5	0	0	0	0	100
Spilje (Sarmat 1, 33%)	9.5	10.6	80	0	0	0	20
Spilje (Sarmat 2, 33%)	10.6	11.7	0	0	0	0	100
Spilje (Sarmat 3, 33%)	11.7	12.7	80	0	10	0	10
Spilje (Badenian)	12.7	15.5	30	10	15	15	30
Haloze	15.5	17.2	30	15	15	10	30

4.2 1D-calibration results

Calculated and measured calibration data for all wells are shown in Figure 21 and Figure 23. The applied heat flow data are compiled inTable 3. The strongly elevated heat flow values in Table 2 (indicated by warm colors) are necessary to obtain the vitrinite reflectance trends, that were observed in the wells.

Table 3 - Calibrated 1D heat flow values for all time slices and wells.

Wells	Age [Ma]	0	1	5.5	6.5	7.1	8.25	9.2	9.5	10.6	11.7	12.7	14	15	15.5	16	17	ΔHF [mW/m²]
	Mg-6	60	62	70	70	70	70	70	70	90	90	160	160	160	160	160	160	
	Pg-5	50	52	60	70	80	80	80	80	80	100	150	150	150	150	115	100	
	Pg-6	50	52	60	70	80	80	80	80	80	100	150	150	150	150	115	100	
	Rak-1	40	55	60	65	65	65	65	65	65	65	65	65	65	65	65	65	
	Lipa-1	48	48	50	50	50	70	70	70	70	70	70	70	70	70	70	70	
	Dok-1	70	70	70	70	70	70	70	70	70	70	70	70	70	70	70	70	
	Ljut-1	55	58	70	70	70	70	70	70	70	70	70	70	70	70	70	70	
	Gb-1	52	55	70	70	70	70	70	70	70	70	70	70	70	70	70	70	
	Sre-1	67	62	60	60	65	65	65	65	65	65	65	65	65	65	65	65	
	Mrt-1	52	50	40	50	60	70	70	70	70	70	70	70	70	70	70	70	
	Dan-3	72	71	70	70	70	70	70	70	70	70	70	70	70	70	70	70	
	Pec-1	63	61	50	50	50	70	70	70	70	70	70	70	70	70	70	70	
	Pichla-1	60	60	60	70	70	70	70	70	70	70	100	120	170	200	230	250	
	Mureck-1	60	60	60	70	70	70	70	70	70	70	110	150	220	250	300	300	
	Radk.-2	50	50	50	50	50	50	50	50	50	50	100	120	150	200	450	500	
	Som-1	75	75	75	75	75	75	75	75	75	75	210	380	500	550	535	500	
	Benedikt-1	65	65	65	65	65	65	65	65	65	65	300	500	500	500	500	500	

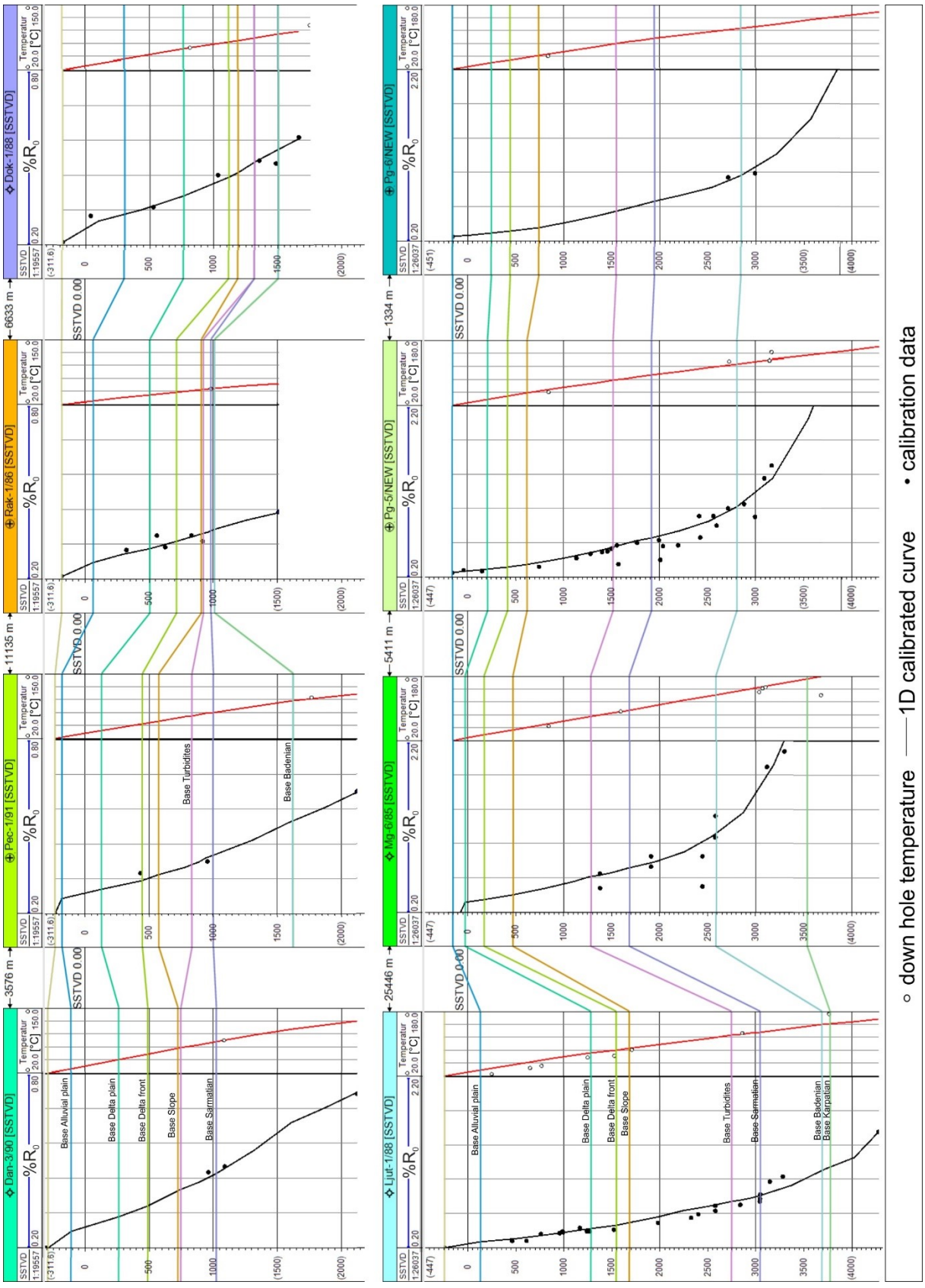

Figure 21 – Depth plots showing measured and calculated vitrinite reflectance (%Ro) and temperature data (1D-models).

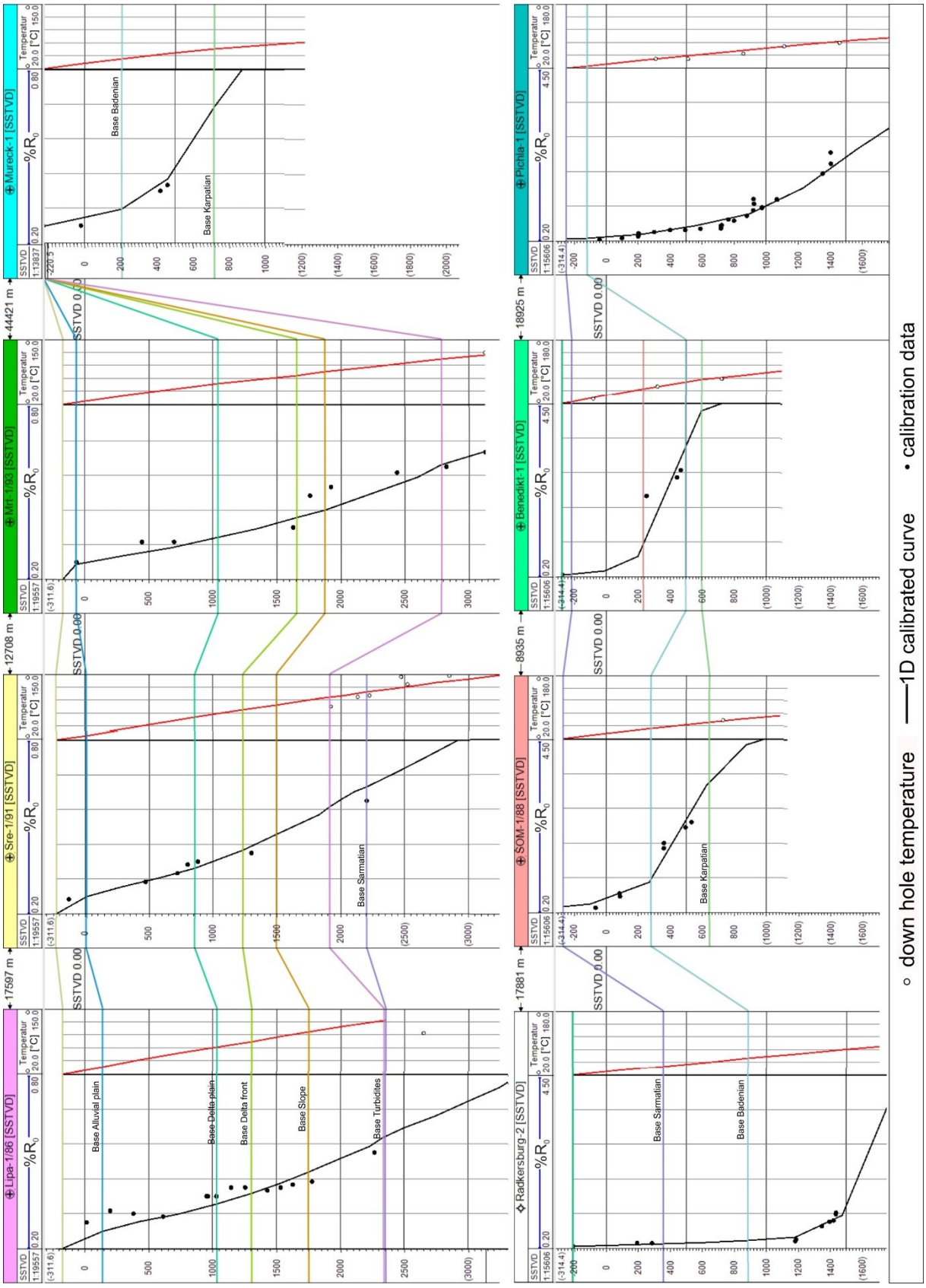

Figure 23 - Depth plots showing measured and calculated vitrinite reflectance (%Ro) and temperature data (1D-models).

4.3 3D model

4.3.1 Model Building

4.3.1.1 Model resolution – Simple Grid

It has to be noted, that this is a basin-scale model of the Mura-Zala Basin. The main purpose is to investigate its thermal evolution, the timing and amount of hydrocarbon generation, and the position of possible hydrocarbon accumulations. It, therefore, cannot be compared with a reservoir model, which uses much higher resolution in the vicinity of a proven single reservoir or prospect and relies on more precise and denser input data than this basin model does.

Different iterations of the model were calculated with different resolutions (cell thicknesses between 100 m and 5 m). The following dimensions were found to be practical regarding a compromise between necessary degree of accuracy and acceptable processing times:

Horizontal resolution: 250 m x 250 m

Vertical resolution (max. cell thickness):

Sandstone (reservoir layers):	20 m
Shale (source rock layers):	50 m
Marl (source rock layers):	50 m
Shale (seal layers):	100 m
Silt (overburden):	100 m
Conglomerate (overburden):	100 m

4.3.1.2 Stratigraphic horizons

Stratigraphic horizons of the Mura-Zala Basin were compiled by Dejan Šram using the JewelSuite of Baker Hughes (Šram et al., 2015). These horizons, kindly provided by the Geological Survey of Slovenia, formed the basis for the geometric model. The data was delivered as triangle meshes.

At first, the horizons were imported one by one into Petrel. To obtain further editable surfaces, the horizons were converted into point sets, consisting between about 10000 and 23000 points, depending on the irregularity of the horizon. Those points where then rejoined to form a new surface in Petrel by using Minimum Curvature interpolation, with influence radius set to ½ cell, interpolation set to average of points and point weighting set to inverse distance squared.

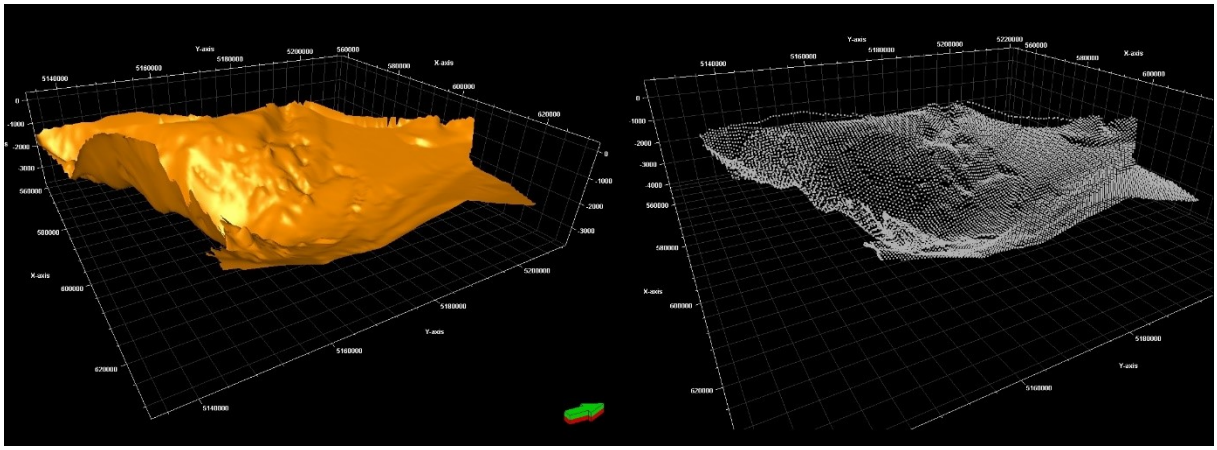

Figure 24 - On the left, the "Base turbidites" horizon as triangle mesh, on the right, the same horizon converted to points.

4.3.1.3 Extension into Austria, Hungary and Croatia

The boundaries of the horizons provided by Šram et al. (2015) are cut along the Slovenian border. Since political borders are not geological borders and considering, that relevant parts of the petroleum system may be located in the Austrian and Croatian parts of the basin, those parts needed to be added to the horizons. Accordingly, the missing parts were defined through polygons based on a Karpatian base map (Figure 25).

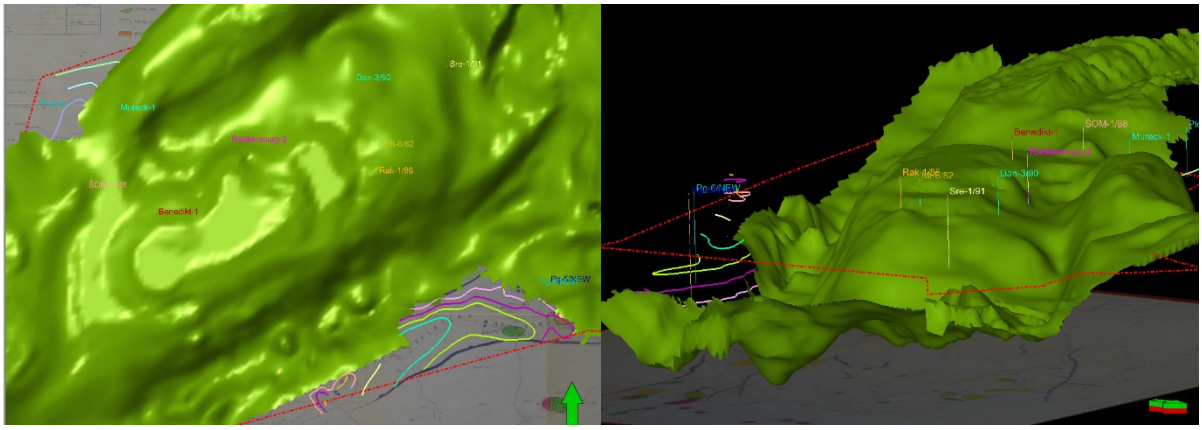

Figure 25 - Updating the horizons in Austrian and Croatian territory.

4.3.1.4 Model refinement Lendava area

For the purpose of this thesis, the area around the city of Lendava was not sufficiently defined. Published seismic profiles and schematic cross-sections (e.g. Figure 13, Figure 15) were georeferenced and used to model the Ormosko-Selnica-Anticline (Figure 26) which forms the structural traps for the Petisovci field in Slovenia, the Zebanec field in Croatia and the Lovaszi and Ujfalu field in Hungary. In addition, the two main faults that define the flower structure and the fault that separates the Petisovci field from the Lovaszi field where integrated in the model.

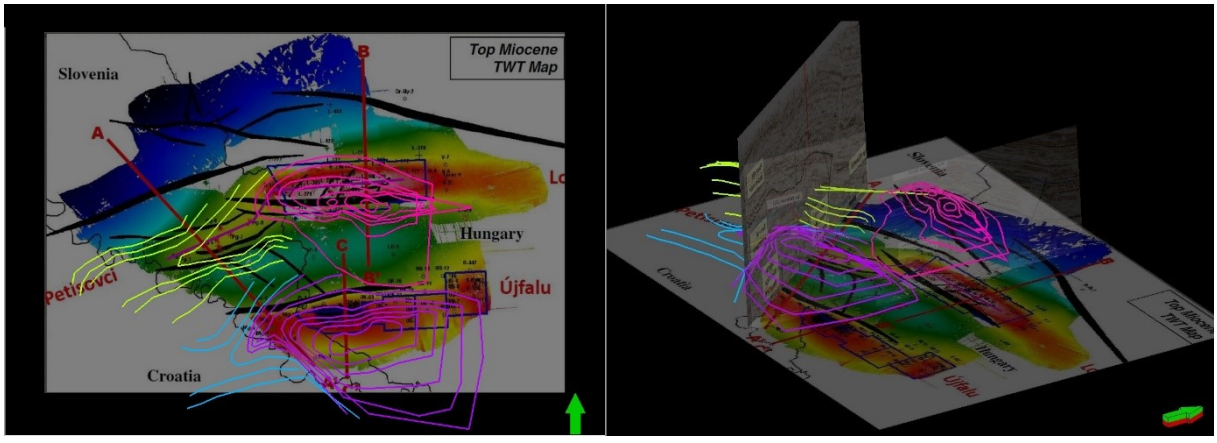

Figure 26 - Modelling of the folds accommodating the most important hydrocarbon reservoirs in Slovenia.

4.3.1.5 New model boundary

The horizons needed to be continuous throughout the whole model inside the newly chosen area of interest, shown in Figure 9, which now includes small parts of Austria, Hungary and Croatia as well. The imported horizons are only defined along their actual occurrence, so particular caution had to be taken where formations where pinching- or cropping out, so the

different horizons would not intersect randomly and create wrong information on its borders. Also, the area where the basement reaches the surface was excluded for this model.

4.3.1.6 QC and Artefacts

As a last step in modelling the geometry, a general QC of the horizons was carried out and several interpolation artefacts, which occurred for example along strongly varying gradients of slopes due to the algorithms used in the process of modeling the surfaces, were removed.

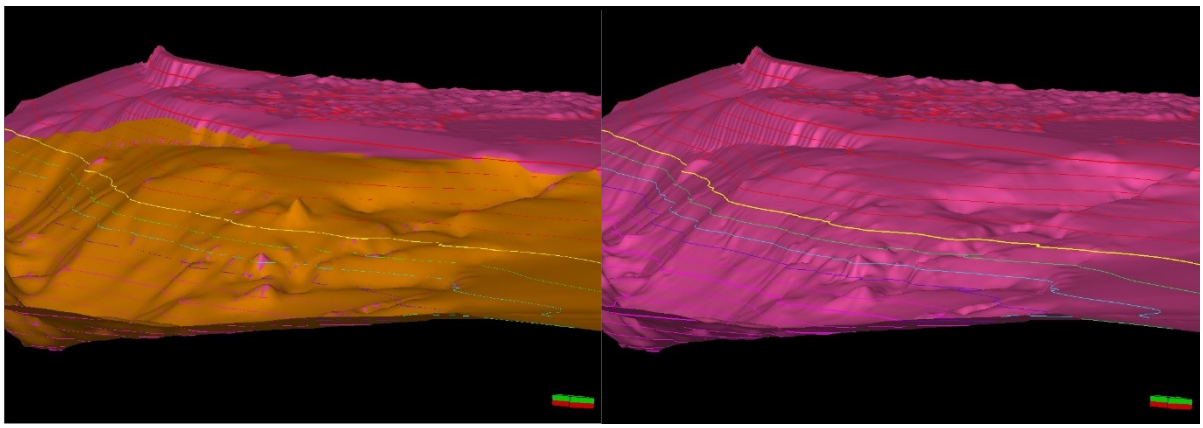

Figure 27 - Removing artifacts from the original surfaces (orange: original, pink: eddited).

4.3.2 Upscaling

In this model, three different properties were available for upscaling to the respective cell thickness.

- Hydrogen Index (HI)
- Total Organic Carbon (TOC)
- Lithology

For the sake of simplicity and due to minor impact of the slightly alternating lithology (see section “Sensitivity analysis”) the upscaling of the lithology was executed, but the results were not used in favor of using a simple layer cake model.

As described earlier, the source rock in this area is not particularly promising. To enhance the chance for noticeable generation, the upscaling for TOC as well as the HI were both done by a “Maximum” averaging method, which assigns every cell the highest discrete value found among its vertical extension.

4.3.3 Populating

The three properties mentioned above had to be distributed in the three dimensional space of the model. This was done by two different approaches for the different properties.

For TOC and HI, a Random Gaussian Simulation was used. Further, the S1 and S2 values were populated in the same fashion.

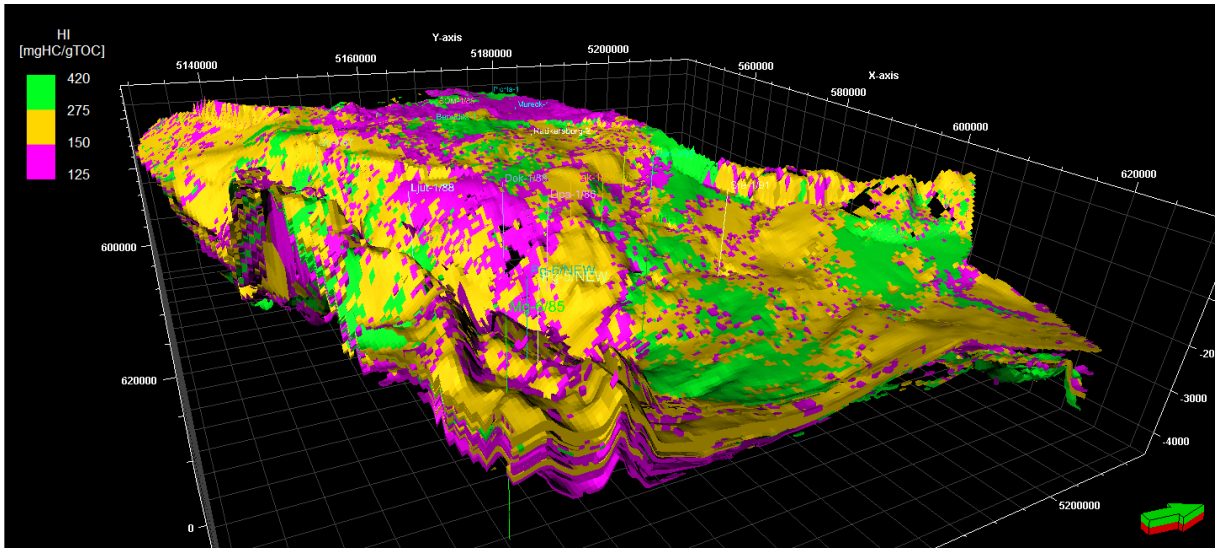

Figure 28 - Populated source rock distribution, filtered for TOC values over 0.5% and with a HI of at least 125

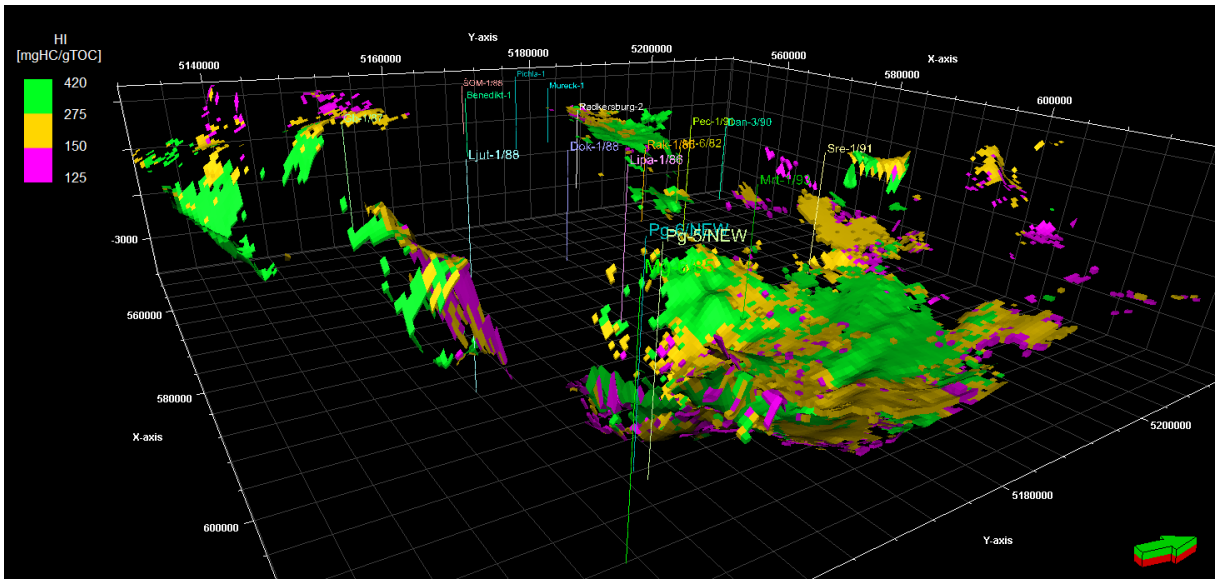

Figure 29 - Source rock distribution, filtered by "fair" or better source rock potential; S1 >0.5, S2 > 2.5, TOC >0.5%

For the lithology, a very rudimental approach was used. Consequently to the sparse information about the lithology, a population “by zone” was chosen. The formations were subdivided in percentages of sand, marl, shale, silt and conglomerate in the same fashion as it was done in the 1D models (Table 2). Additionally those percentage layers were split into multiple sequences of thinner sand/shale/sand/shale packages, to give a better representation of narrowly layered multiple reservoir horizons rather than one very thick layer of e.g. reservoir sandstone with a thickness of more than a hundred meters. The result can be seen in Figure 30 and Figure 31.

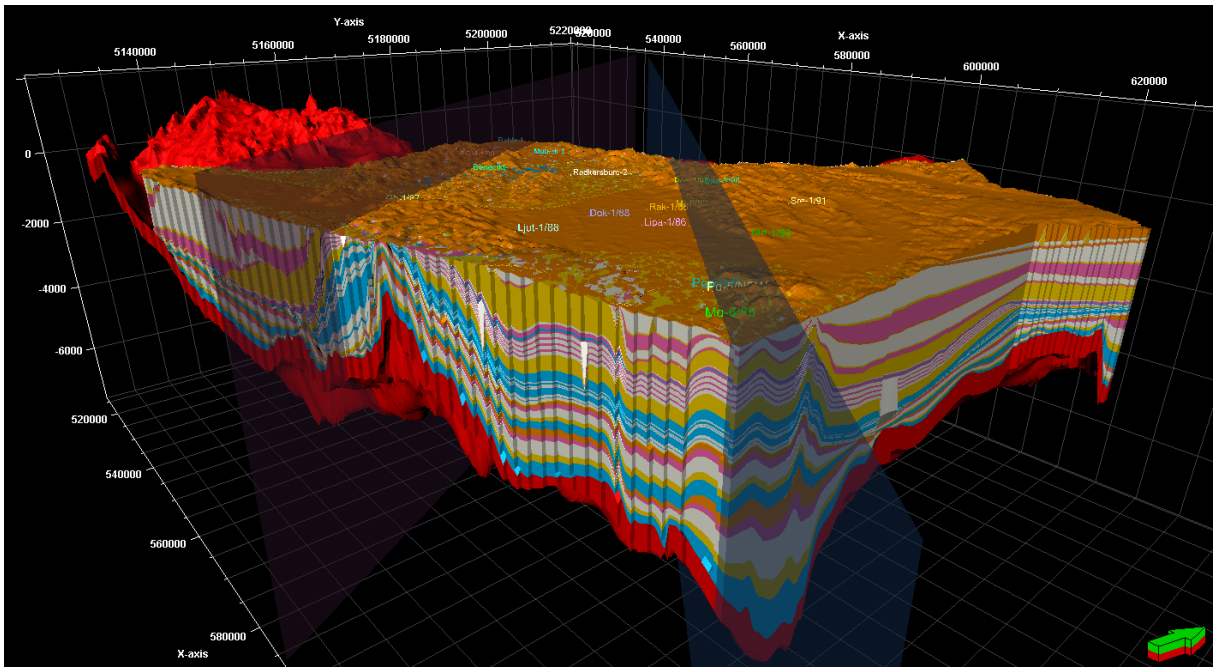

Figure 30 - Model with populated facies, including the locations of cross section A-A' and D-D'

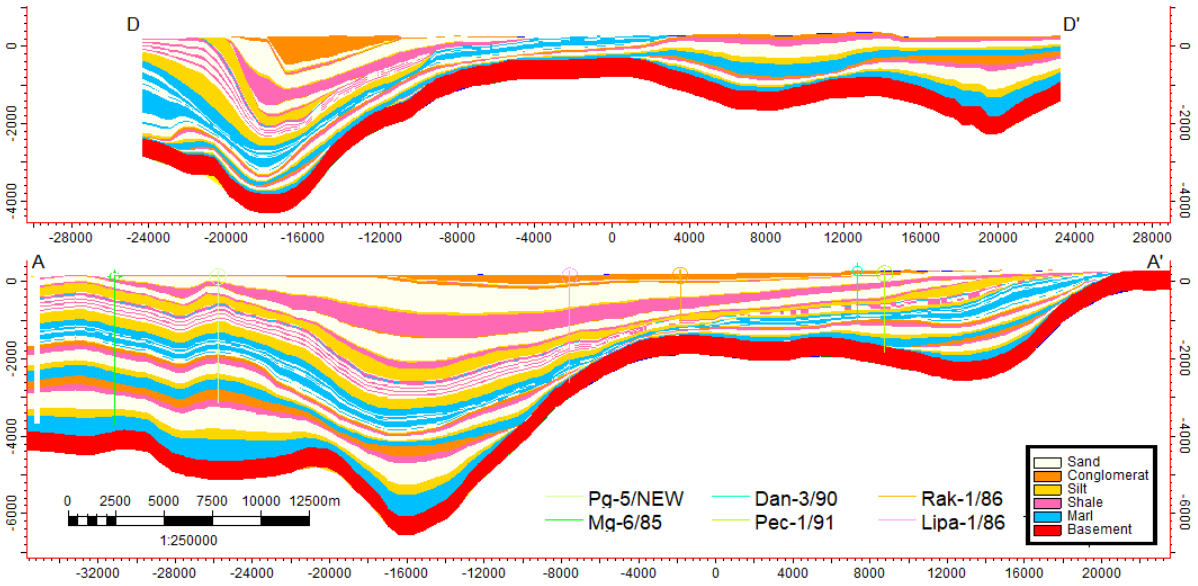

Figure 31 - Cross sections A-A' and D-D', showing the facies distribution

4.4 Petroleum System Model

To convert the 3D model to a petroleum system model, the Simple Grid has to be connected to the following objects:

- A facies table
- A chronostratigraphy
- A fault history (optional)

For the facies table, the "5 facies" definition, already used for the 1D model (Figure 20) was used. The same goes for the chronostratigraphy (Figure 18) which was also defined earlier

within the 1D modelling process. The events had to be connected to the corresponding horizons (Figure 32).

Event	Age [Ma]	Horizon				
Period			Facies	Kinetic	TOC [%]	HI [mgHC/gTOC]
Topographie	0.00	Topographie				
Ptuj-Grad Fm.			From Property '5_facies'	From Property '5_facies'	From Property 'TOC'	From Property 'HI'
Base Aluvial Plain	5.50	Base Alluvial Plain				
Mura Fm.			From Property '5_facies'	From Property '5_facies'	From Property 'TOC'	From Property 'HI'
Base Delta Plain	6.50	Base Delta Plain N				
Mura Fm. (Delta Front)			From Property '5_facies'	From Property '5_facies'	From Property 'TOC'	From Property 'HI'
Base Delta Front	7.10	Base Delta Front N				
Lendava Fm.			From Property '5_facies'	From Property '5_facies'	From Property 'TOC'	From Property 'HI'
Base Slope	8.25	Base Slope				
Lendava Turbidites (80%)			From Property '5_facies'	From Property '5_facies'	From Property 'TOC'	From Property 'HI'
Base Turbidites 1	9.20	17				
Lendava Fm. (Turbidites 20%			From Property '5_facies'	From Property '5_facies'	From Property 'TOC'	From Property 'HI'
Base Turbidites 2	9.50	Base Turbidites				
Spilje - Sarmat 1			From Property '5_facies'	From Property '5_facies'	From Property 'TOC'	From Property 'HI'
Base Sarmat 1	10.60	Base_Sarmat_1				
Spilje - Sarmat 2			From Property '5_facies'	From Property '5_facies'	From Property 'TOC'	From Property 'HI'
Base Sarmat 2	11.70	Base_Sarmat_2				
Spilje - Sarmat 3			From Property '5_facies'	From Property '5_facies'	From Property 'TOC'	From Property 'HI'
Base Sarmat 3	12.70	Base Samart				
Spilje Fm. (Badenian)			From Property '5_facies'	From Property '5_facies'	From Property 'TOC'	From Property 'HI'
Base Badenian	15.50	Base Badenian				
Haloze Fm.			From Property '5_facies'	From Property '5_facies'	From Property 'TOC'	From Property 'HI'
Base Karpatian	17.20	Base Kapart				
Basement			From Property '5_facies'	From Property '5_facies'	From Property 'TOC'	From Property 'HI'
Basement	30.00	Base Basement				

Figure 32 – Property assignment for the petroleum system

In addition, assignments for the properties **facies**, **TOC** and **HI** had to be made. Here different approaches have been applied. For all three models, the lithology distribution described earlier was used.

- The first model was assigned with the populated values for TOC and HI from the upscaled well logs, but later filtered to take only "fair" source rocks (HI ≥125 mg HC/g TOC and TOC ≥0.5%) into account, setting all cells to zero that did not meet the requirements.
- The second model was modified in a similar way as the first one, but the threshold for the hydrogen index was lowered to HI ≥ 25 mg HC/g TOC, while keeping the 0.5% TOC threshold.
- In the third model, every shale and marl cell was assigned with a HI of 500 and a TOC of 10%. These (unrealistic) high values were used to test the influence of an excellent source rock on the migration/accumulation behavior.

4.4.1 Erosion

Post-Miocene erosion occurred in different parts of the basin, which also influenced the thermal evolution of rock layers. The erosion was mainly driven by extrusion through post Pontian compressional tectonics (Horváth et al., 2015). The amount of erosion was calibrated by the 1D models. It occurred in the very south east of the basin along the Donat Fault (Figure 33b) and in the northwest, in the vicinity of the Kozjak- and Pohorje Block (Figure 33a). In the southeast, parts of the Putj-Grad Formation were eroded, with thickness up to 900 m, while in the northwest, sedimentation was stagnating since Badenian times, which led to erosion of parts of the Spilje Formation within the last 5 million years. Erosion cannot be modeled in Petrel, so the

model was exported to PetroMod for the refinement process. For this purpose, erosion maps had to be created and assigned to the corresponding time periods. To reconstruct paleogeometry and erosion, events were created to last for 3 Ma, starting at 5.5 Ma, which was identified as time of full deposition (Figure 34-Figure 37).

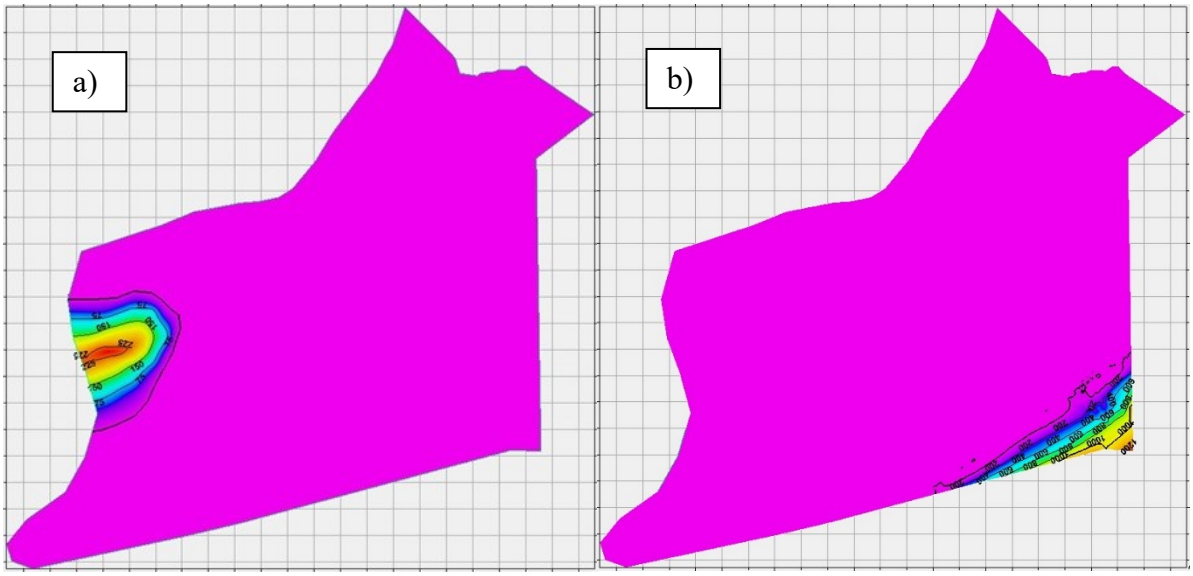

Figure 33 - Erosion during the last 5 Ma; on a) the eroded thickness of the Spilje Fm. is shown. On b) the eroded thickness of the Ptuj-Grad Fm. can be seen.

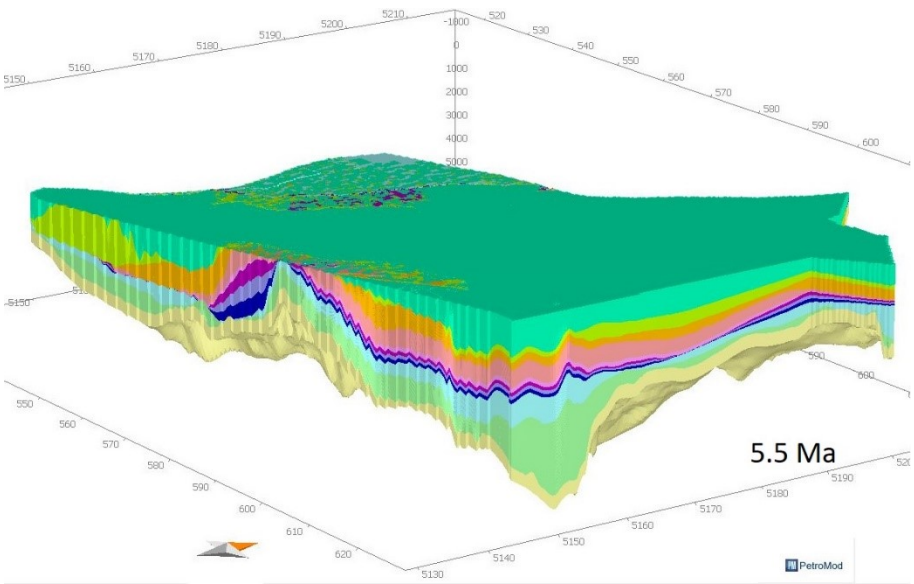

Figure 34 - The top greenish layer shows the thickness of the Mura Formation at the time of full deposition

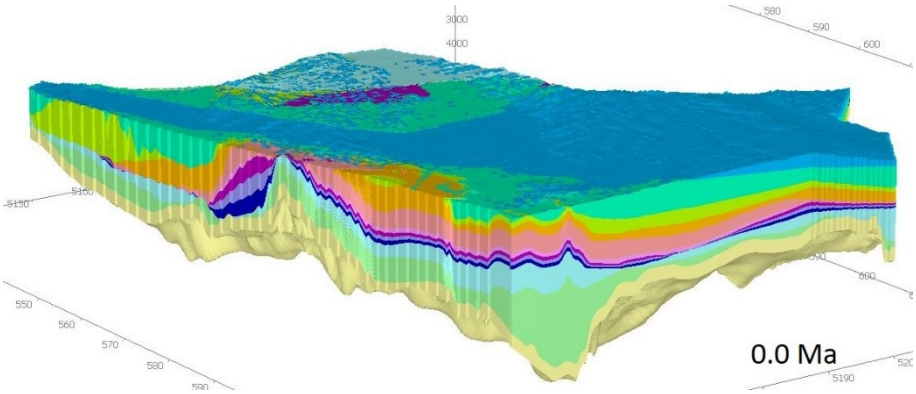

Figure 35 - Basin architecture at present day, with the south-eastern part of the Mura Formation eroded

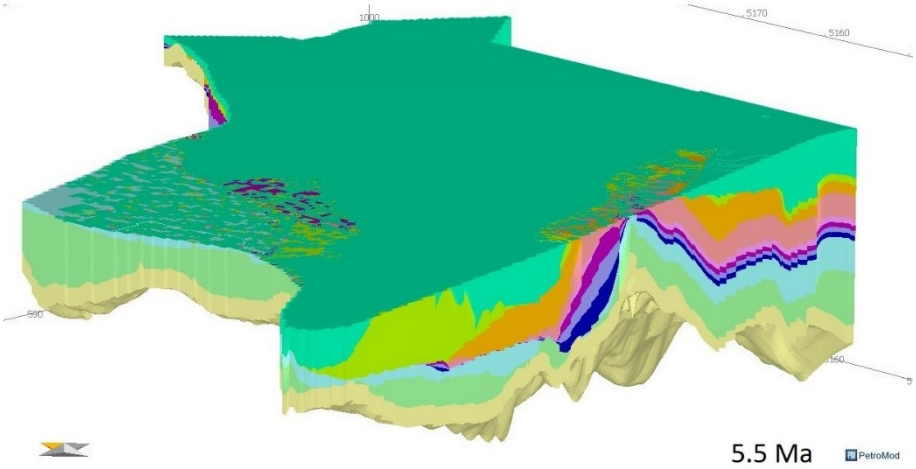

Figure 36 – Basin structure at 5.5 Ma. Note that the light blue layer (Spilje Formation) is still present in the NE of the model

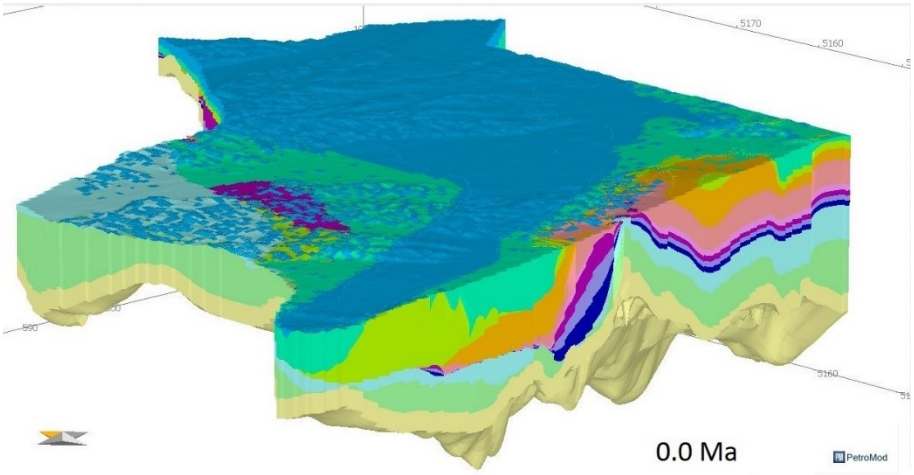

Figure 37 - Until today, the Spilje Formation in this part of the basin was fully eroded

5 Simulation

To be able to run a 3D PSM, boundary conditions have to be defined. In contrast to a 1D PSM, point information has to be expanded to maps. The simulator used is the Hermes Simulator (©Schlumberger) that is embedded in the PetroMod 3D software package. Beside the boundary conditions, the simulator options have to be chosen.

5.1 Simulator options

5.1.1 Run control

The run control offers different options for the simulation of the temperature and pressure histories. Regarding temperature, it is possible to choose between "multi 1D temperature", which calculates in 1 dimension only, and "2D/3D temperature". "Multi 1D temperature" saves calculation time, but neglects lateral heat transport. In contrast, "2D/3D temperature" provides a full 2D/3D temperature calculation and much more accurate results. Therefore, this option was used for the simulations.

For pressure calculation "2D/3D pressure run" is available, which enables the calculation of overpressure. Alternatively a "hydrostatic pressure run" can be applied, considering pore pressure equals hydrostatic pressure. For the needs and amount of information available in this model, the hydrostatic pressure run was sufficient.

5.2 Boundary Conditions

5.2.1 Heat flow

Moving from point information (1D mode) to the 3D space, the heat flow information for each borehole had to be converted into heat flow maps for every time slice. For this, different interpolating algorithms are available in the software, each one resulting in a different spatial distribution, but all honoring the input data. For the distribution of the data in this thesis, Kriging was used as the algorithm of choice, because it is considered the best unbiased linear estimator (Matheron, 1962). Moreover, for areas without data, the results are biased towards the mean, what for most scenarios in the heat flow distribution seems a good guess. To honor the basin geometry, collocated Co-Kriging (Matheron, 1962) was applied, using the basin geometry (water depth) at each time slice as secondary variable, with a correlation coefficient of 0.6. This means that if a high heat flow has been observed in a structural low and a low heat flow in a structural high, the software assume elevated heat flows also in depression without heat flow information. This approach prevents isolines from boldly crossing geological structures. The range for correlation of data points in the Kriging algorithm was chosen with 23 km in either direction. An example in the difference of using kriging, co-kriging and convergent interpolation, which is a control point oriented algorithm that retains trends in areas with little data, while honoring details in areas where data exists (Schlumberger, 2015) is shown below (Figure 38).

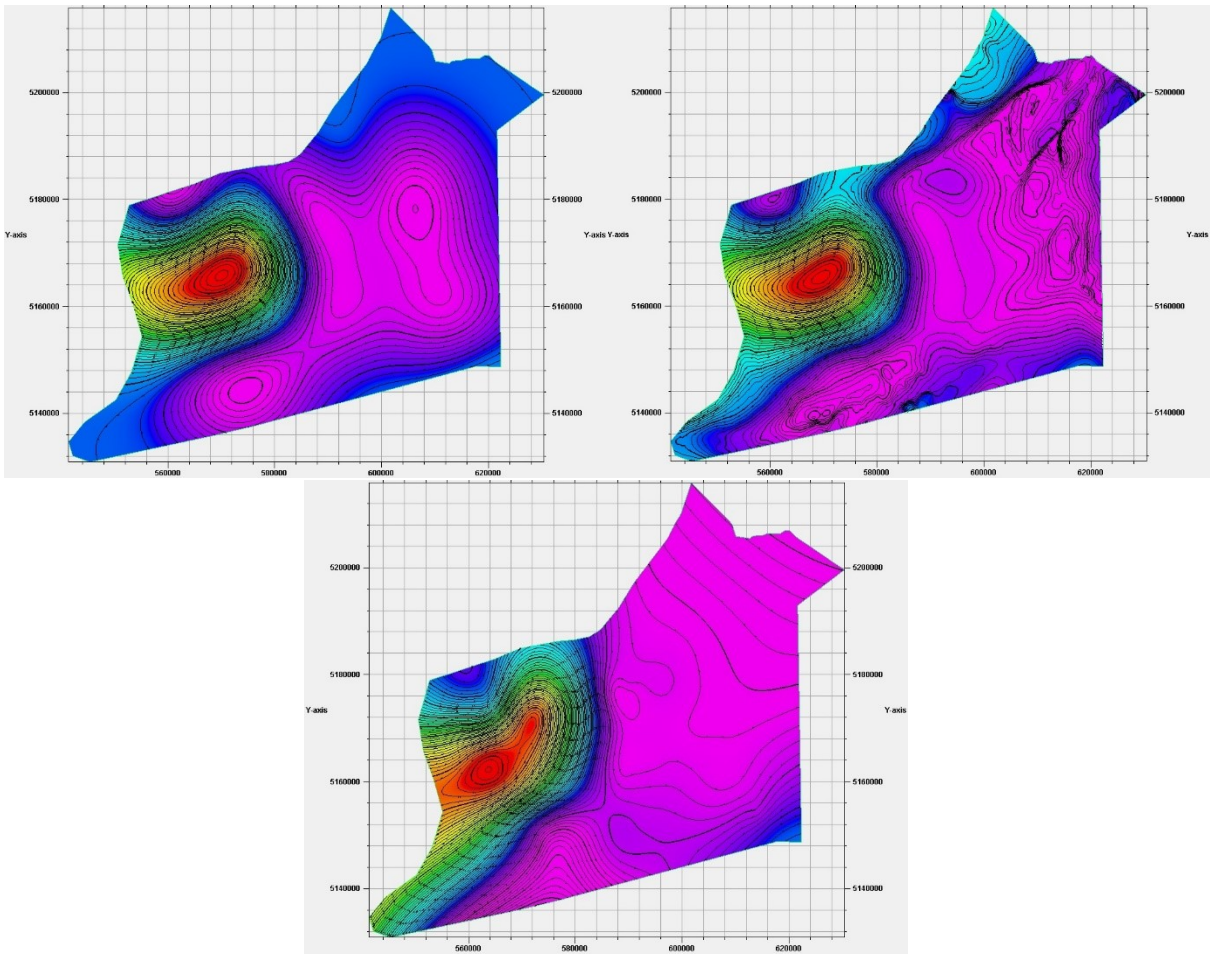

Figure 38 – Heat flow at 17.2 Ma interpolated by conventional kriging (top left), co-kriging (top right) and convergent interpolation (bottom). It is visible, that conventional krigig and co-kriging show an overall simmilar appearance, where co-kriging also resambles the basin structure to a certain degree. Convergent interpolation is trend oriented and only data point driven, letting e. g. the north-east of the basin with very little data look like a staircase.

5.2.2 PWD (Paleo water depth)

Paleo water depth describes the mean water depth at a certain location at a certain time in history. It influences the basin geometry and is also necessary to use estimate the sediment water interface temperature (Figure 39). The PWD maps used in this simulation were based on data applied by Hasenhüttl et al. (2001) for their 1D models. Convergent interpolation was used for the interpolation.

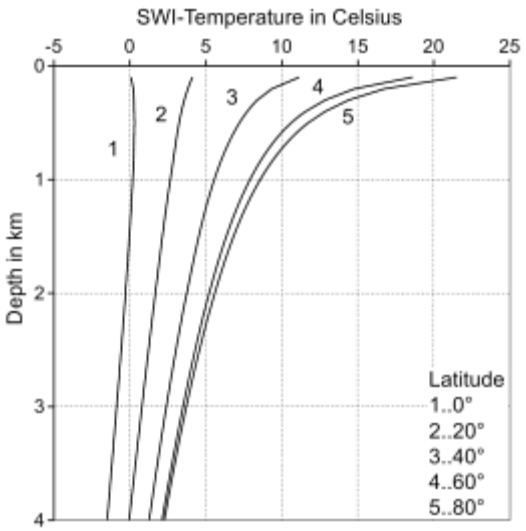

Figure 39 - Present day sediment-water-interface curves dependent on latitude and depth (Beardsmore and Cull, 2001)

5.2.3 SWIT (Sediment Water Interface Temperature)

The sediment water-interface temperature (SWIT) is the upper boundary of the heat flow problem, while the basal heat flow is the lower one. According to the heat conductivity law, the temperature difference between two locations causes the heat flow q (Hantschel and Kauerauf, 2009). For this model the function "Auto SWIT" was used, determining the SWIT by using the Global Mean Surface Temperature as suggested by Wygrala (1989) and taking the PWD into account.

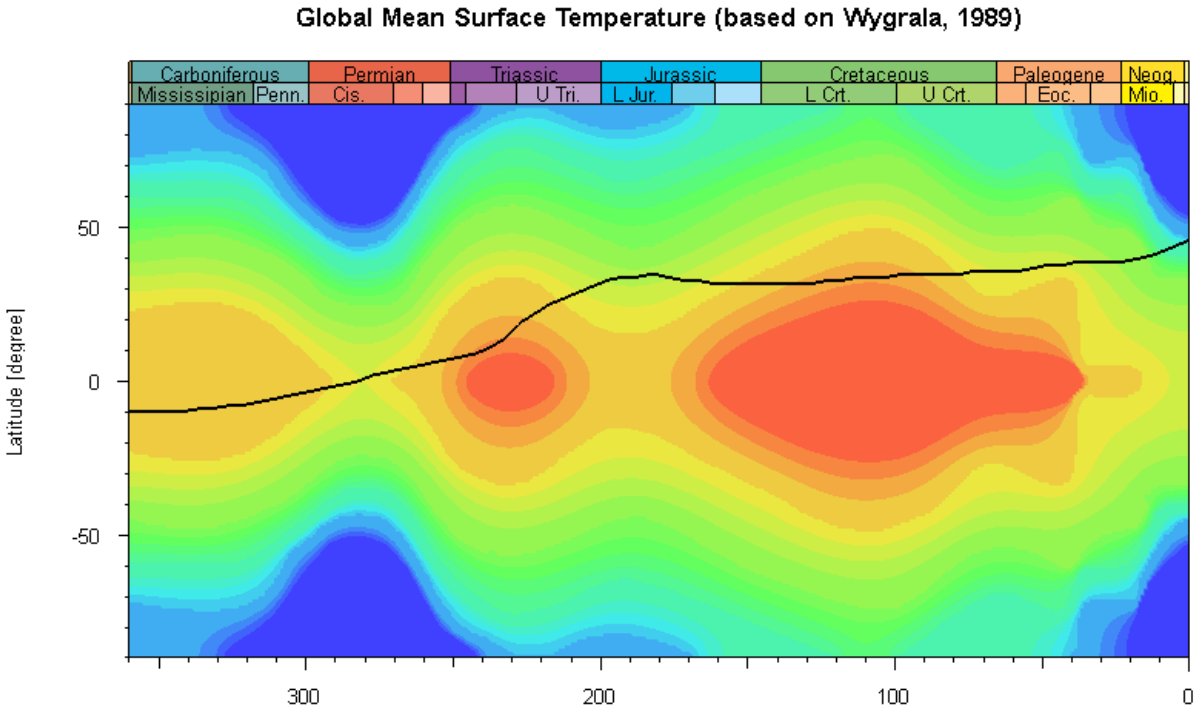

Figure 40 - Paleo-surface temperatures by Wygrala (1989). The black line shows the location 33°N through time.

5.3 Calibration Process

Moving from 1D to 3D in thermal modeling, implies that heat can now not only come from the base of the model and the lithology itself (i.e. radiogenic heat production) or can only escape in one direction through the surface, but that every cell in the model radiates heat into every neighboring cell or receives heat from it. That means that the heat flow in the neighborhood has a big impact on the temperatures reached in every cell. Therefore, it was likely that the calibrated heat flows from the 1D models would not result in a good fit with calibration data in the 3D model. Additionally, due to the use of co-kriging, the change of heat flow in one point of the model can influence the heat flow distribution on the very other end of the model. This led to a partly significant change from the 1D heat flows to the heat flows in the 3D model. The differences between heat flows in the 3D and 1D models are shown in Table 4 (compare Tables 2 and 4).

Table 4 -Heat flow difference between the calibrated 1D models and the calibrated 3D model (1D - 3D).

Wells	Age [Ma]	0	1	5.5	6.5	7.1	8.25	9.2	9.5	10.6	11.7	12.7	14	15	15.5	16	17	ΔHF [mW/m²]
	Mg-6	0	0	0	0	0	0	0	0	0	0	0	0	0	0	0	0	
	Pg-5	0	0	0	0	0	0	0	0	0	0	0	0	0	0	0	0	
	Pg-6	0	0	0	0	0	0	0	0	0	0	0	0	0	0	0	0	
	Rak-1	-10	0	0	0	0	0	0	0	0	0	0	0	0	0	0	0	
	Lipa-1	-5	-5	-5	-3	-3	0	0	0	0	0	0	0	0	0	0	0	
	Dok-1	-5	-5	-5	-5	-5	-5	-5	-5	-5	-5	-5	-5	-5	-5	-5	-5	
	Ljut-1	0	3	15	15	15	15	15	15	15	-30	-30	-30	-30	-30	-30	-30	
	Gb-1	0	0	0	0	0	0	0	0	0	0	0	0	0	0	0	0	
	Mrt-1	0	0	0	0	0	0	0	0	0	0	0	0	0	0	0	0	
	Som-1	0	0	0	0	0	10	10	10	10	10	10	10	10	10	10	10	
	Dan-3	0	0	0	0	0	0	0	0	0	0	0	0	0	0	0	0	
	Pec-1	0	0	0	0	0	10	10	10	10	10	10	10	0	0	0	0	
	Pichla-1	0	0	0	0	0	0	0	0	0	0	20	40	40	40	15	-10	
	Mureck-1	0	0	0	0	0	0	0	0	0	0	30	30	60	50	80	80	
	Radk.-2	0	0	0	0	0	0	0	0	0	0	0	0	0	25	-30	-30	
	Som-1	0	0	0	0	0	0	0	0	0	0	0	30	10	50	35	0	
	Benedikt-1	0	0	0	0	0	0	0	0	0	0	0	-100	-100	-100	-100	-100	

6 Simulation Results

6.1 Calibrated heat flow 3D

6.1.1 Heat flow 0 Ma – 17.2 Ma

6.1.1.1 Synthetic well log fit

Like in the 1D model, the simulated calibration data was fitted to the measured data. For this purpose, synthetic well logs through the calculated attribute "Sweeney&Burnham(1990)_EASY%Ro" were created at the well locations. The best fit is presented beneath (Figure 41 & Figure 42). In , the heat flow values through time for the 3D calibrated model are listed.

Table 5 - Heat flow values for the 3D calibrated model

Wells	Age [Ma]	0	1	5.5	6.5	7.1	8.25	9.2	9.5	10.6	11.7	12.7	14	15	15.5	16	17	ΔHF [mW/m²]
	Mg-6	60	62	70	70	70	70	70	70	90	90	160	160	160	160	160	160	
	Pg-5	50	52	60	70	80	80	80	80	80	100	150	150	150	150	115	100	
	Pg-6	50	52	60	70	80	80	80	80	80	100	150	150	150	150	115	100	
	Rak-1	40	55	60	65	65	65	65	65	65	65	65	65	65	65	65	65	
	Lipa-1	53	53	53	53	53	70	70	70	70	70	70	70	70	70	70	70	
	Dok-1	75	75	75	75	75	75	75	75	75	75	75	75	75	75	75	75	
	Ljut-1	55	55	55	55	55	55	55	55	55	100	100	100	100	100	100	100	
	Gb-1	52	55	70	70	70	70	70	70	70	70	70	70	70	70	70	70	
	Sre-1	67	62	60	60	65	65	65	65	65	65	65	65	65	65	65	65	
	Mrt-1	52	50	40	50	60	60	60	60	60	60	60	60	60	60	60	60	
	Dan-3	72	71	70	70	70	70	70	70	70	70	70	70	70	70	70	70	
	Pec-1	63	61	50	50	50	60	60	60	60	60	60	60	70	70	70	70	
	Pichla-1	60	60	60	70	70	70	70	70	70	70	80	80	130	160	215	260	
	Mureck-1	60	60	60	70	70	70	70	70	70	70	80	120	160	200	220	220	
	Radk.-2	50	50	50	50	50	50	50	50	50	50	100	120	150	175	480	530	
	Som-1	75	75	75	75	75	75	75	75	75	75	210	350	490	500	500	500	
	Benedikt-1	65	65	65	65	65	65	65	65	65	65	300	600	600	600	600	600	

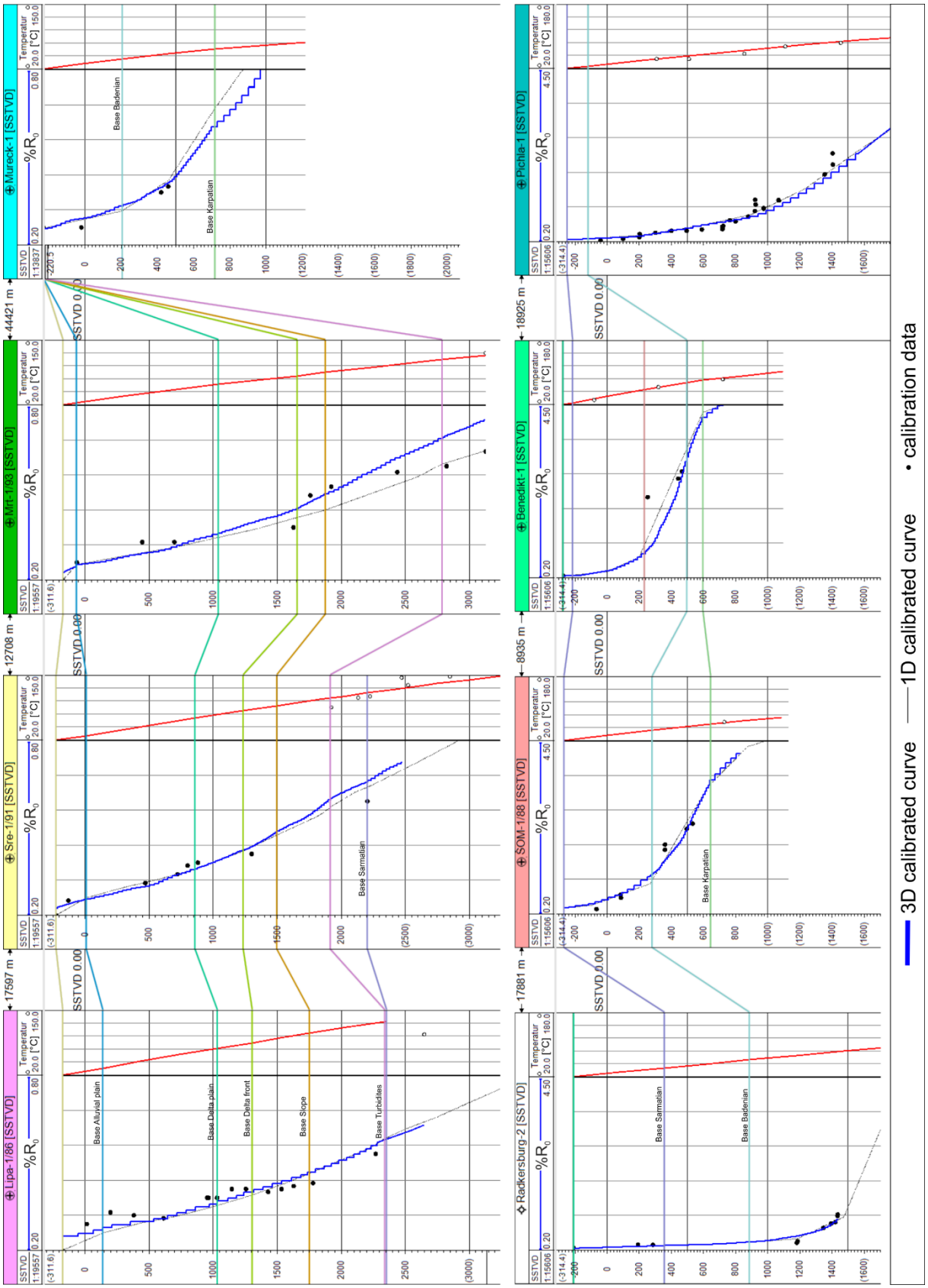

Figure 41 – Calculated and measured calibration data (%R_0; formation temperature) from the 3D model, extracted through synthetic well logs.

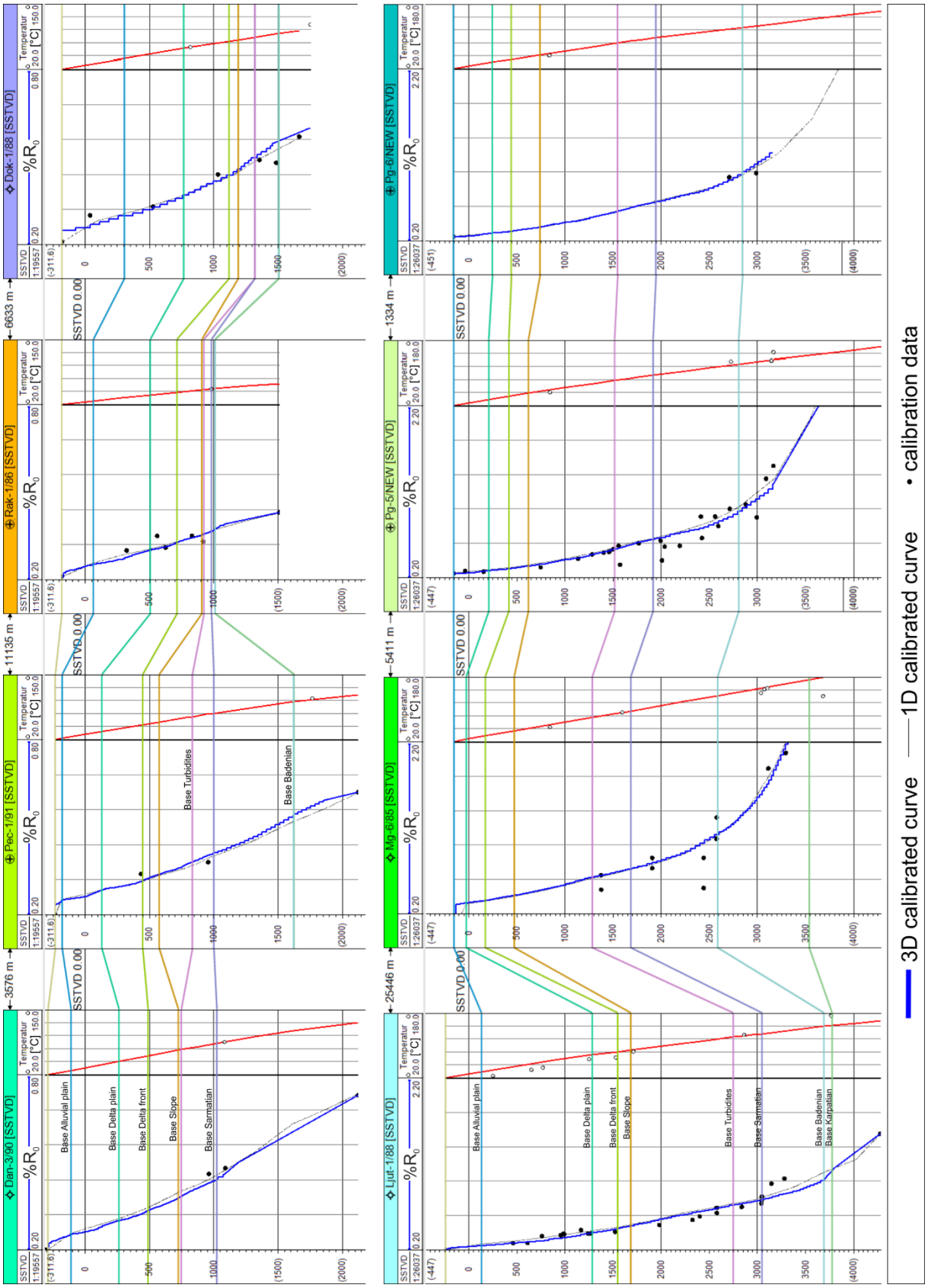

Figure 42 - Calculated and measured calibration data (%R_0; formation temperature) from the 3D model, extracted through synthetic well logs.

6.1.1.2 *Heat flow maps*

The heat flow maps, which led to the fit displayed in Figure 41 and Figure 42 are shown in the following (Figure 43 - Figure 49). Strongly elevated heat flow can be observed between 17.2 Ma and 12.7 Ma in the south-east and the north-west of the model, probably connected to volcanism and plutonism (Sachsenhofer et al., 1998; Pamic & Pécskay, 1996; see 8).

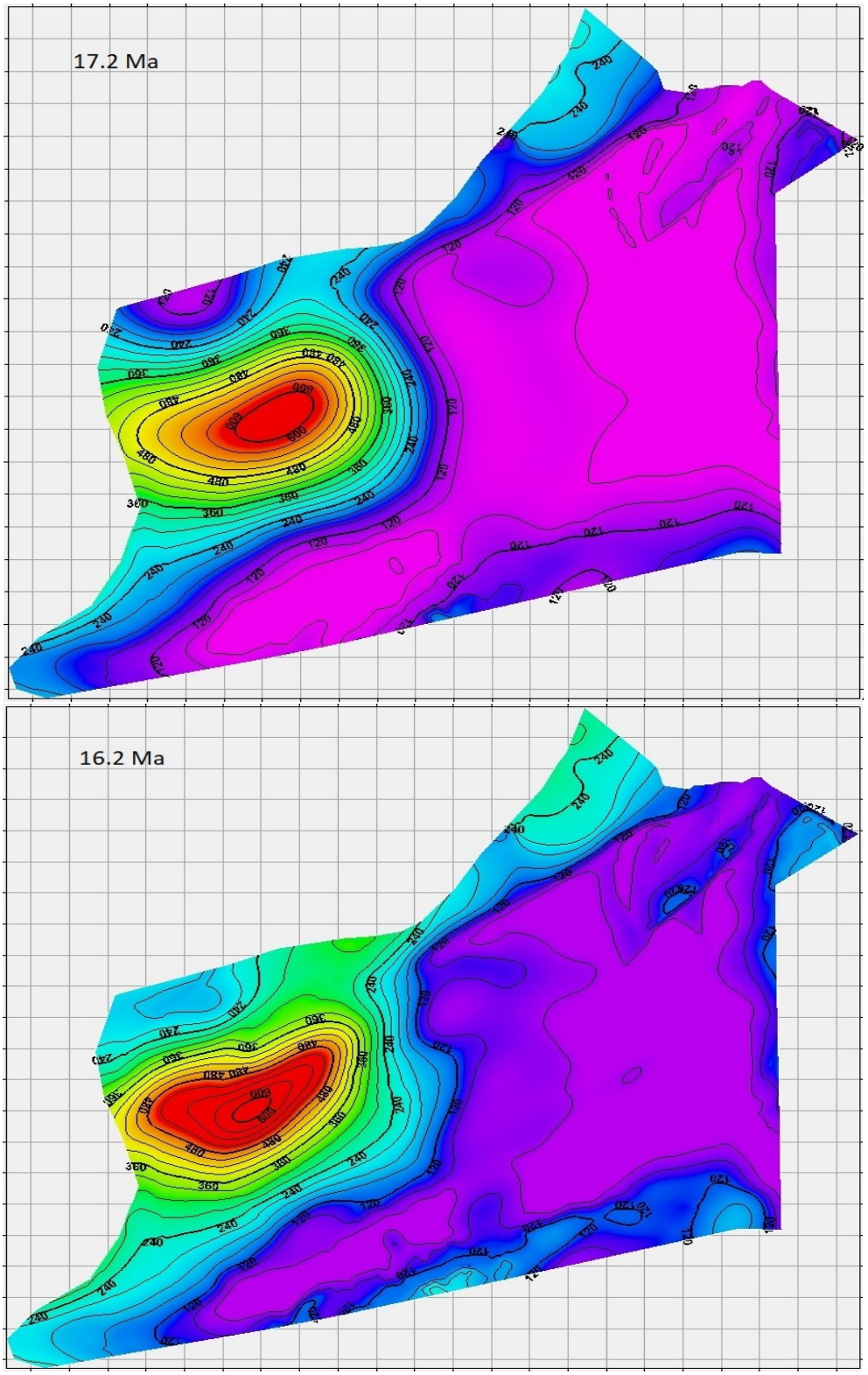

Figure 43 - Heatflow distribution in the basin at 17.2 Ma and 16.2 Ma.

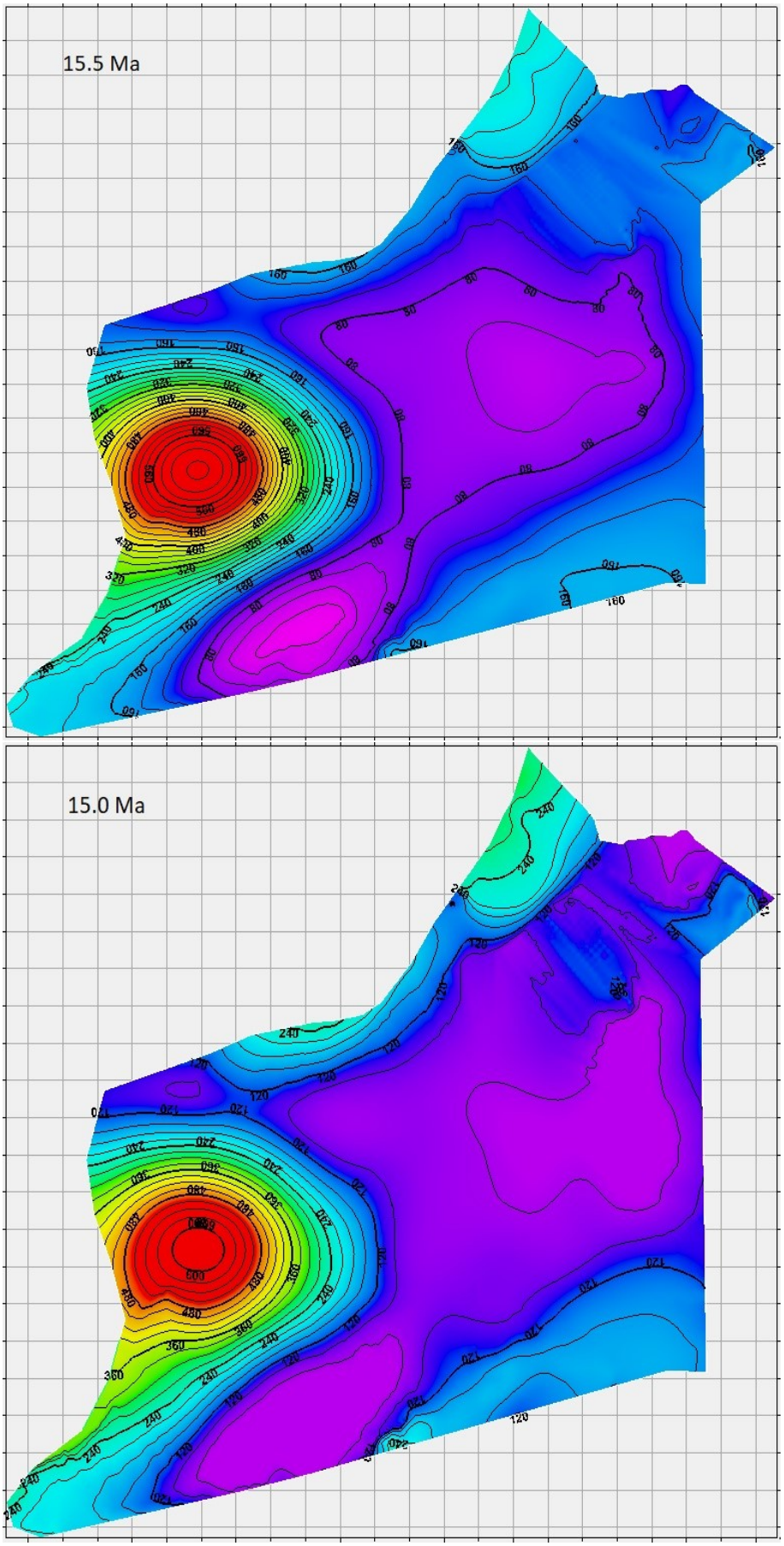

Figure 44 - Heatflow distribution in the basin at 15.5 Ma and 15.0 Ma.

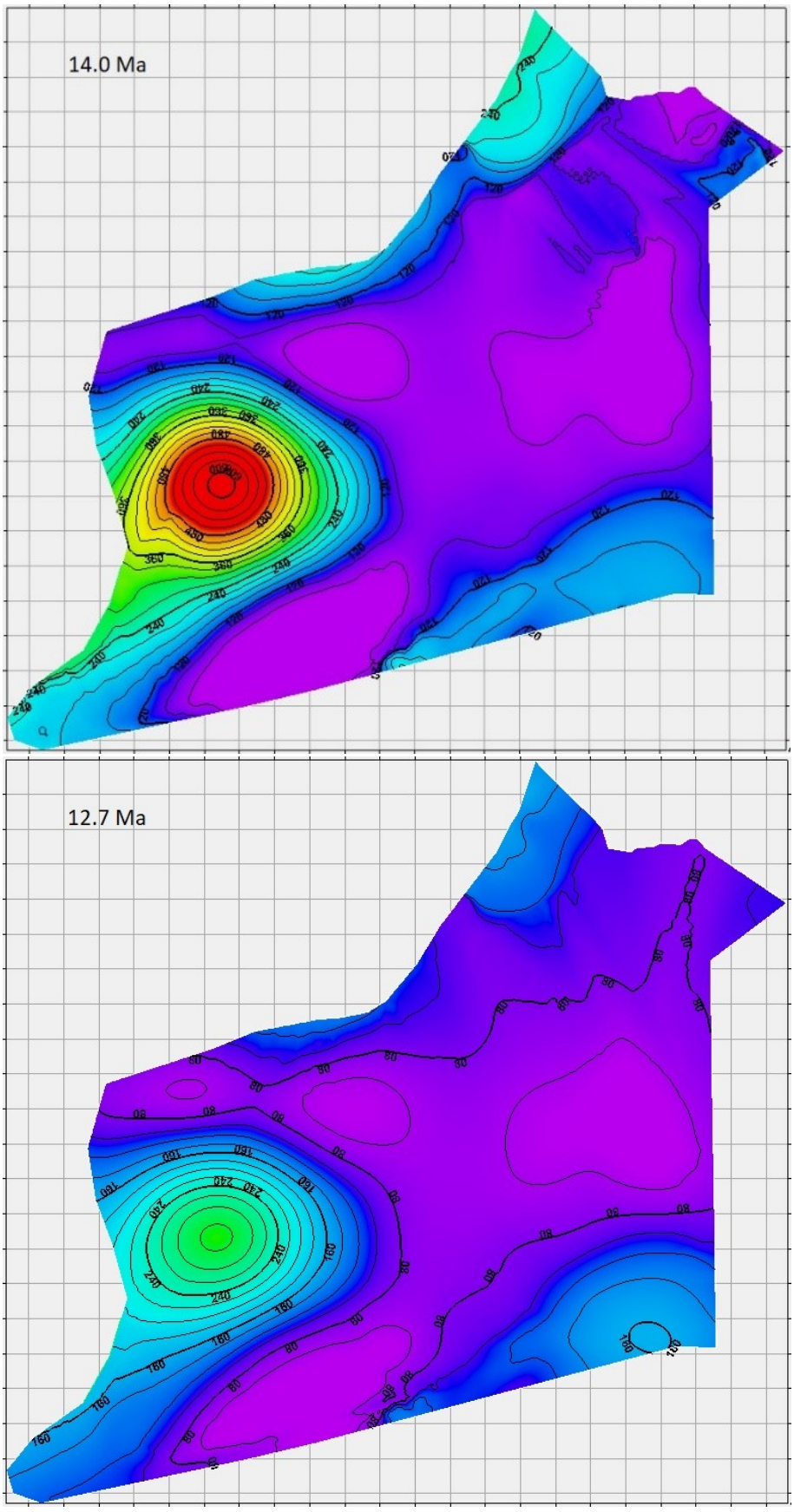

Figure 45 - Heatflow distribution in the basin at 14.0 Ma and 12.7 Ma.

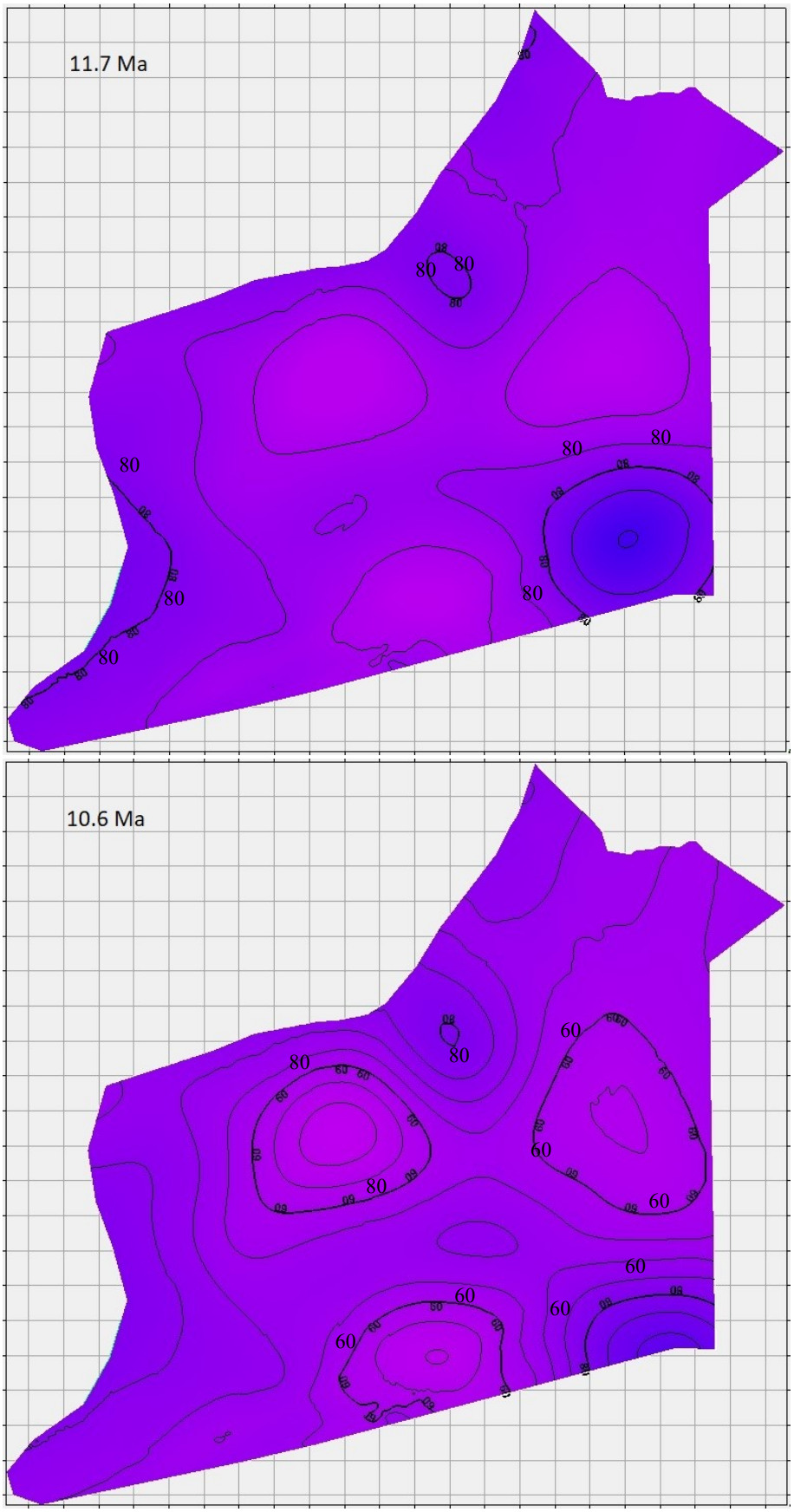

Figure 46 - Heatflow distribution in the basin at 11.7 Ma and 10.6 Ma.

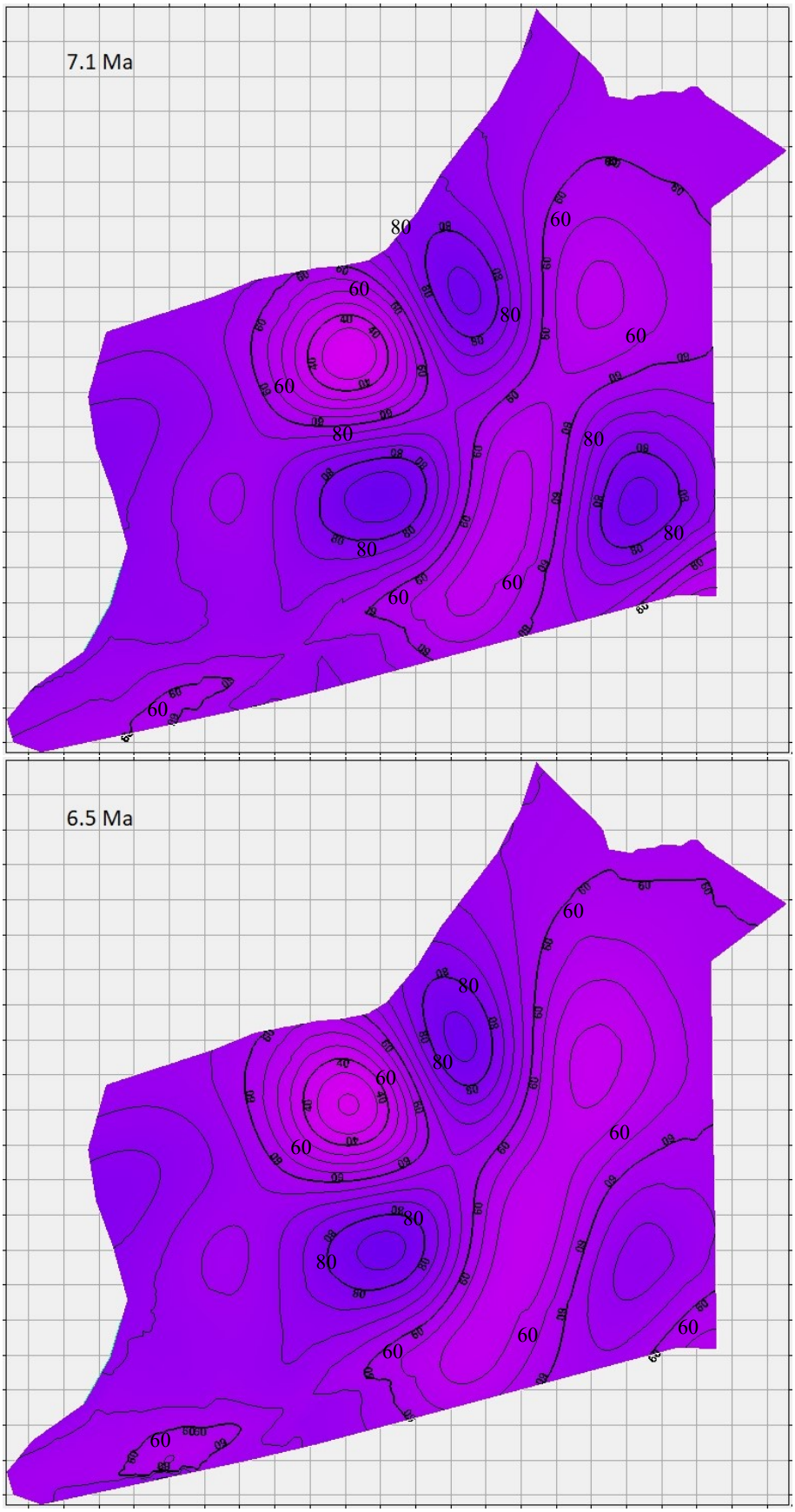

Figure 47 - Heatflow distribution in the basin at 7.1 Ma and 6.5 Ma.

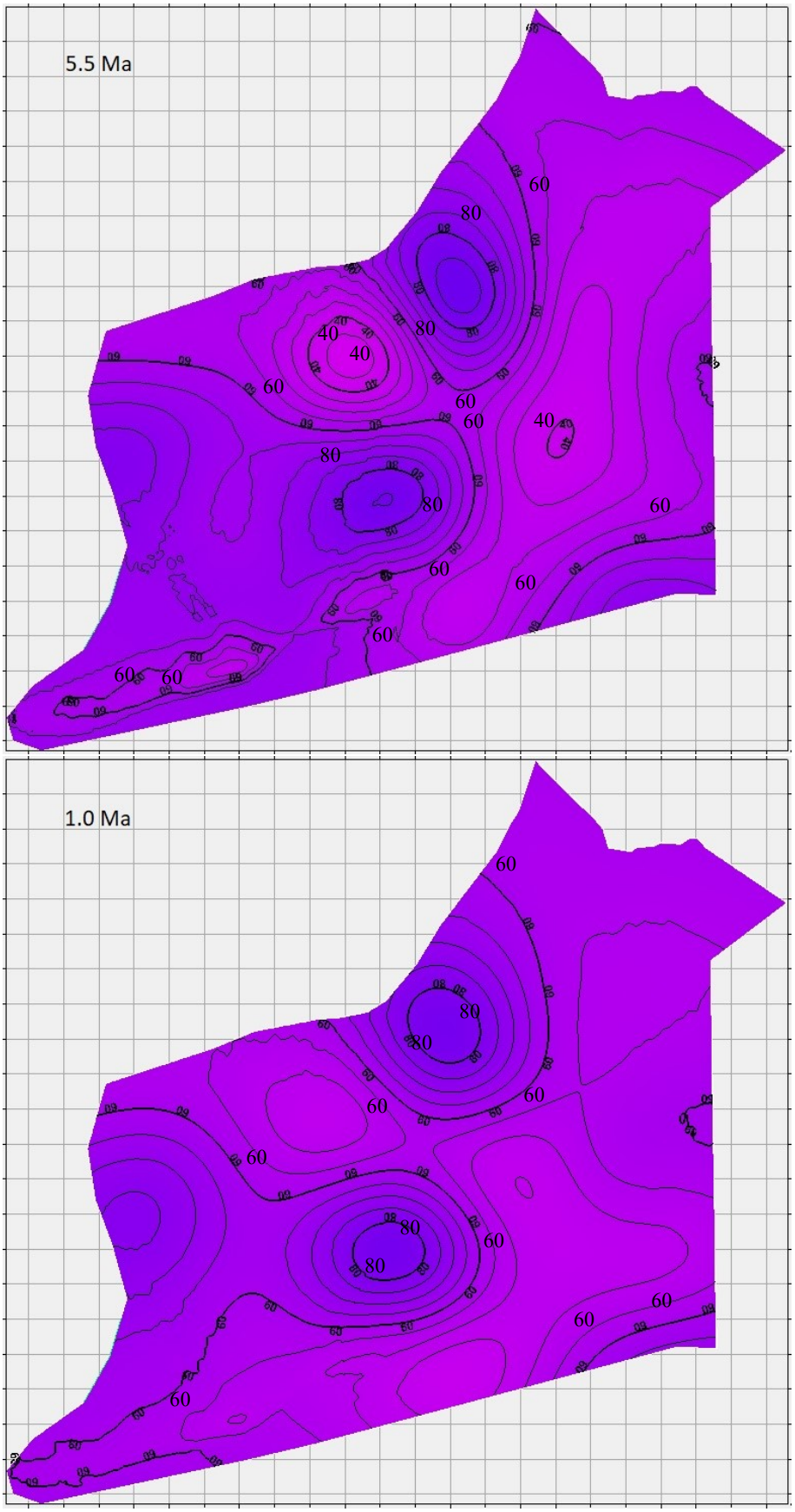

Figure 48 - Heatflow distribution in the basin through time.

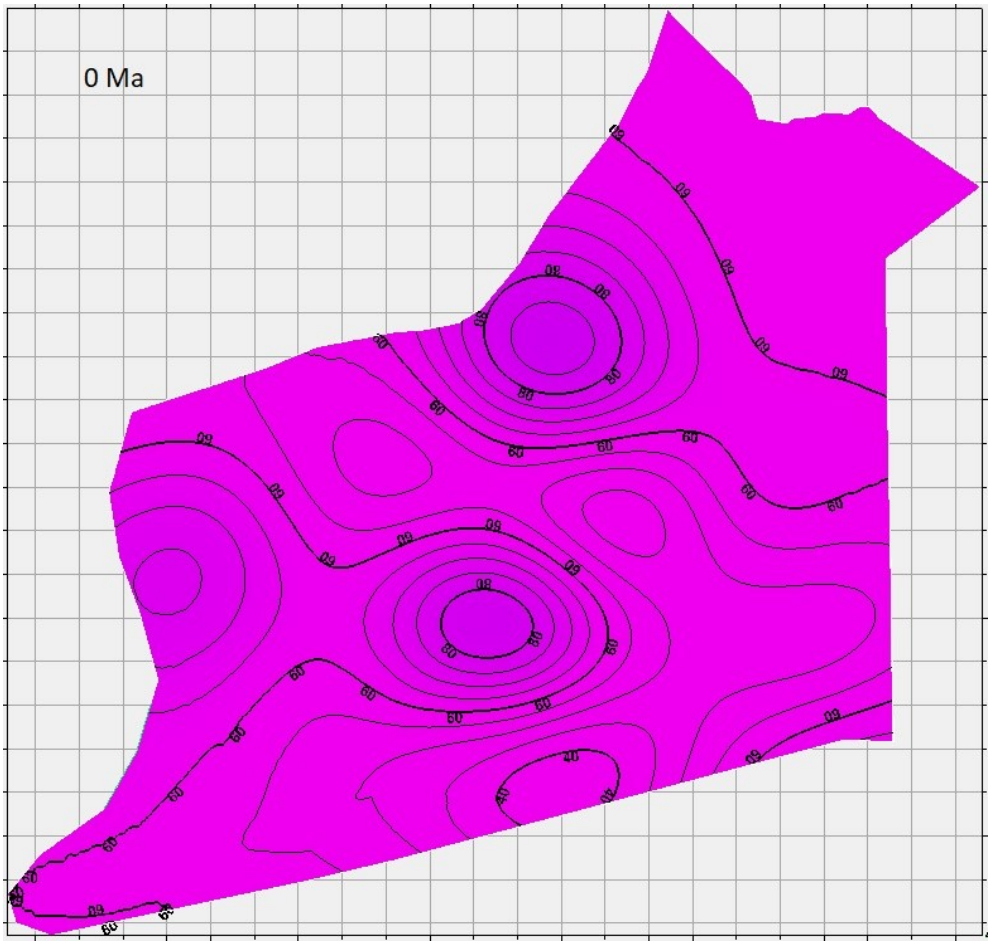

Figure 49 - Present day heat flow, calibrated to vitrinite reflectance and down hole temperature data.

6.2 Maturity & Generation

The simulation with the calibrated heat flow maps leads to reconstructions of source rock maturity in the basin during different time slices. Together with the kerogen type present in the source rock, the maturity evolution controls the timing of hydrocarbon generation and the type of the generated hydrocarbons (Figure 50). For the visualization, vitrinite reflectance was chosen, as it is the best and most widely used maturity indicator, and as it has been available for all wells.

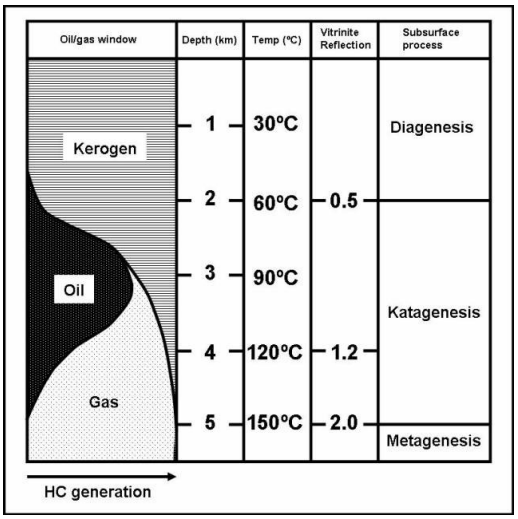

Figure 50 - Hydrocarbon generation & vitrinite reflectance (oilandgasgeology.com)

No distinct source rock layers are present in the Mura-Zala Basin (e.g. Hasenhüttl et al., 2001). In contrast, organic matter rich rocks are more or less irregularly distributed. Therefore, hydrocarbon generation was investigated using two scenarios with different source rock distributions and generation kinetics:

6.2.1 Generation scenario 1 (Case 1)

Source rock distribution: The source rock was distributed as shown in the chapter "population". Then all cells with less than 0.5% TOC were excluded from the calculation. Further, all cells with an HI of less than 25 were also excluded. That means that only "fair" or "good" source rocks with at least hydrogen-poor Type III kerogen was used for the calculation. For this case, the kinetic for TIII Kerogen (Crack) by Tissot in Waples (1992) was choosen.

6.2.2 Generation scenario 2 (Case 2)

The source rock distribution is generally the same as in "Case 1", but the HI cut-off was set to 125, resulting in source rock quality of at least Type II/IIb. For this case, the kinetic for TII Kerogen (Crack) by Tissot in Waples (1992) was chosen. Compared to Case 1, that means that for example the lower parts of the Haloze Formation (Karpatian) do not have any source rock or generation potential. Based on the used kinetic data set, hydrocarbon generation locally commences at a maturity of less than 0.6%Rr. Therefore, the generation map does not fit exactly the maturity map which assumes maturity at 0.6% and above.

6.2.3 Vitrinite reflectance, temperature & generation – cross sections and maps

Model results (vitrinite reflectance, temperature, amount of generated hydrocarbons) are presented in this section along cross sections and maps (stratigraphic horizons) for different time slices. The results are visualized using the same type of template, which is explained in (Figure 51):

A: The moment in time, at which the profiles and horizons were extracted.

B: The maturity distribution along the specified horizon (e.g. base Badenian).

C: The paleo-temperature distribution along the specified horizon.

D: The maturity distribution in the basin along the profiles A-A' and D-D' (see Figure 9 for position of profiles).

E: The paleo-temperature distribution in the basin along the profiles A-A' and D-D'.

F: The generated bulk mass of hydrocarbons in the formation overlaying the horizon specified in B and C.

Note, that the vertical exaggeration of the A-A' profile is 2:1, while it is 3:1 for the D-D' profile.

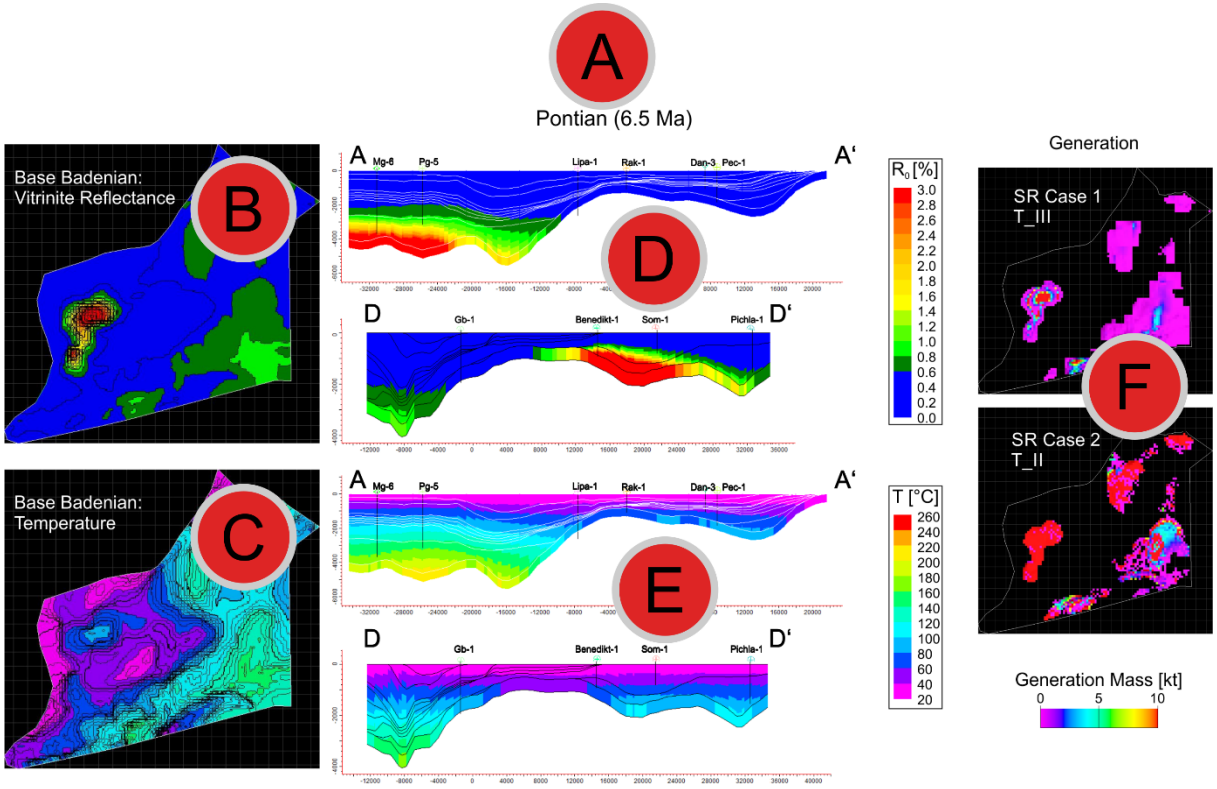

Figure 51 - Explanation of the visualization template (see text for details)

6.2.3.1 15.5 Ma (Figure 52)

At 15.5 Ma (Early Badenan), strongly elevated heat flow in the northwestern (Somat area; up to 600 mW/m²) and southeastern parts of the basin (Lendava area;) resulted in an extremely high geothermal gradient. Consequently, early hydrocarbon generation commenced at depths of only 300 to 600 m in the Haloze Formation. However, only very minor volumes have been generated (Case 1:T_III: 13000 kg), because the source rock is of inferior quality. No source rocks are present in the Haloze Formation in Case 2 and, therefore, generation is absent.

6.2.3.2 12.7 Ma (Figure 53-Figure 54)

Heat flow in the Somat area decreased during Late Badenian time, but was still elevated at the onset of the Sarmatian (). This caused a strong increase in maturity at the base of the Karpatian while also parts of the base of the Badenian horizon reached the oil window. Therefore, the Haloze Formation is already mature to over mature in parts, making generation in the bespoken areas possible and likely.

6.2.3.3 11.7 Ma (Figure 55 - Figure 56)

By the end of the Sarmatian, heat flow normalized and reached values between 50 mW/m² and 70 mW/m² in the Somat area, which then remained constant until present day. In the Lendava area, heat flow was around 100 mW/m² and declined to ~80 mW/m² one million years later. Consequently, maturity stayed essentially the same beside the expected increase due to deeper burial in areas that were not affected by the strongly elevated heat flow in Karpatian/Early Badenian times. Since the main source rocks are mainly expected in Badenian and Sarmatian layers, virtually no additional hydrocarbons were generated.

6.2.3.4 6.5 Ma (Figure 57 - Figure 59)

About 8 Ma ago, the Ljutomer Trough started to become the deepest trough in the basin. Despite moderate heat flow and consequently moderate thermal gradients, Badenian and subsequently Sarmatian sediments became mature due to their burial depth. The first Badenian sediments that were not subject to the early Miocene heating events became mature at about 8.25 Ma. At 6.5 Ma, the whole base of the Badenian layer was in the oil window along the Ljutomer Trough. Sarmatian sediments in the deeper parts of the trough also reached vitrinite reflectance values of 0.6%Rr and more. The Sarmatian was further subdivided into the layers Sarmat 1-3 (Figure 18). In Figure 59, for the SR case 1 (T_III), the layer Sarmat 2 is displayed to give a good visual representation of generation, because Sarmat 1 is producing almost nothing in this scenario, while SR case 2 (T_II) shows Sarmat 1, but Sarmat 2 was also producing in the 10 kt magnitude. According to the simulation used in this study, the Sarmat 2 layer includes the best source rocks in the Sarmatian succession.

6.2.3.5 Present Day (Figure 60 - Figure 64)

From the Pontian until today, thermal subsidence continued. As described above (chapter "Erosion"), the maximum thickness of the Mura Formation was reached at 5.5 Ma. Later, the upper part of the Mura Formation became eroded. This resulted in a pull-up of the maturity pattern in the very south-eastern corner of the model area compared to the pattern at 6.5 Ma (Figure 59). The thermal subsidence caused that additional parts of the Haloze Formation became mature in the deeper parts of the basin and that significant parts even reached gas window maturity. The deepest parts in the Ljutomer Trough became highly over mature, with vitrinite reflectance values exceeding 3%Rr. The Spilje Formation (Badenian) followed the same structure, with deeper parts entering the gas window and a slight spatial extension of mature rocks. The Sarmatian part of the Spilje Formation became mature along the whole axis of the Ljutomer Trough and east of the Murska Sobota Block, with the deepest parts getting into the gas window. As mentioned above, the Sarmat 2 layer has the best source rock potential, and therefore is displayed on the "Generation" map for SR case 1. For SR case 2, the Sarmat 1 layer is displayed, whereas the Sarmat 2 layer shows basically the same pattern as the Sarmat 1 layer in this case. Moving to the Lendava Formation, oil-mature rocks can be found at its base along the axis of the Ljutomer Trough. The shallowest rocks reaching the oil window are located at the top of the turbiditic section of Lendava Formation (Figure 64), where a small area corresponding to the very deepest part of the Ljutomer Trough reached vitrinite reflection values of about 0.6%Rr.

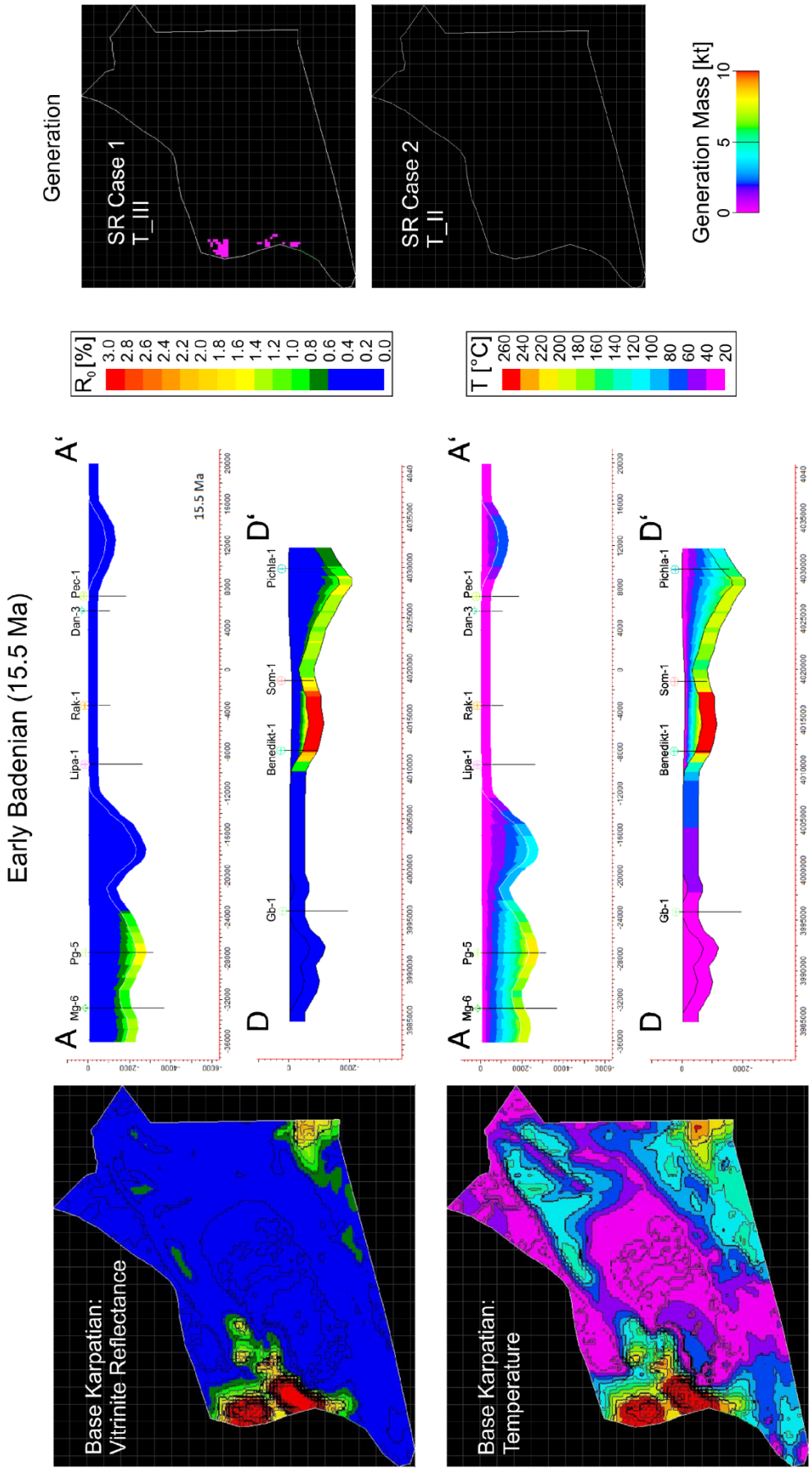

Figure 52 - Vitrinite reflectance and temperature distribution along the base of the Haloze Formation (Karpatian) 15.5 Ma ago. The generation refers to generation in the Haloze Formation.

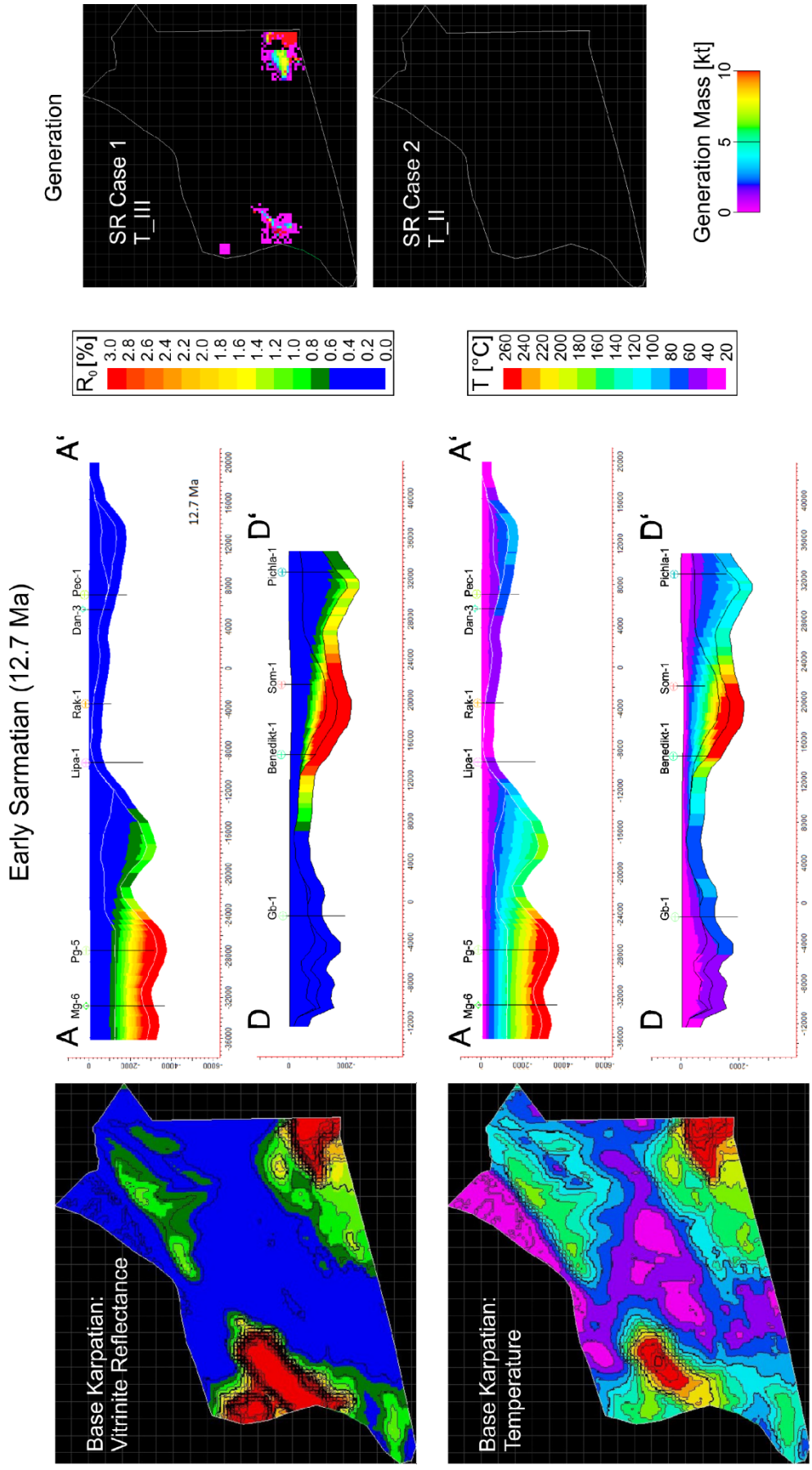

Figure 53 - Vitrinite reflectance and temperature distribution along the base of the Haloze Formation (Karpatian) 12.7 Ma ago. The generation refers to generation in the Haloze Formation.

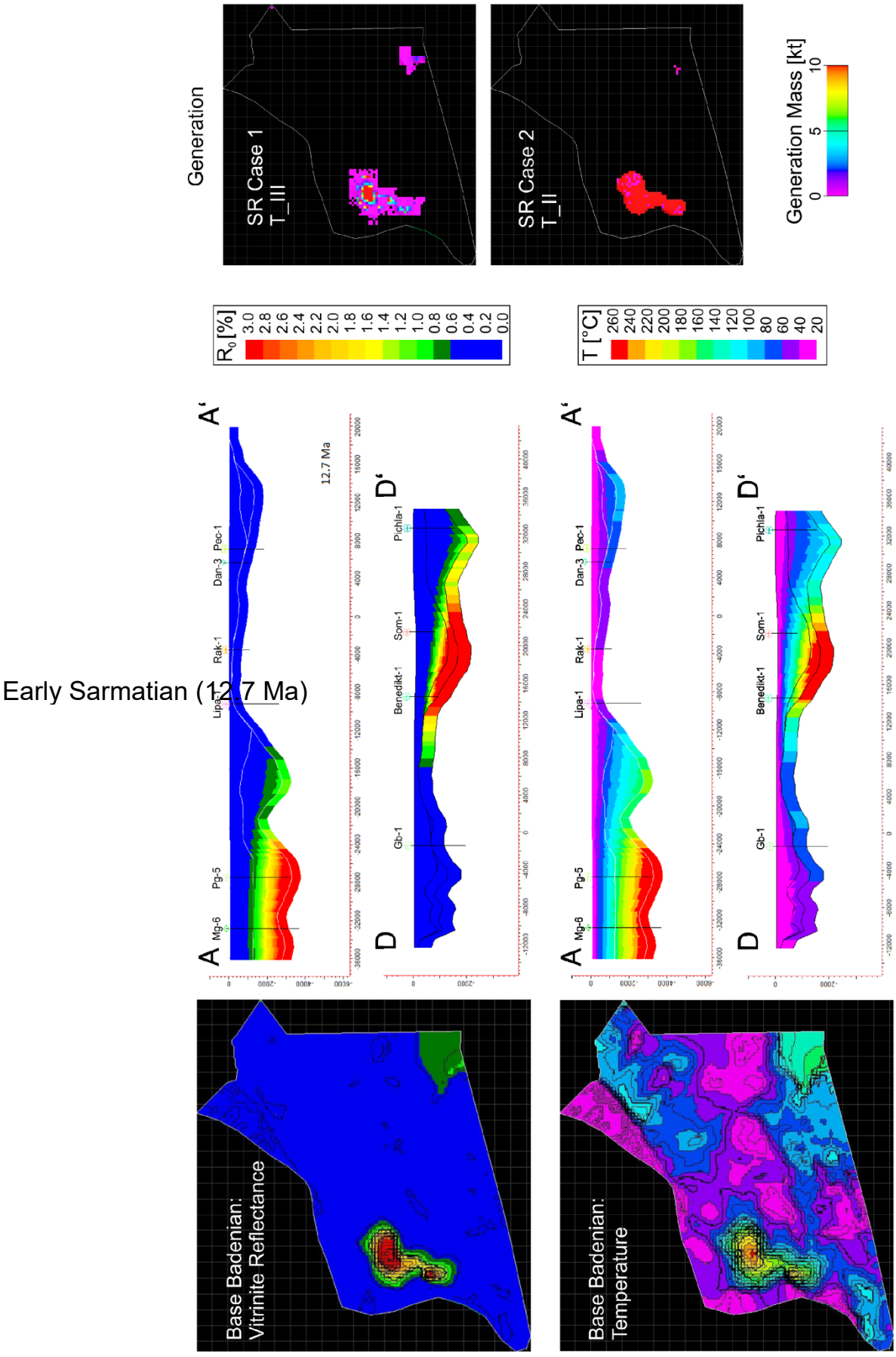

Figure 54 - Vitrinite reflectance and temperature distribution along the base of the Spilje Formation (Badenian) 12.7 Ma ago. The generation refers to generation in the Spilje Formation (Badenian).

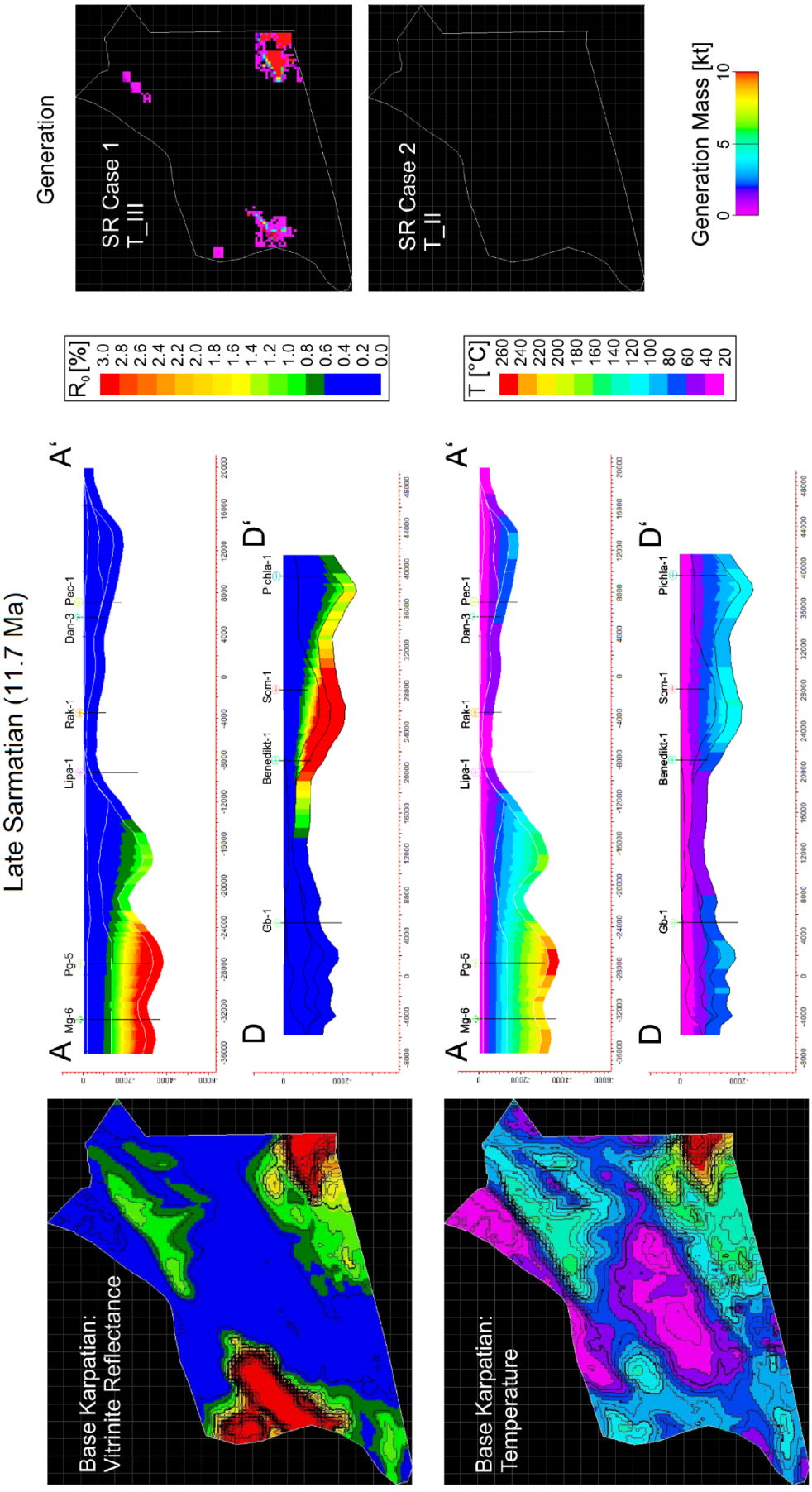

Figure 55 - Vitrinite reflectance and temperature distribution along the base of the Haloze Formation (Karpatian) 11.7 Ma ago. The generation refers to generation in the Haloze Formation.

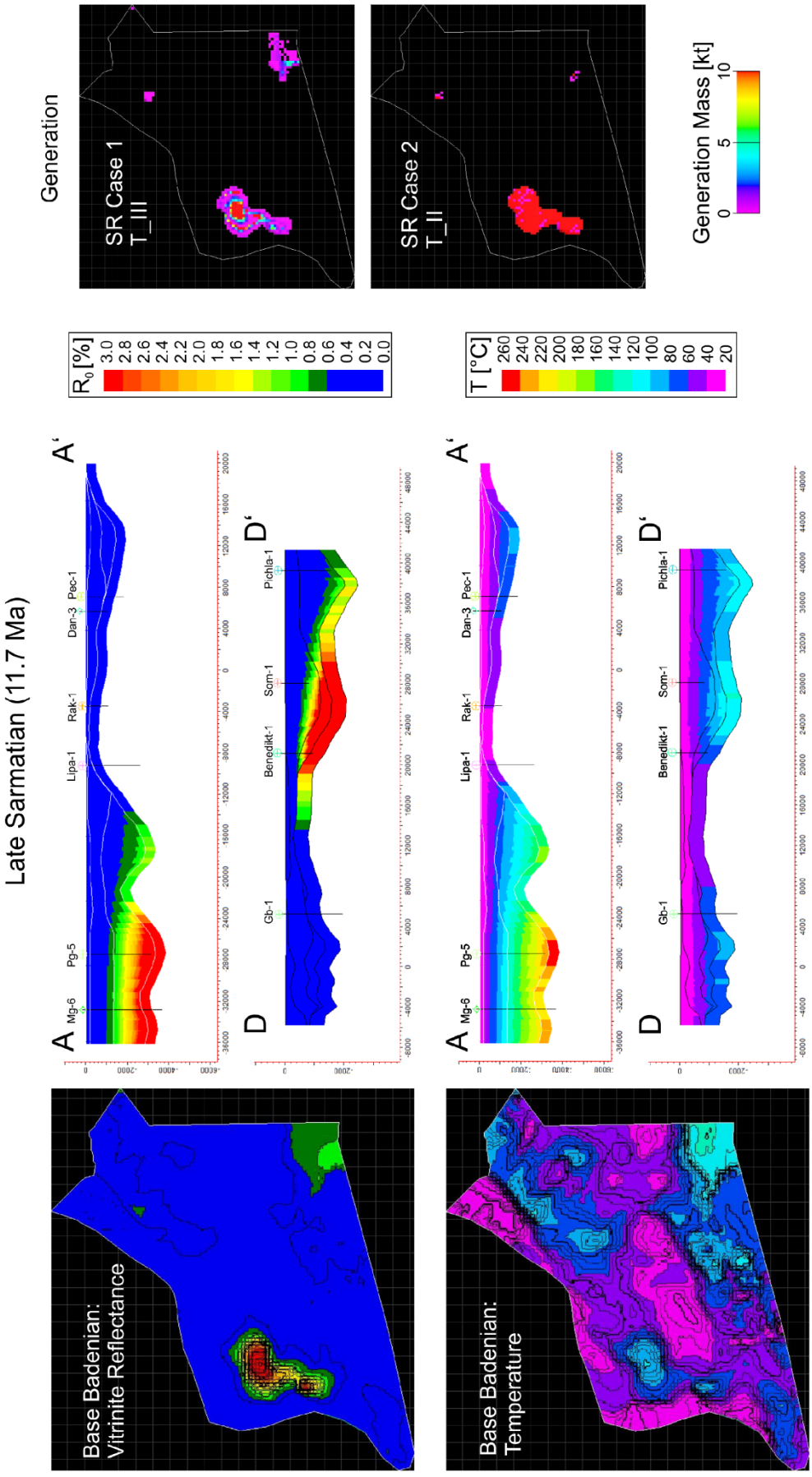

Figure 56 - Vitrinite reflectance and temperature distribution along the base of the Spilje Formation (Badenian) 11.7 Ma ago. The generation refers to generation in the Spilje Formation (Badenian).

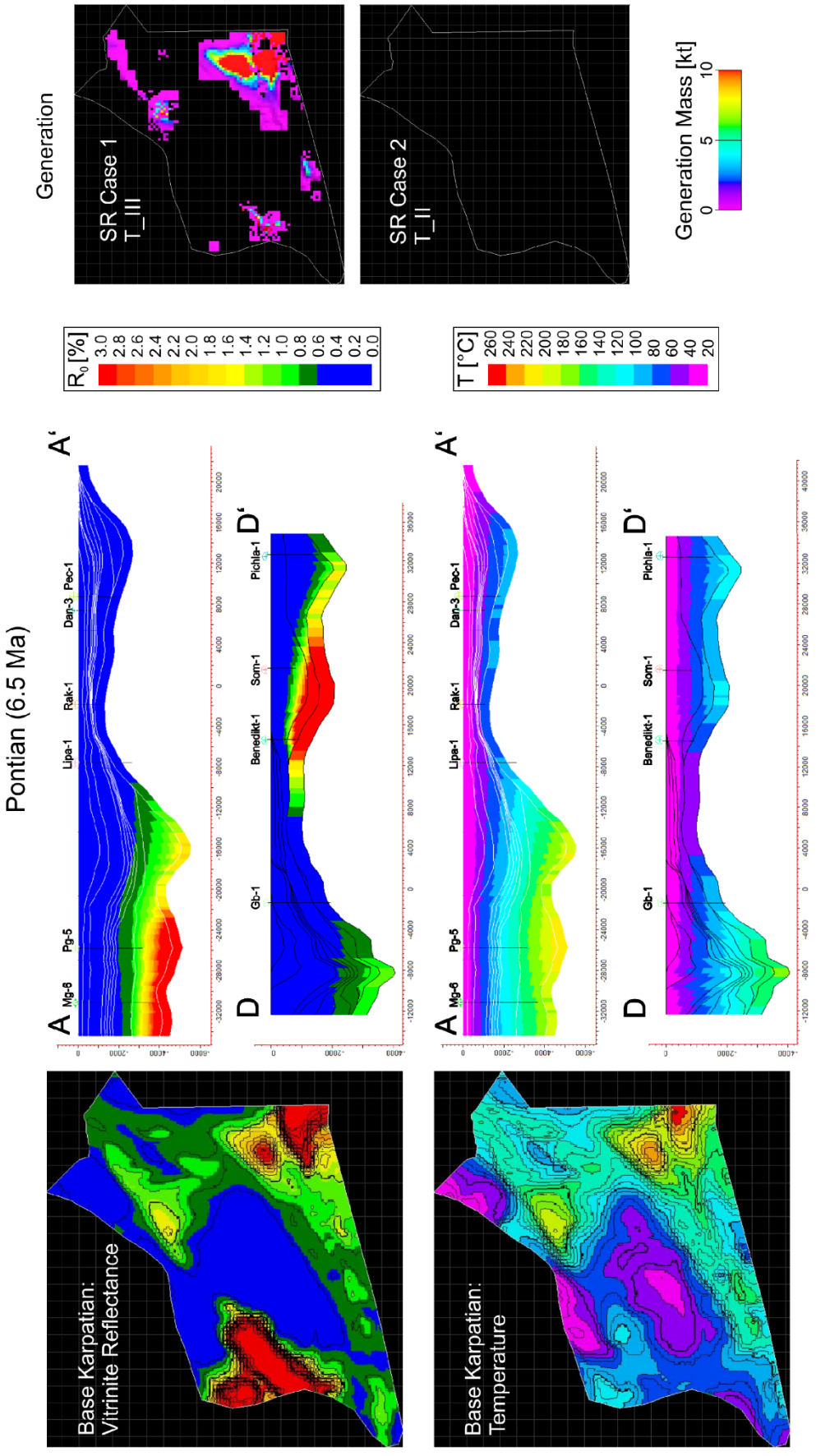

Figure 57 - Vitrinite reflectance and temperature distribution along the base of the Haloze Formation (Karpatian) 6.5 Ma ago. The generation refers to generation in the Haloze Formation.

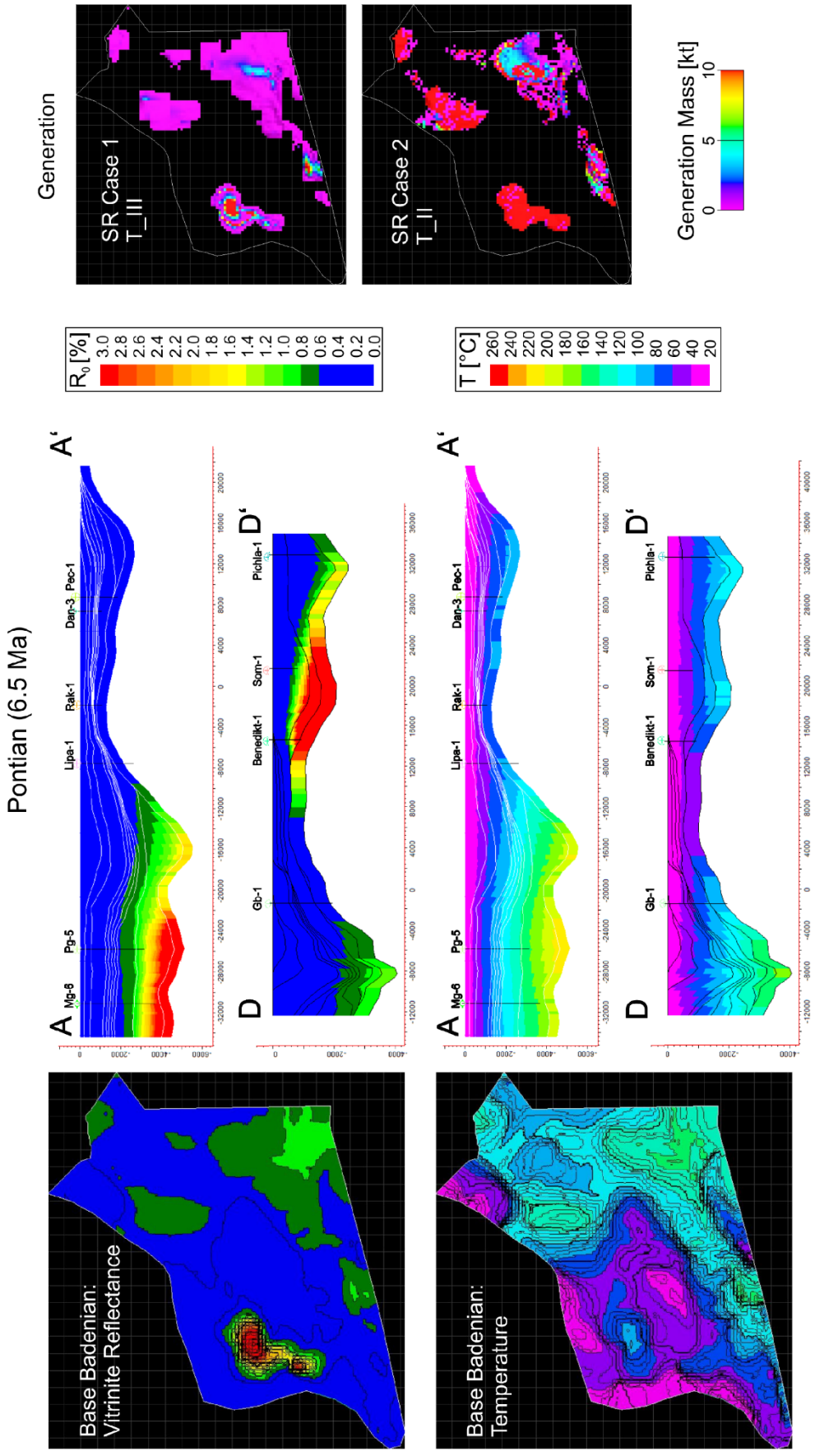

Figure 58 - Vitrinite reflectance and temperature distribution along the base of the Spilje Formation (Badenian) 6.5 Ma ago. The generation refers to generation in the Spilje Formation (Badenian).

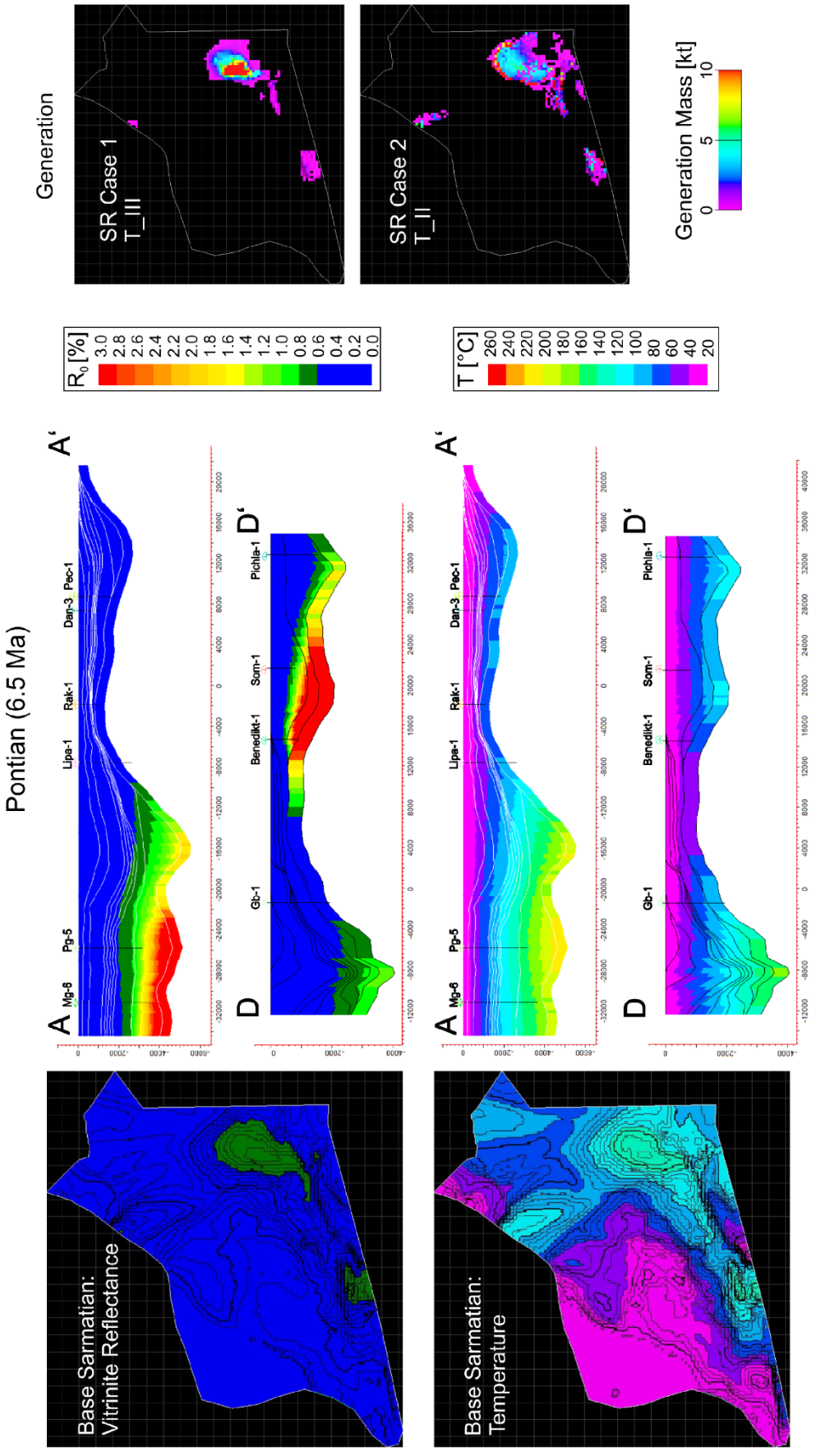

Figure 59 - Vitrinite reflectance and temperature distribution along the base of the Spilje Formation (Sarmatian) 6.5 Ma ago. The generation refers to generation in the Spilje Formation (Sarmatian).

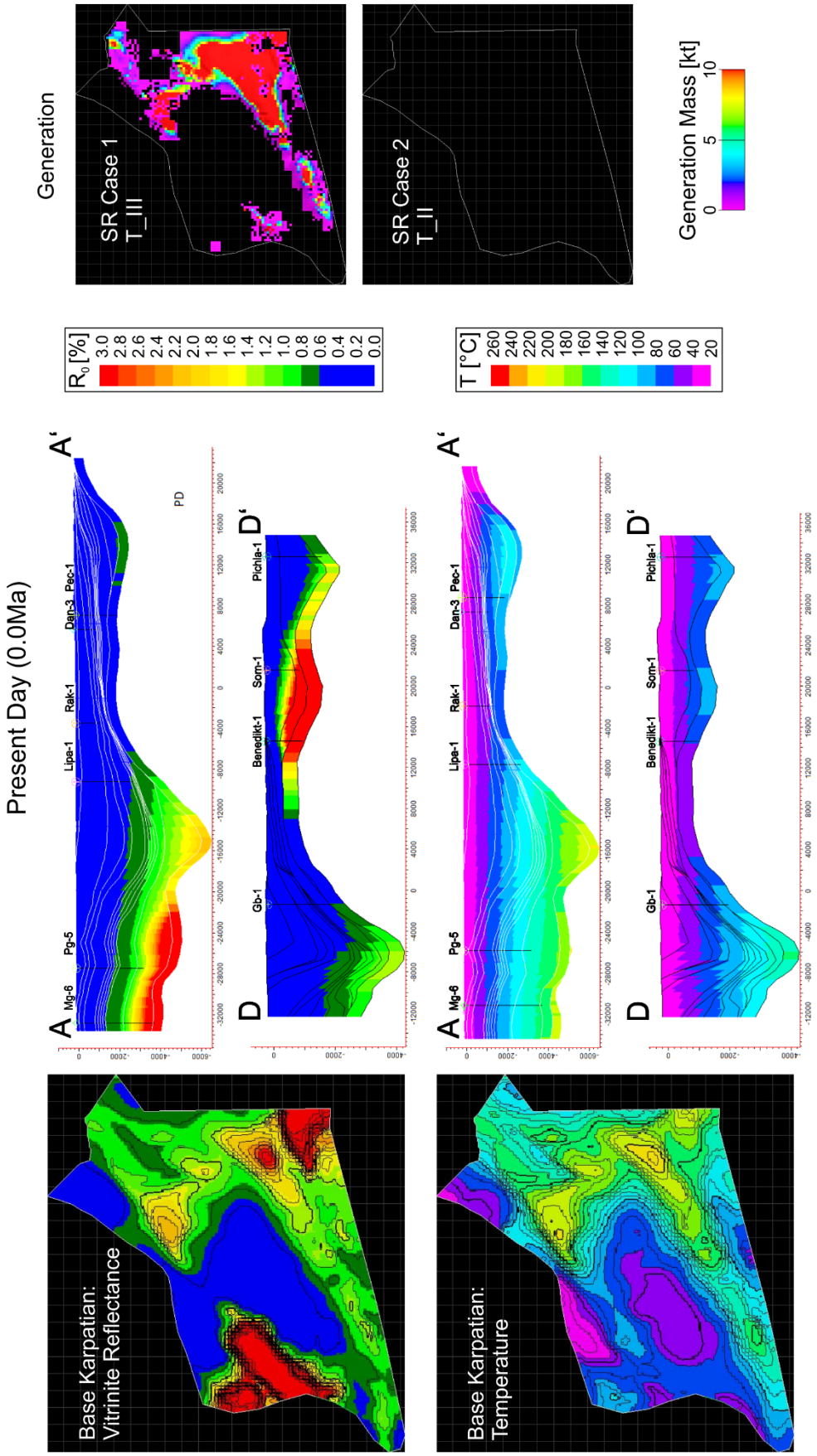

Figure 60 - Vitrinite reflectance and temperature distribution along the base of the Haloze Formation (Karpatian) at present day. The generation refers to generation in the Haloze Formation.

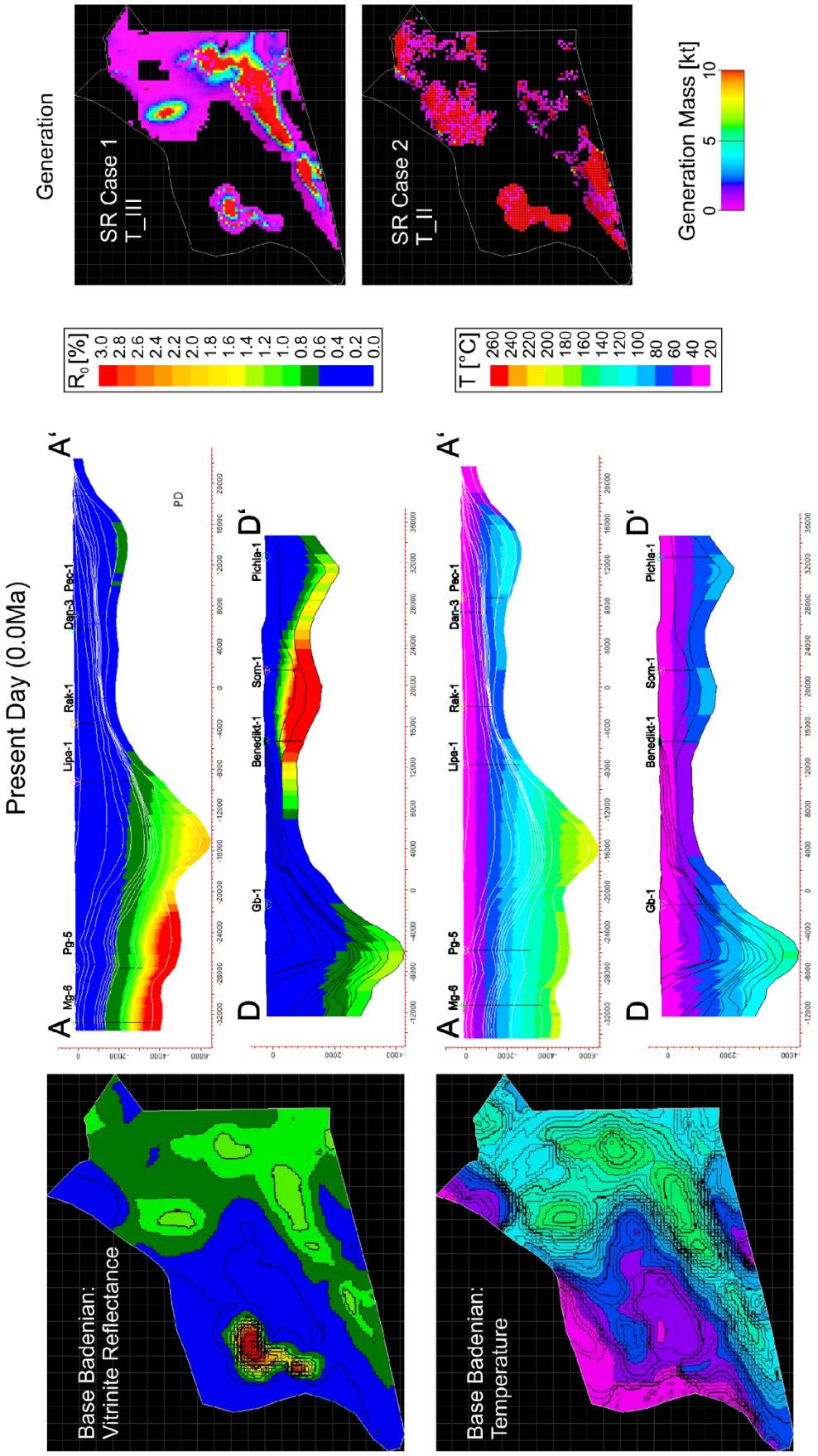

Figure 61 - Vitrinite reflectance and temperature distribution along the base of the Spilje Formation (Badenian) at present day. The generation refers to generation in the Spilje Formation (Badenian).

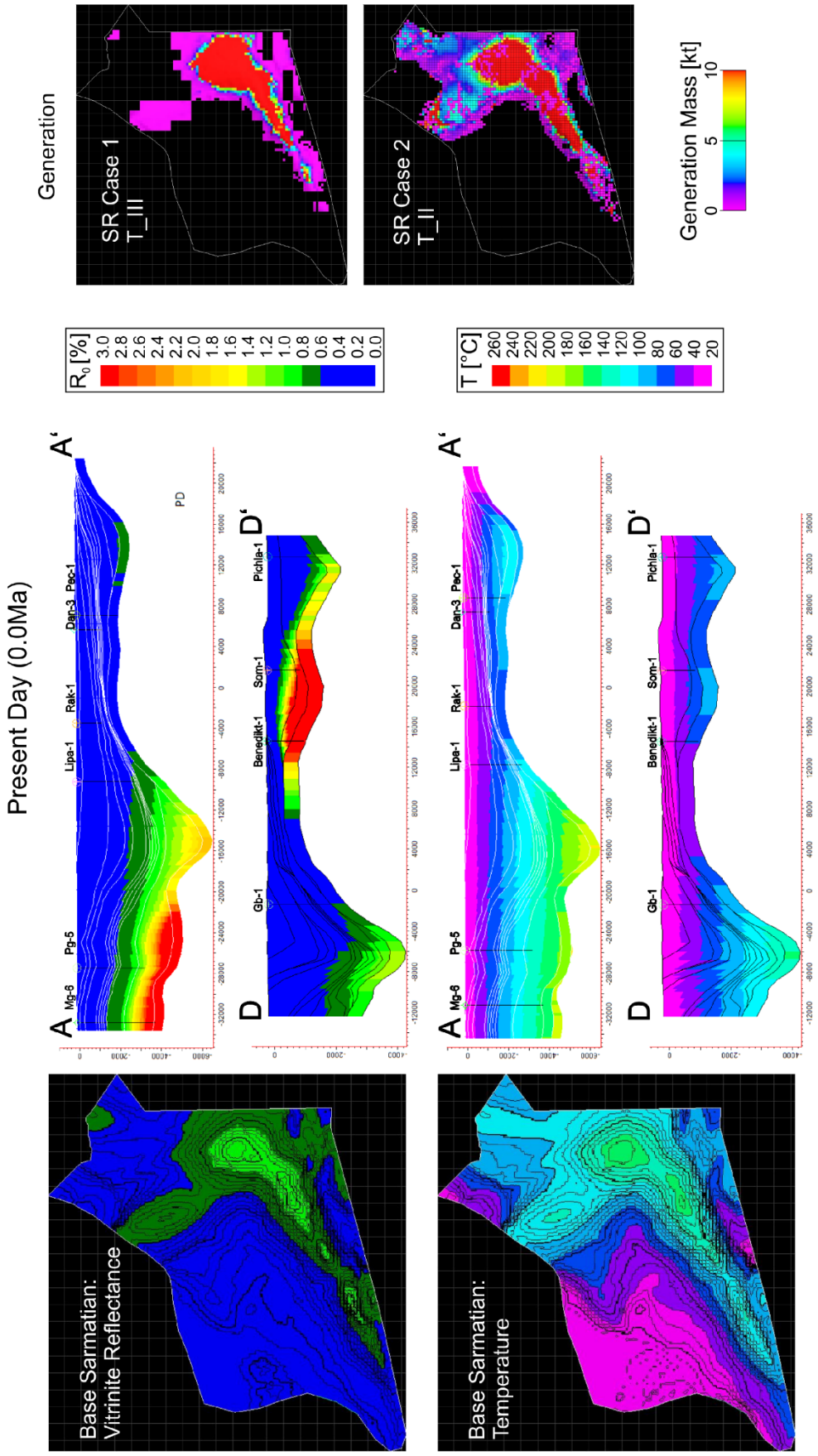

Figure 62 - Vitrinite reflectance and temperature distribution along the base of the Spilje Formation (Sarmatian) at present day. The generation refers to generation in the Spilje Formation (Sarmatian).

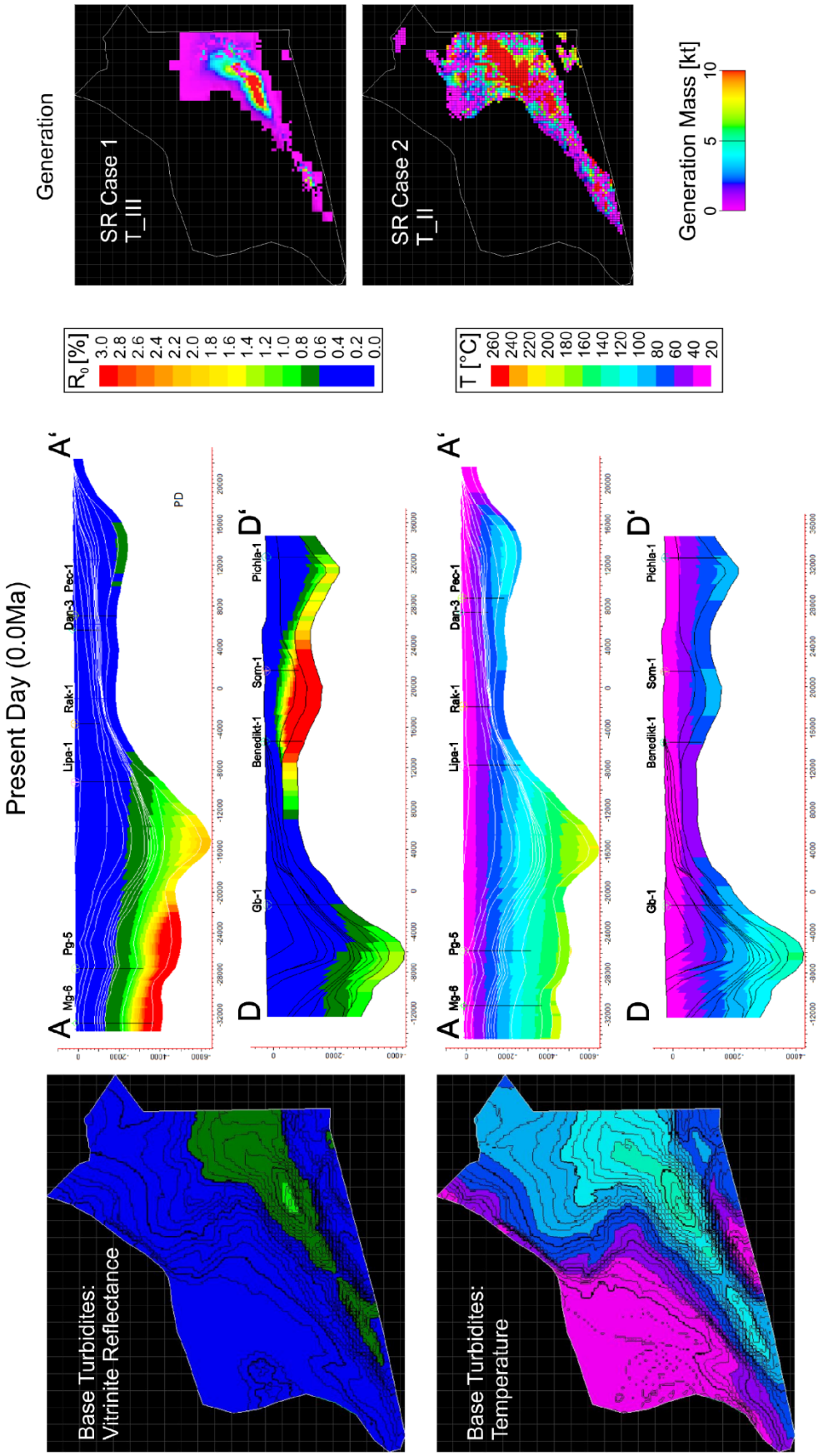

Figure 63 - Vitrinite reflectance and temperature distribution along the base of the Lendava Formation (Turbidites) at present day. The generation refers to generation in the Lendava Formation (Turbidites)).

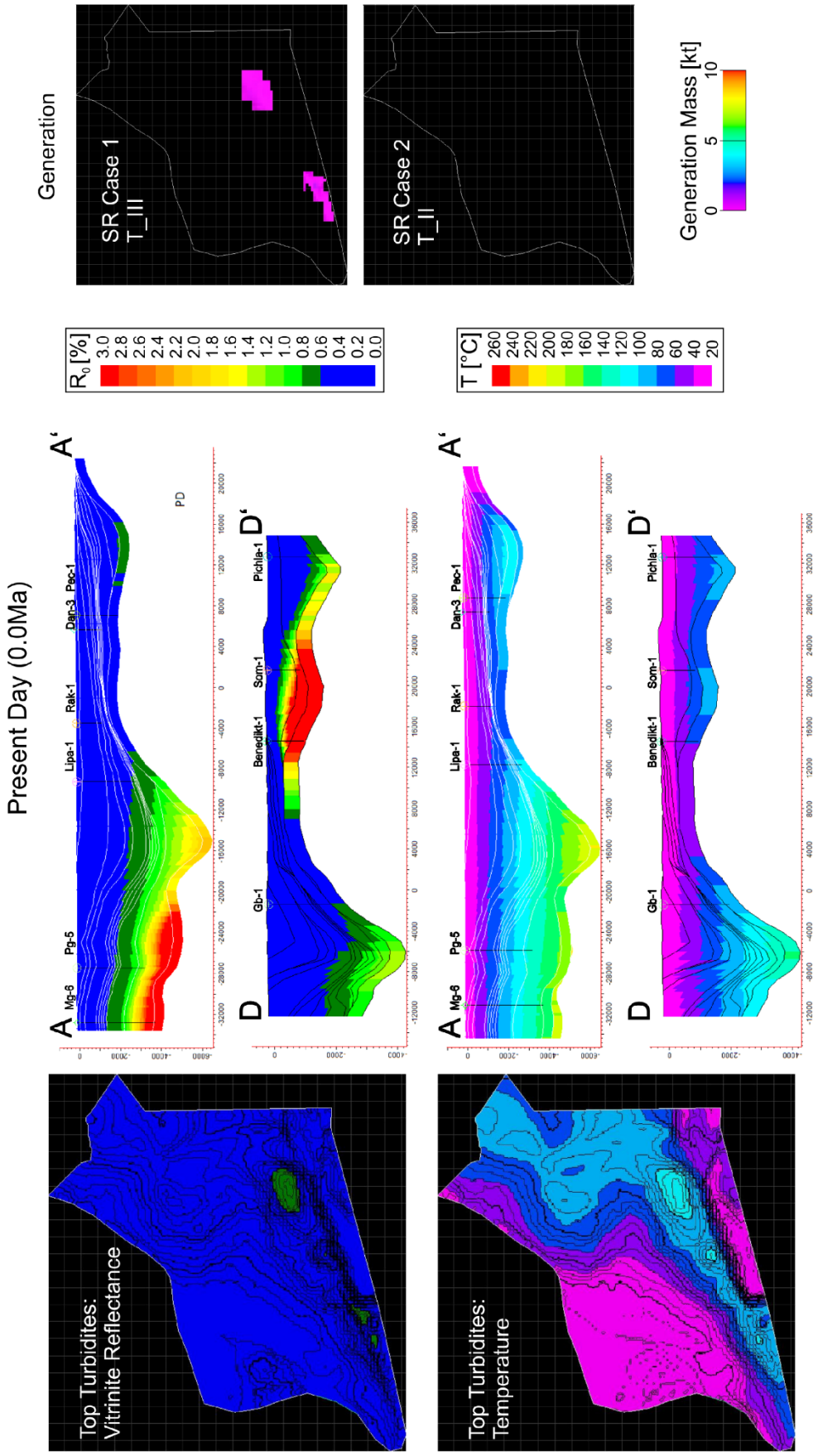

Figure 64 - Vitrinite reflectance and temperature distribution along the top of the Lendava Formation (Turbidites) at present day. The generation refers to generation in the Spilje Formation, above the turbiditic sequence.

In Figure 65, the present day maturity along all four profiles shown in Figure 9 are displayed.

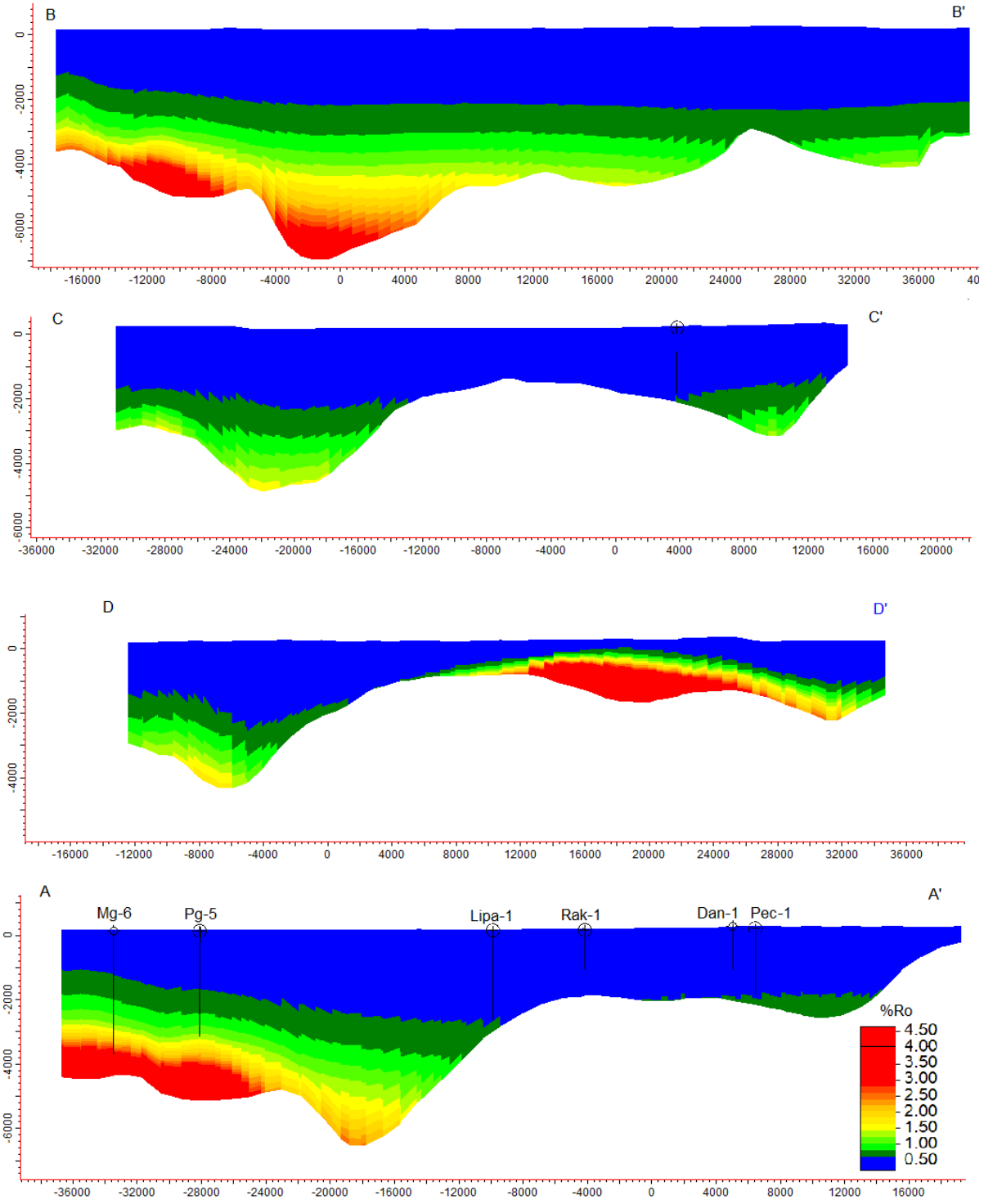

Figure 65 - Present day maturity along 4 profiles. The location of the profiles is shown in Figure 9.

6.3 Accumulations and hydrocarbon migration

The two different generation scenarios described in 6.2 resulted in different accumulations as shown in 6.3.1 and 6.3.2. The locations of the modeled accumulations in 2D and 3D are shown, as well as the flow paths, highlighting the secondary migration pathways. As a result of the model type (layer cake model), most of the accumulations are found where hypothetical pinch-outs of the sandstone reservoir layers occur. The most important accumulation of commercial interest, the Petišovci Field in the Petišovci-Lovászi-Antiform, is filled with less than 6*10^6 m³ oil (surface conditions) for the generation scenario 2 (6.2.2) and less than 1*10^6 m³ oil (surface conditions) for generation scenario 1 (6.2.1)

The third scenario depicted here (6.3.3), is as described in 4.4**Error! Reference source not found.**. This hypothetical scenario was run, because the simulations based on hard data could not fill the Petišovci field to the known extend. It uses the source rock distribution of the generation scenario case 1 (6.2.1), but additionally assigning every shale and every marl source rock properties with a TOC of 10%, a hydrogen index of 500 mg HC/g TOC and source rock kinetics of Tissot in Waples (1992) for TII Kerogen (Crack). In this last "hypothetical" scenario, more than 136*10^6 m³ (surface conditions) oil are found in the accumulation simulating the Petišovci field, with another 346*10^6 m³ oil (reservoir conditions) lost to the surface in the process.

6.3.1 Scenario 1

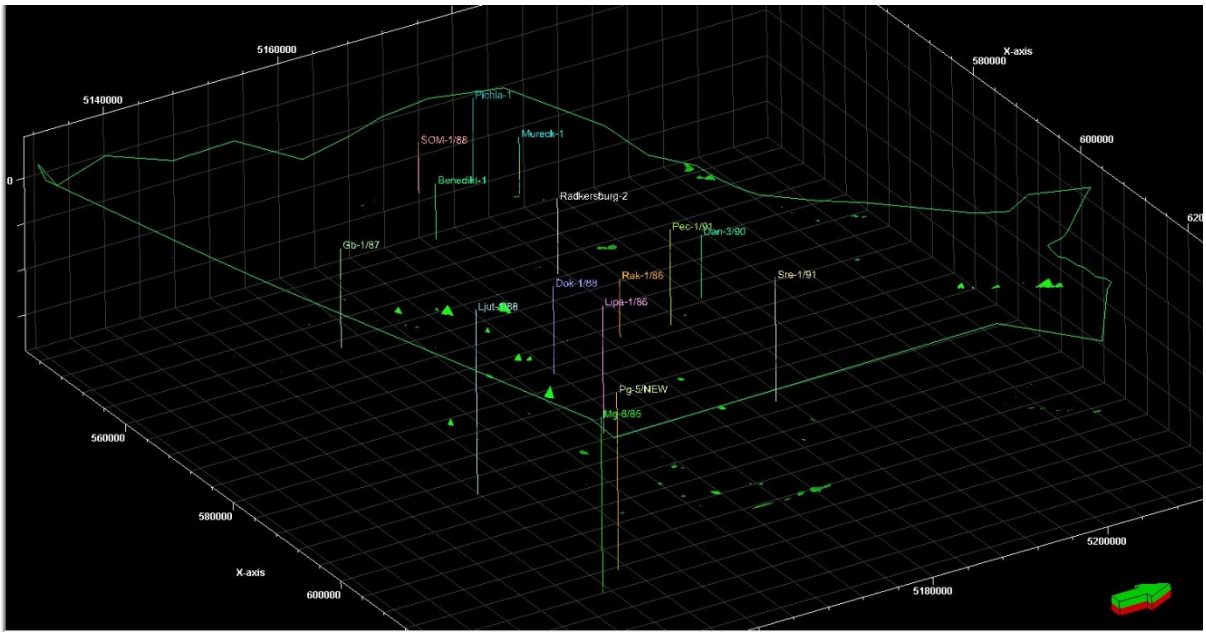

Figure 66 - Accumulations for source rock case 1 (6.2.1) – 3D

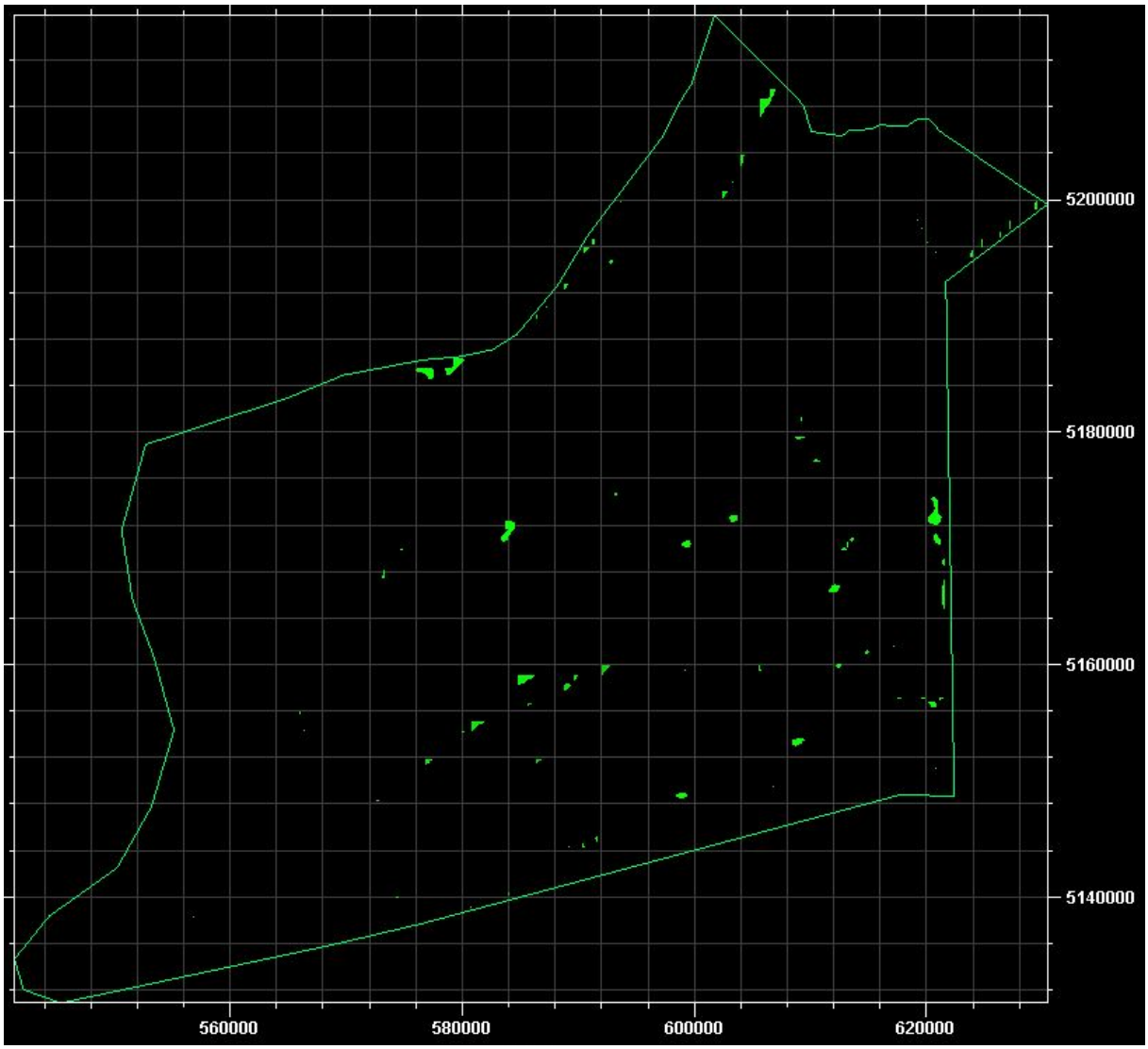

Figure 67 - Accumulations for source rock case 1 (6.2.1) - 2D

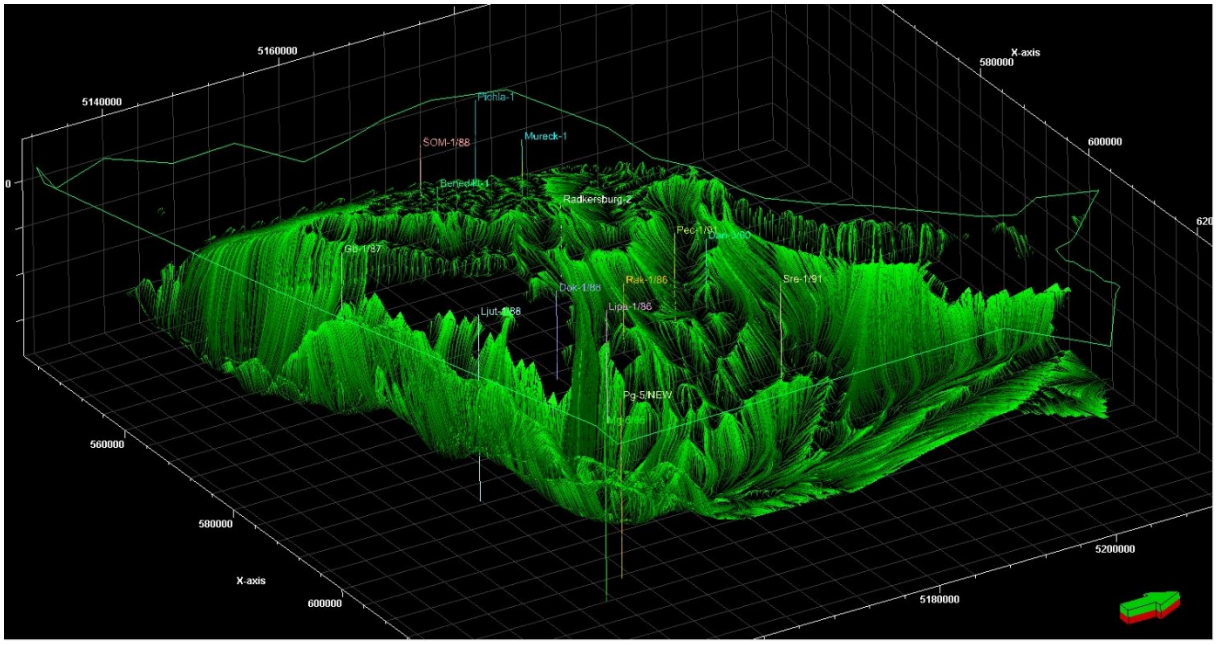

Figure 68 – Flow paths for source rock case 1 (6.2.1)

6.3.2 Szenario 2

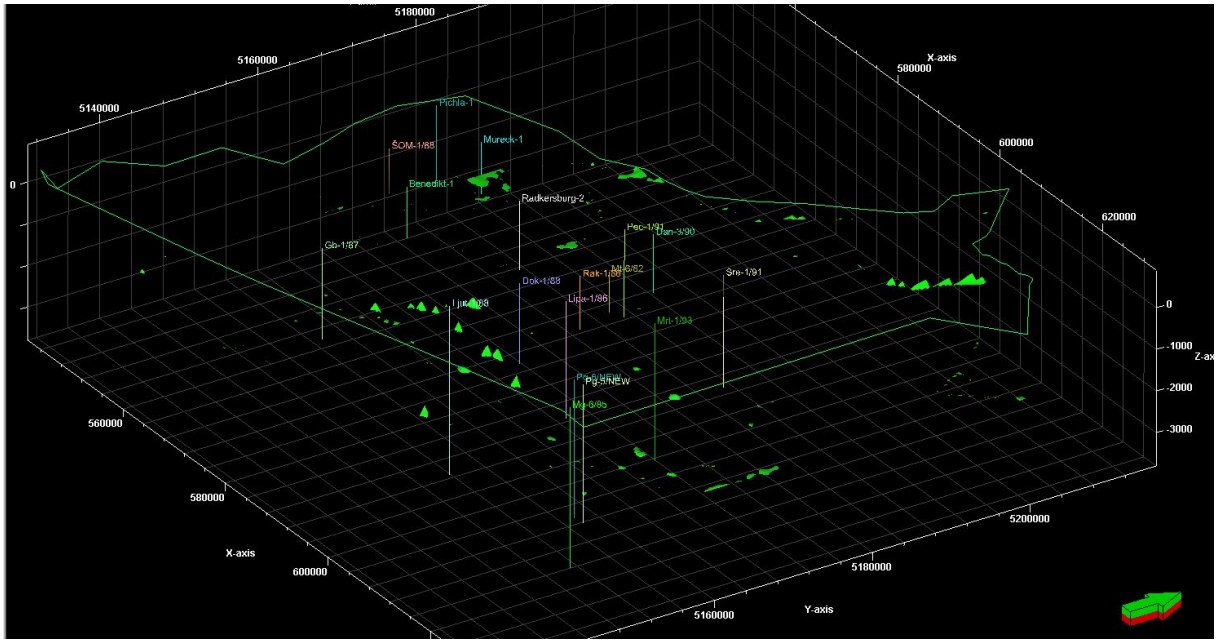

Figure 69 - Accumulations for source rock case 2 (6.2.2) - 3D

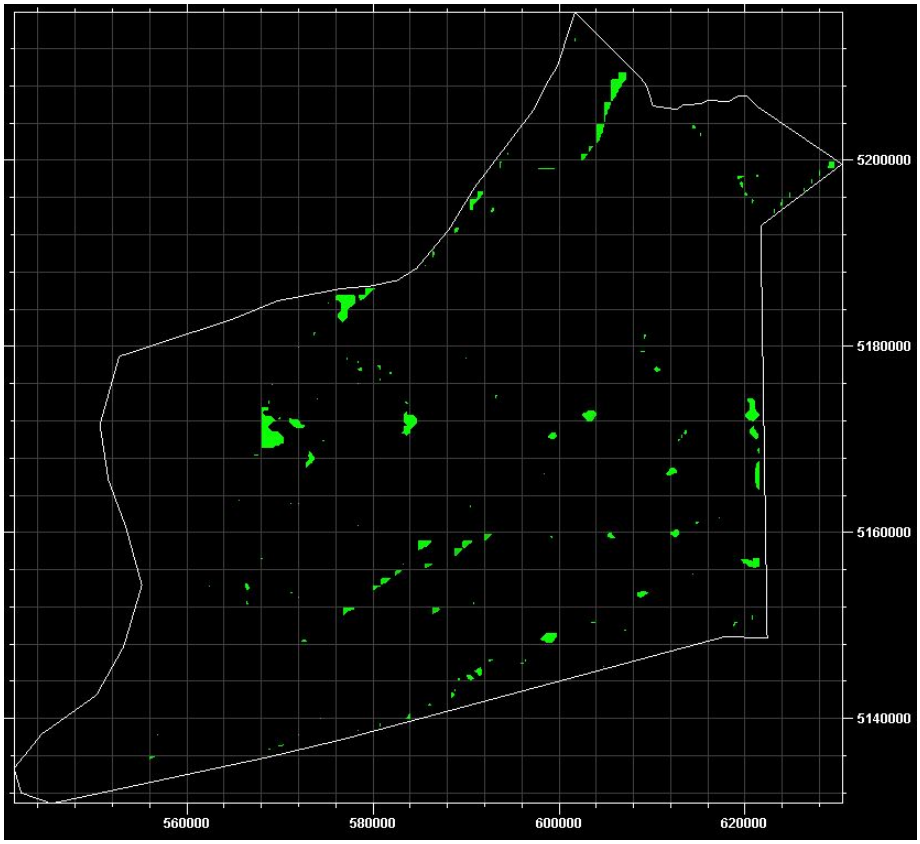

Figure 70 - Accumulations for source rock case 2 (6.2.2) – 2D

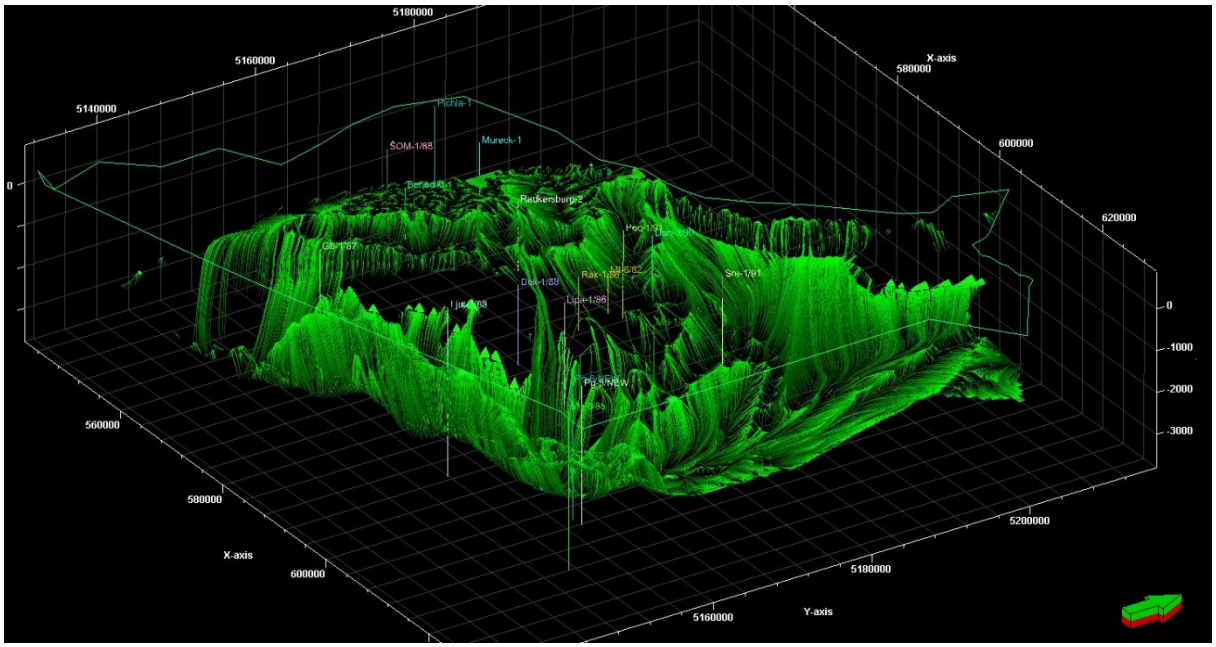

Figure 71 – Flow paths for source rock case 2 (6.2.2)

6.3.3 Scenario 3

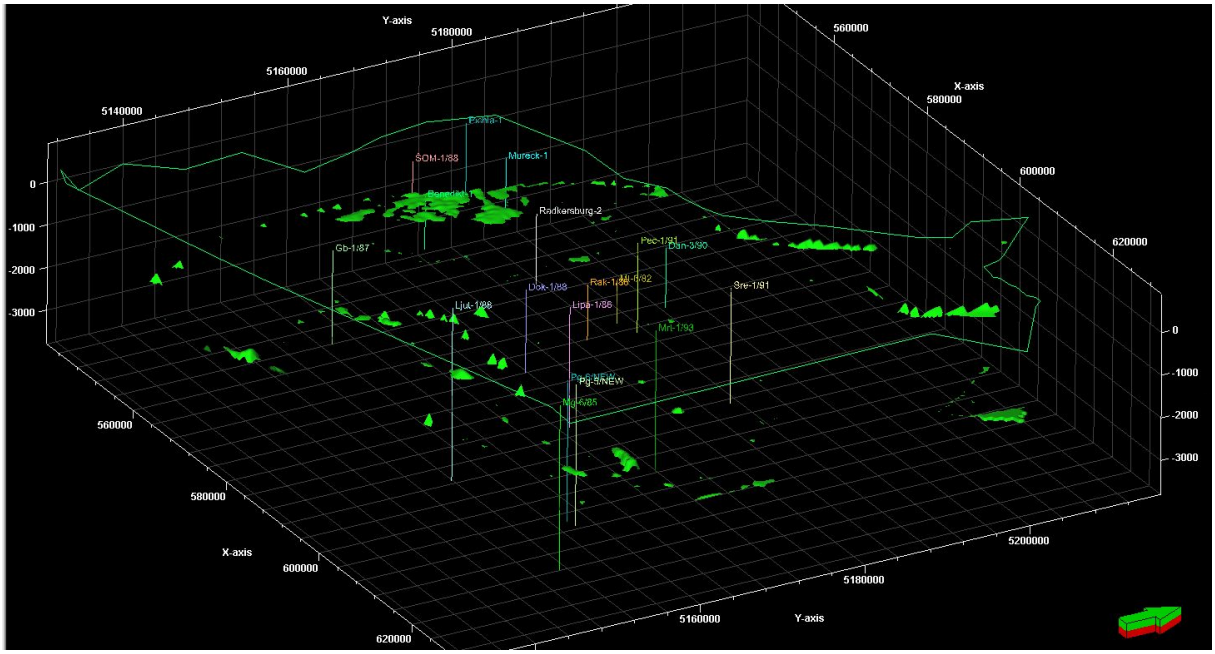

Figure 72 - Accumulations for source rock case 3 (6.3) – 3D

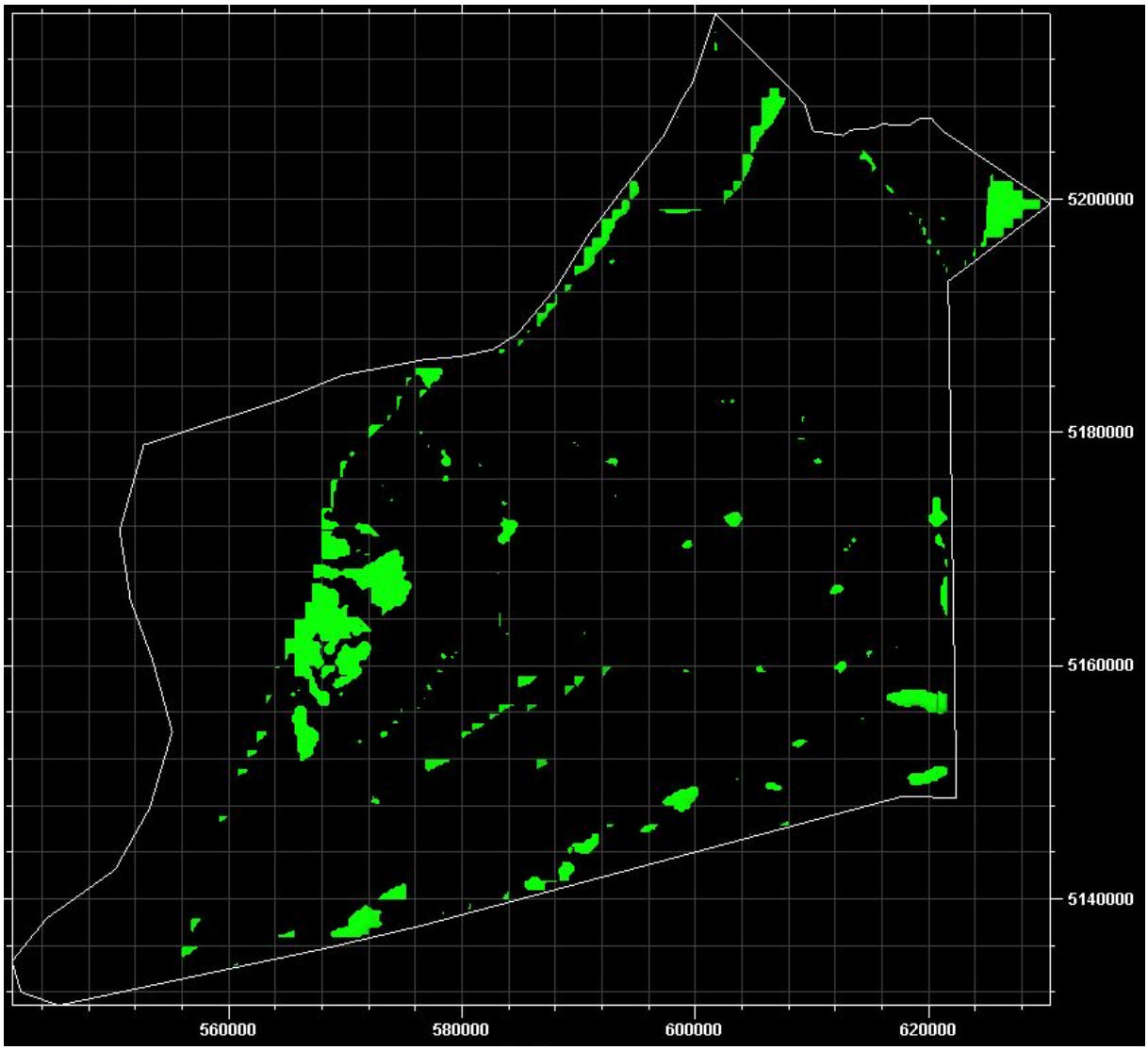

Figure 73 - Accumulations for source rock case 3 (6.3) – 2D

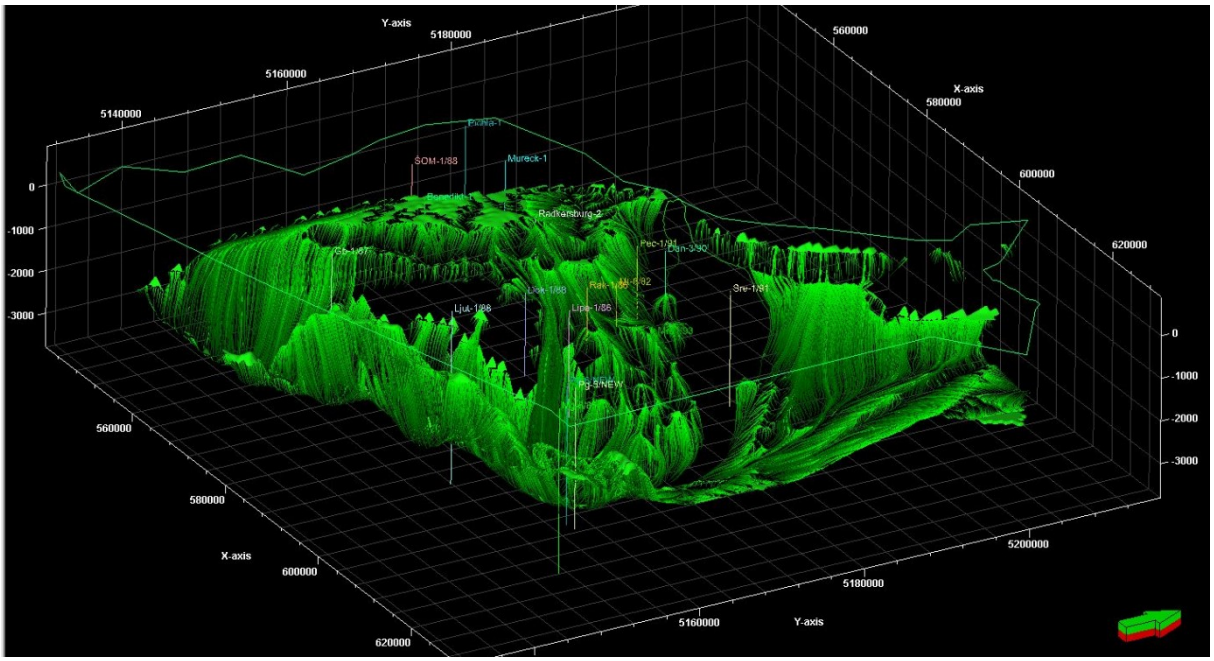

Figure 74 – Flow paths for source rock case 3 (6.3)

7 Sensitivity Analysis

This chapter deals with the influence of different model assumptions on the main calibration parameter, vitrinite reflectance [$\%R_0$]. A model can only be as good as its input data and is strongly dependent on the assumptions made, based on data analysis to fill the space without hard data. Here we assess the deviation of vitrinite reflectance caused by the change of certain model parameters, like different lithology content of the formations, paleo-bathymetry deviating from the assumptions made by Hasenhüttl et al. (2001) and the influence of a change in recent heat flow on the maturity patterns in the basin, by applying a published heat flow map published by Gosar et. al. (2005) in different time steps back from present day.

To demonstrate the influence throughout the model, 4 wells with a set of very diverse properties and allocated in very different positions were chosen;

Table 6 - Properties of the wells chosen to represent the sensitivity analysis

	HF[mW/m²]											Horizons Penetrated	TVD
Age [Ma]	0	1	5.5	6.5	7.1	11.7	12.7	15	15.5	16	17		
Ljut-1	55	58	70	70	70	70	70	70	70	70	70	9	4048
Som-1	75	75	75	75	75	75	210	500	550	535	500	3	1100
Pg-5	50	52	60	70	80	80	150	150	150	115	100	8	3324
Pichla-1	60	60	60	70	70	70	70	170	200	200	200	2	1815

7.1 Lithology

Lithology has a very big influence on the heat distribution inside the earth. It determines the thermal gradient mainly by two properties; thermal conductivity and radiogenic heat production. Thus, we expect the highest deviation in $\%R_0$ with a change of this parameter, since the lithology across all wells was unified in the 3D model for each formation. The results for this analysis are shown in Figure 75 and Figure 76. The column left to the %R0 chart shows the lithology used in the predictions by Hasenhüttl (2001) and Sachsenhofer (1998, 2001) which corresponds to the red curve in the $\%R_0$ chart, while the column to the right of the $\%R_0$ chart shows the lithology assigned to the well by the 3D model corresponding to the blue curve. For both cases the same, final heat flow presented in was used.

It became clear that variations in lithology are expressed to a satisfying amount through the assumptions made concerning an average lithology for the different formations (Table 2) and

therefore have a minor effect on vitrinite reflectance trends with the exception of the Somat well, characterized by a very high paleo-heat flow.

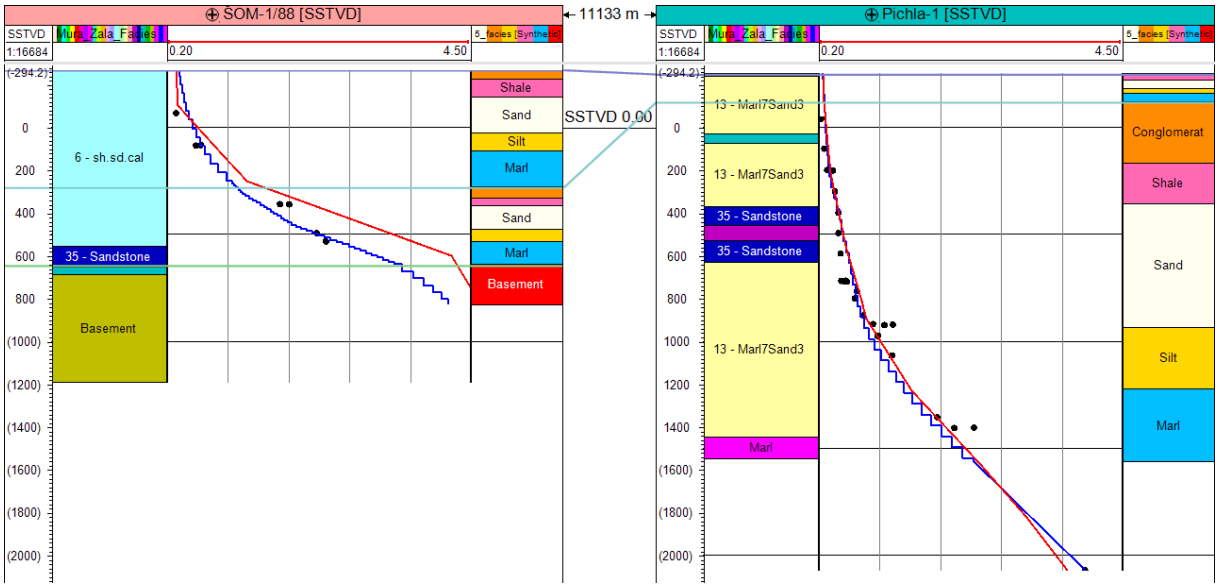

Figure 75 - Deviation in %R_0 with different lithologies assigned. The blue line shows the fit with the "5 facies" approach, the red one the "detailed lithology"

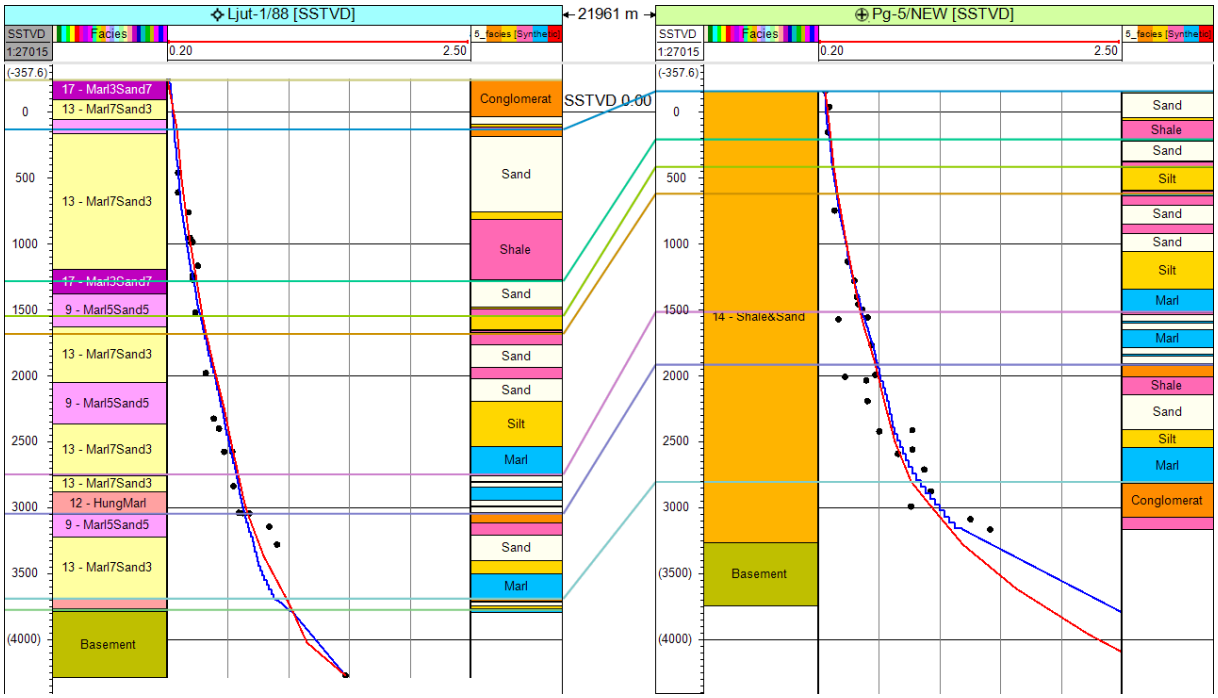

Figure 76 - Deviation in %R_0 with different lithologies assigned. The blue line shows the fit with the "5 facies" approach, the red one the "detailed lithology"

7.2 Paleo water depth

Paleo water depth (PWD) influences the heat distribution by changing the temperature at the surface of the sediments. While the mean temperature 10 meters beneath the surface in Mediterranean climate only drops about 2°C compared to the surface, at depths greater than 2000 meters it reaches about 4°C and therefore changes up to 20°C in total.

For the evaluation of the influence of PWD, two additional scenarios ("PWD 1000" and PWD realistic" where created to compare to the PWD maps actually used for the model calculation ("base case"). The inputs for those cases are shown in Table 7.

Table 7 - PWD scenarios used for the PWD sensitivity analysis.

	PWD Realistic	PWD 1000	„Base case" (1D)			
Age [Ma]	All wells [m]	All wells [m]	Som-1 [m]	Pg-5 [m]	Pichla-1 [m]	Ljut-1 [m]
0	0	0	0	0	0	0
1	5	200	0	0	0	5
5.5	5	1000	0	3	0	35
6.5	10	1000	0	5	0	35
7.1	150	1000	0	10	0	35
8.25	150	1000	0	15	0	35
9.2	150	1000	0	20	0	35
9.5	500	1000	0	20	0	40
10.6	1000	1000	0	25	0	40
11.7	500	1000	5	30	0	40
12.7	500	1000	100	35	0	40
14	500	1000	100	40	0	40
14.5	500	1000	100	45	0	40
15	500	1000	100	50	0	40
15.2	500	1000	100	50	0	40
15.5	500	1000	100	50	0	50
16.25	500	1000	100	100	0	50
17	500	1000	100	100	0	50
30	500	1000	0	0	0	50

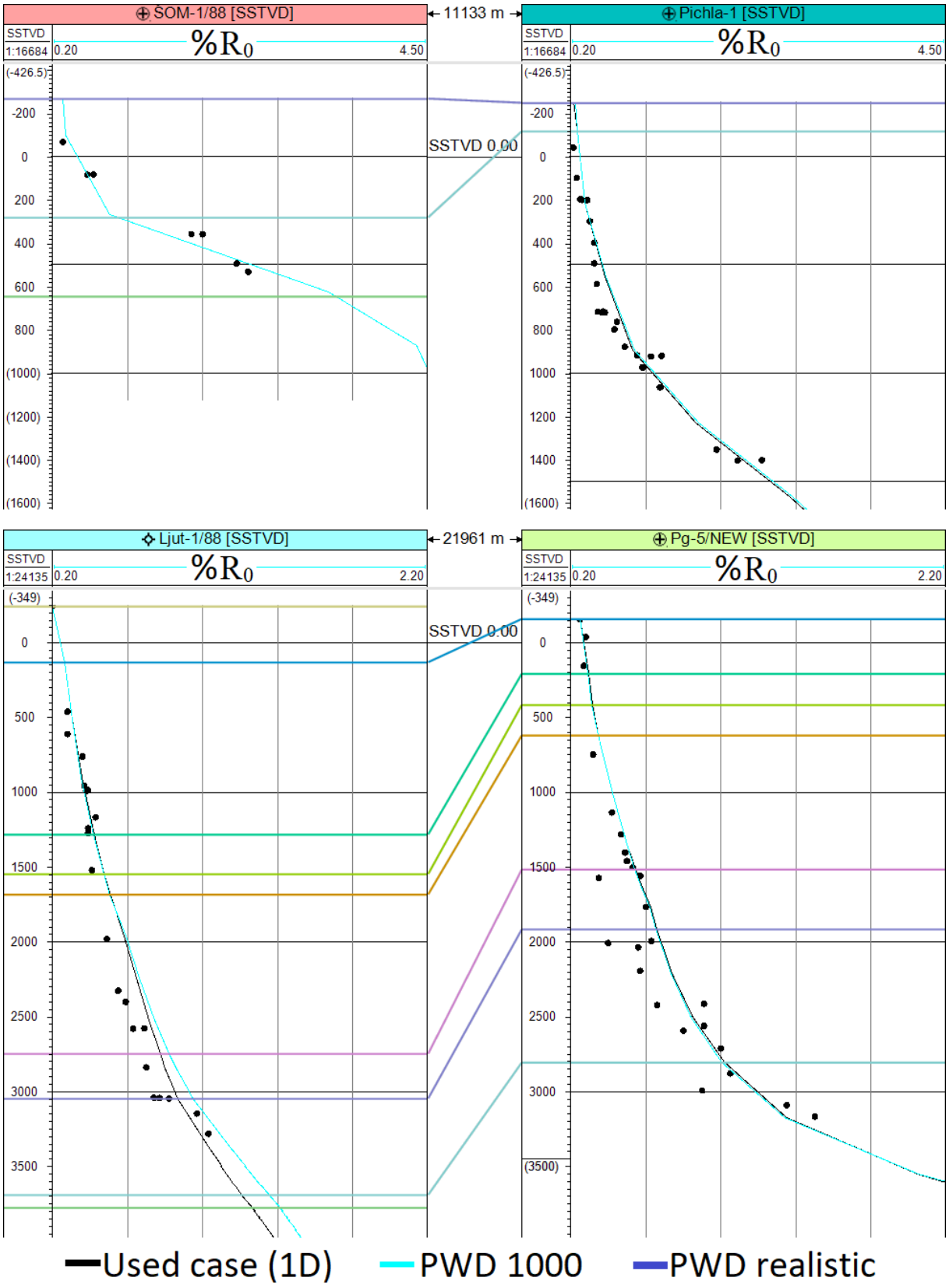

The differences caused by the three different PWD cases are minimal and in three of the four wells used for the demonstration, practically non-existing. Therefore the calculated vitrinite reflectance trends overlie each other. Only for the Ljut-1 well, the PWD 1000 case results in a

slightly increased vitrinite reflectance below 2700 m MD, compared to the “base case” and the “PWD realistic” case.

7.3 Present day heat flow

The present day heat flow distribution has been determined by calibrating calculated temperature trends against measured formation temperatures. Since the Mura-Zala basin was also subject to intensive geothermal investigations e.g. the T-Jam project (Rman et al., 2011) and the quality of the received borehole temperature data is partly hard to evaluate, a present day heat flow map published by Gosar et al. (2005) (Figure 77) was used for comparison. The results are displayed in Figure 78. To visualize the effect, 4 wells with the highest deviation in heat flow between the map published by Gosar and the HF map generated for this thesis have been chosen (Figure 79). It is clearly visible that a heat flow as proposed by Gosar et al. (2015) would have to be a very recent development. If this heat flow would have been present 1 Ma ago, the calculated vitrinite reflectance values would exceed the measured ones significantly. An alternative reason for the high deviation between the expected values in the thesis and the values proposed by Gosar et al. (2015) could be heat transfer through convection.

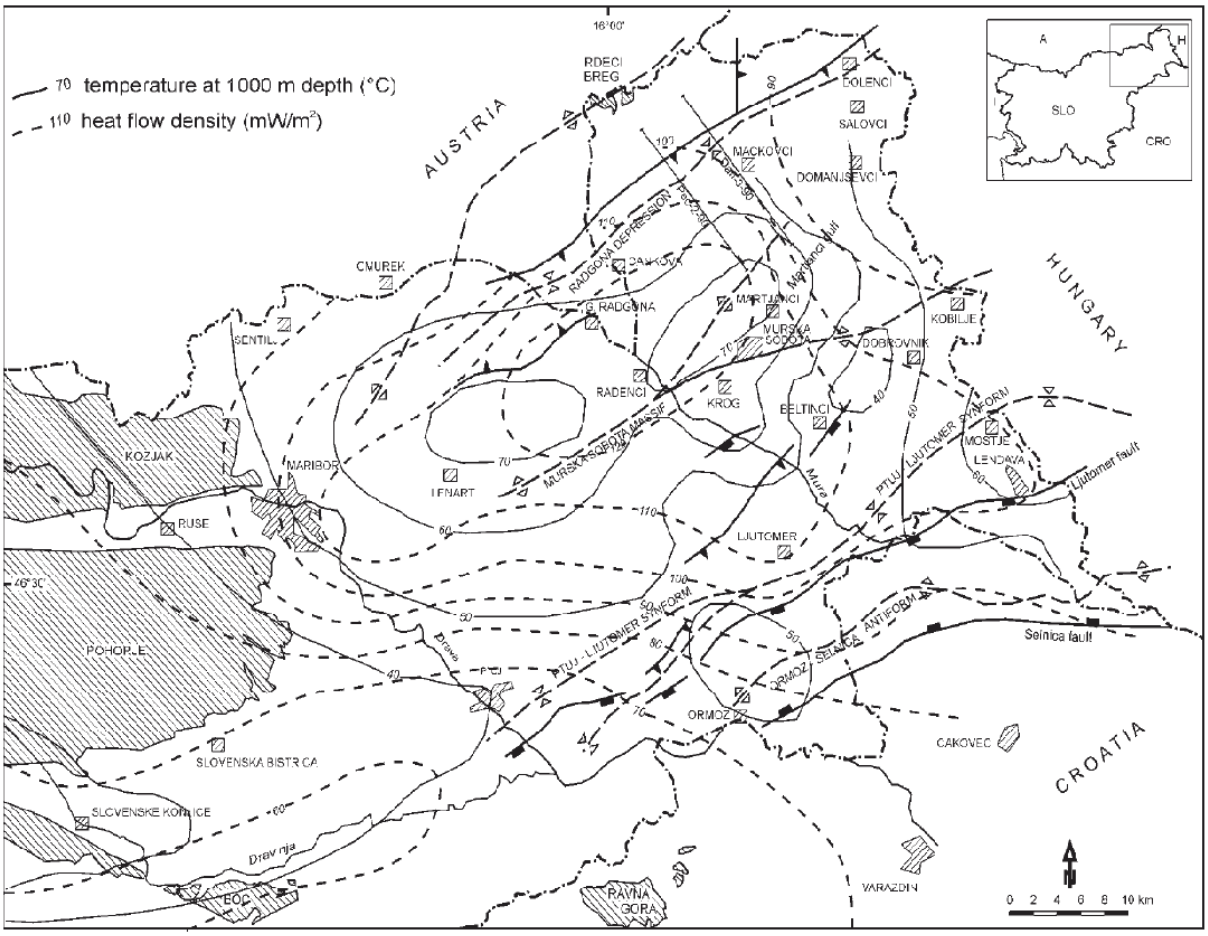

Figure 77 - HF and temperature map published by Gosar et. al. 2005, after Rajver et al. 2002 (temperatur) and after Ravnik et. al 1995 (HF)

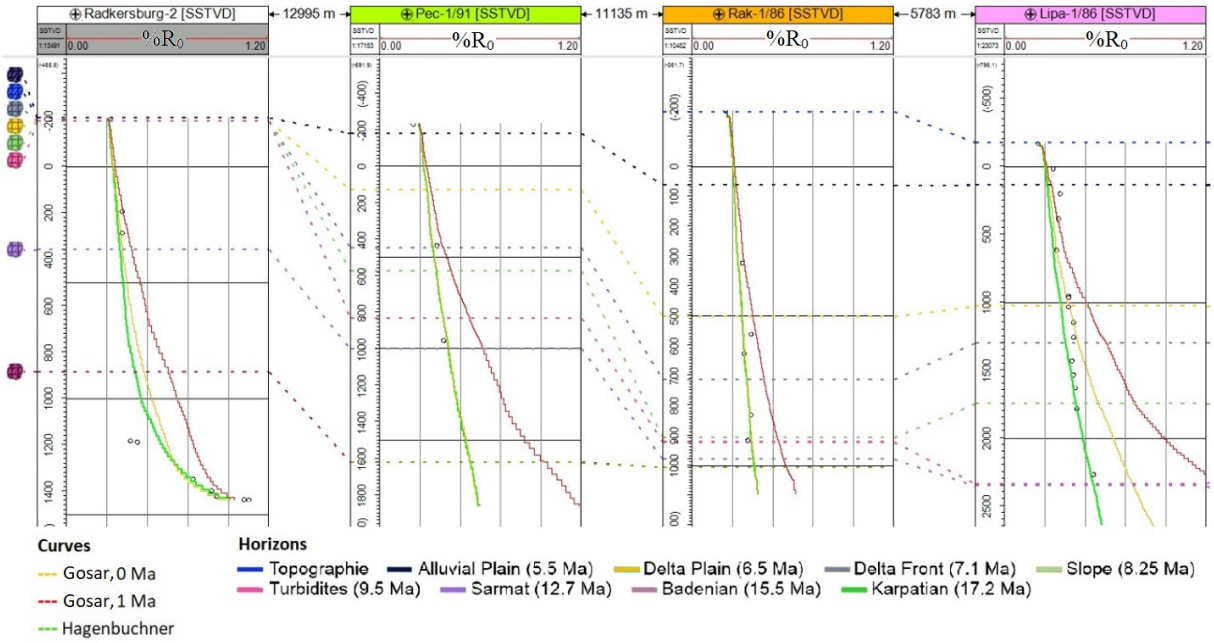

Figure 78 - Influence of different heat flow (HF) scenarios on %R_0. The green curve shows the HF history constructed in this model, orange a linear change to HF Gosar from 1 Ma to now, red a linear change from 5.5 Ma to 1 Ma, staying constant until today.

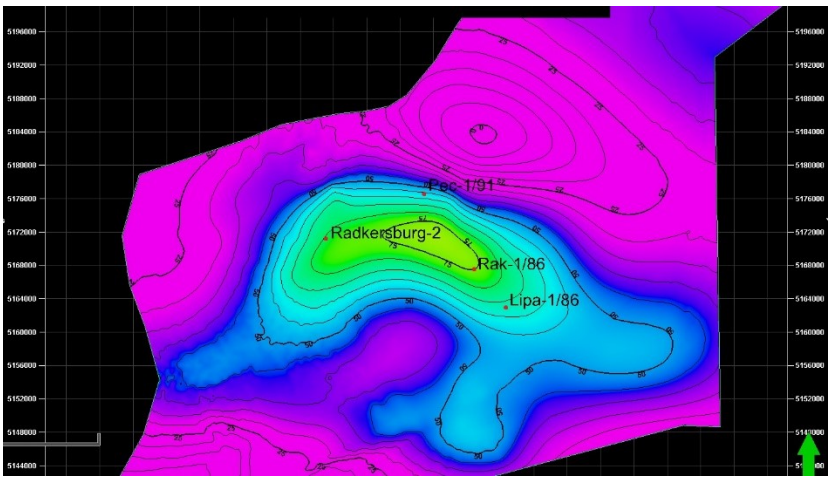

Figure 79 - HF deviation between Gosar et al. 2005 and the present day map generated in this thesis (Figure 49)

8 Discussion and Conclusions

Based on a 3D structural model of the Mura-Zala Basin (Sram et al., 2015), a 3D petroleum systems model was built. In comparison to former 1D models of the thermal history of the basin (Hasenhüttl et al., 2001), it allows an improved reconstruction of paleo-heat flows. Moreover, it provides new insights into the timing of hydrocarbon generation and migration.

The Mura-Zala Basin is characterized by extremely high Badenian paleo-heat flows caused probably by shallow magma chambers related to Miocene magmatic activity. At the same time heat flow varied strongly in a lateral direction. Because a 1D approach cannot consider lateral conductive heat transport, the reconstructed paleo-heat flow values derived from the 3D model differ partly considerably from paleo-heat flow values derived from the 1D models (Table 4). This is especially valid for the "hot spots" (areas of plutnonism and volcanism). Apart from that, the new 3D model confirms the general heat flow evolution of the Mura-Zala Basin as reconstructed by Sachsenhofer et al. (1998 & 2001) and Hasenhüttl et al. (2001).

Potential source rocks in the Mura-Zala Basin occur in Badenian, Sarmatian and Pannonian units, but a clearly defined prominent source rock layer is missing. Moreover, most source rocks have relatively low TOC contents (<2 %) and relatively low HI values (mostly below 400 mg HC/g TOC), as often observed in Neogene rocks in the western part of the Pannonian Basin (Clayton & Koncz, 1994). Badenian successions are generally poor in organic matter and have low HI values, while Sarmatian successions have "good" oil potential by Peters' (1986) classification. "Fair" to "good" source rock potential is also abundant in Upper Miocene levels, but those are mainly immature in the Mura-Zala Basin (6.2.3).

The oil window as well as the gas window has been reached in different parts of the Mura-Zala basin (see maturity maps) at different time steps. An **early generation phase** happened most likely already in Karpatian to Badenian times in the area of the Ormoz-Selnica Anticline. Elevated heat flow in the western continuation of this structure (Boc Anticline) is proven by vitrinite reflection and fission track data (Sachsenhofer et al., 2000) and by the good fit in the Pg-5 and Mg-6 wells, considering this Karpatian/Early Badenian heat flow event. Badenian volcanism in north Croatia (Pamic & Pécskay, 1996) is a possible heat source for this event. In the Somat area, this strongly elevated heat flow in the Karpatian/Early Badenian is obvious due to the vitrinite reflection patterns found in the area. A possible explanation offered by Sachsenhofer (1998) is a shallow Karpatian/Early Badenian pluton, situated between the western Pohorje dacites and the Miocene volcanoes in the Styrian Basin. At the moment it is unclear, if prolific source rocks exist in Karpatian succession. But even in this case, the early generated hydrocarbons were most likely lost to the surface due to an absence of a trap.

During Pannonian time, deep burial caused maturation of Miocene sediments despite of moderate heat flows (see 6.2.3). This **second generation phase** probably ceased, at least in most parts of the basin, due to Pliocene basin inversion. The traps for the Lovászi and Petišovci field obviously formed only through the basin inversion in post Pontian time, therefore earlier generated hydrocarbons have a low preservation potential, although entrapment in older structures and re-migration into the present traps is also possible (Hasenhüttl et al., 2001).

The accumulation volumes calculated with the two purely statistically distributed source rock scenarios (Case 1, Case 2) are not sufficient to fill the Petišovci and Lovászi fields and therefore suggest that the oil and gas are not sourced exclusively by Badenian and Sarmatian source

rocks. This can have multiple reasons. The lower Karpatian succession has been rarely reached by drilling operations in the Mura-Zala basin, especially in the deeper parts of the Ljutomer Trough. Hence, prolific source rocks in Karpatian horizons may have been overlooked. In general, the number of source rock data throughout the basin is not overwhelming. Sachsenhofer et al. (1994) found, that the lower Karpatian succession in the adjacent Styrian Basin (Styrian Schlier) contains rocks with higher TOC and HI values than used in the model of the Mura-Zala Basin, with an exception in the Somat area. Indeed, much higher volumes of hydrocarbons were generated during the early generation phase in the Somat area than in the rest of the basin. This shows that a Karpatian source rock with similar petroleum potential than the Styrian Schlier would yield much higher and more realistic hydrocarbon volumes. Oil/gas to source rock correlations were not carried out so far for the Slovenian oil and gas fields. Therefore, the possibility exists that oil and gas were generated from an older, Mesozoic source rock. Upper Triassic source rocks (e.g. Rhaetian Marl) have not been detected in Slovenia yet, but contribute significantly to hydrocarbon generation in Hungary (Clayton & Koncz, 1994). Permo-Carboniferous dark-grey to black, clayey siltstone, as it was found in the Hungarian part of the Ormoz-Selinca Anticline, might also have hydrocarbon potential (Bérci-Makk & Kochansky-Devidé, 1981).

8.1 Limitations of the model

In order to be able to interpret the findings of this thesis better, the limitations of the model are mentioned in the following.

Model Type - The model type used is a layer cake model. This brings limitations in several properties, specifically in facies distribution and migration.

Facies distribution - The facies is modelled in uniform layers, conformably overlying one another. Each layer extends along the whole basin.

Migration - Also caused by the facies distribution, vertical migration is restricted. This is because generated hydrocarbons cannot vertically penetrate the first overlying low permeability layer, that extends over the whole basin (shale, marl…). This means, that a source rock that is generating in one layer, e.g. in the Spilje Formation (Badenian), secondary migration will only happen in the next overlaying high permeability layer (sandstone…) and occur along the boundary to the next low permeability layer, until either a structural trap, like a four way closure in a fold, is reached (until it is filled to the spill point) or the carrier layer pinches out. This results in a very small amount of possible reservoir horizons.

Faults - Beside the three faults that were modelled as described earlier, the model also lacks of faults, which could represent structural seals or flow paths through low permeability lithology.

Scale - As mentioned earlier, the model is in basin scale. Together with the basis of the facies distribution, the lateral extent of accumulations cannot be trusted, since the thickness of the actual layers with reservoir quality is much thinner than represented in this model.

Rock- & flow-properties - The different lithologies in the model are not calibrated to measured rock properties, like actual porosity or permeability data from the lab, but use the standard lithologies and their behaviour embedded in the Petrel © and PetroMod © software packages. Reliable information like core data or well logs to determine those properties were

not available for this study. This might have a big influence on reservoir capacity, over pressure and flow paths in general.

8.2 Outlook

For a more realistic facies distribution, different deterministic and stochastic distribution models could be applied. Related to the current density of wells combined with the relatively good knowledge of depositional facies, object based facies modelling would be a very good approach. Combined with a refined structural model that includes faults, a realistic representation of the whole basin could be archived. Another measure that could be taken in combination with the latter would be facies constrained property modelling. This would limit e.g. source rock properties to actual defined source rock, what would not have made sense in the model as it was built here. The best results are obviously achieved, if 3D seismic cubes for big parts of the basin would be available. This would allow adding reservoir scale models to the basin model and allow property distribution of different kinds based on hard data and seismic attributes, critically enhancing reliability of estimations regarding facies, rock properties and fluid flow properties, as well as structural features.

To get a better understanding of the origin of the hydrocarbons in the Petišovci Field, detailed geochemical investigations of accumulated hydrocarbons (molecular composition, biomarker ratios, isotopy) and potential source rocks would be of great value. Especially answering the question if the hydrocarbons in the reservoirs are exclusively of Miocene origin or if an older source rock has to be taken into account, is critical.

9 Literatur

Bada, G., Horváth,F., Dövényi,P., Szafián,P., Windhoffer,G., Cloething,S.,2007. Present day stress field and tectonic inversion in the Pannonian basin. Global. Planet. Change 58, 165-180.

Bader, A.A.M. 1976: O možnih zalogah nafte in plina v severovzhodni Sloveniji = Possible oil and gas resources in the northeastern Slovenia, BSc thesis (in Slovenian), University of Ljubljana, Faculty of Natural Science and Engineering, Ljubljana: 55 p.

Beardsmore, G. R. & Cull, J. P. 2001. Crustal Heat Flow. A Guide to Measurement and Modelling. x + 324 pp. Cambridge, New York

Bérci-Makk, A., & Kochansky-DevideÂ, V. (1981). Marine Lower and Upper Permian in the oil exploratory well Ujfalu-I (SW-Hungary). Acta geologica Hungarica 24, 117-128.

Clayton, J. L., & Koncz, I. (1994). Petroleum geochemistry of the Zala Basin. American Association of Petroleum Geologists Bulletin 78, 1- 22.

Cloetingh, S.,van Wees, J.D., Ziegler,P.A., Lenkey, L., Beekman, F.,Tesauro, M.,Förster, A., Norden, B., Kaban, M., Hardebol, N., Bonté, D., Genter, A., Guillou-Frottier, L., Ter Voorde, M., Sokoutis, D., Willingshofer, E., Cornu, T., Worum, G., 2010. Lithosphere tectonics and thermo-mechanical properties: an integrated modelling approach for Enhanced Geothermal Systems exploration in Europe. Earth-Sci. Rev. 102, 159–206.

Csontos, L., Vörös, A., 2004. Mesozoic plate tectonic reconstruction of the Carpathian region. Palaeogeogr. Paleoclimatol. Palaeoecol. 210, 1–56.

Dank, V., 1962. Sketch of the deep geological structure of the south Zala basin. Földtani Közlöny, 92, 150-159

Djurasek, S. 1988: Pregledna karta podloge tercijara sa otkrivenim naftnim i plinskim objektima = Overview map of the Tertiary basement with discovered oil and gas objects (in Serbo-Croatian). Nafta Lendava, GeoZS, Archive GeoZS.

Djurasek, S. 1988: Rezultat suvremenih geofozickih istraživanja u SR Sloveniji (1985-1987). Nafta 39, 311-326, Zagreb.

Dolton, G.L. 2006: Pannonian Basin Province, Central Europe (Province 4808) – Petroleum Geology, Total Petroleum Systems, and Petroleum Resource Assessment. Bulletin 2204–B. Reston, Virginia, USGS

Dunkl, I., Grasemann, B., Frisch, W., 1998. Thermal effect on upper plate during core-complex denudation: a case study from the Rechnitz Window, Eastern Alps. Tectonophysics 297, 31–50.

Durasek, S. & Simon, I., 1994. Karpatian Basement Map with possible and proven hydrocarbon accumulations indicated.

Fodor, L. Uhrin, A., Palotas, K., Selmeczi, I., Nador, A., Toth-Makk, A., Scharek, P., Riznar, I. & Trajanova, M. 2011. Geological conceptual model within the frames of the T-JAM project. GeoZS, Ljubljana. MAFI, Budapest.

Fodor, L., Gerdes, A., Dunkl, I., Koroknai, B., Pécskay, Z., Trajanova, M., Horváth, P., Vrabec, M., Jelen, B., Balogh, K. & Frisch, W. 2008: Miocene emplacement and rapid cooling of the Pohorje pluton at the Alpine-Pannonian-Dinaridic junction, Slovenia. – Swiss J. Geosci., Birkhäuser Verlag, 255-271, Basel

Gosar, A. 2005: Seismic reflection investigations for gas storage in aquifers (Mura depression, NE Slovenia). –Geologica Carpathica, 56, 285-294, Bratislava.

Grenerczy, Gy., Sella, G.F., Stein, S., Kenyeres, A., 2005. Tectonic implications of the GPS velocity field in the northern Adriatic region. Geophys. Res. Lett. 32, L163 11.

Haas, J., Kovács, S., Krystyn, L., Lein, R., 1995. Significance of Late Permian-Triassic facies zones in terrane reconstructions in the Alpine-North Pannonian domain. Tectonophysics 242, 19–40.

Handy, M., Schmid, S.M., Bousquet, R., Kissling, E., Bernoulli, D., 2010. Reconciling plate-tectonic reconstructions of Alpine Tethys with the geological–geophysical record of spreading and subduction in the Alps. Earth-Sci. Rev. 102, 121–158.

Hantschel, T., Kauerauf, A. I., 2009. Fundamentals of Basin and Petroleum System Modeling. Springer-Verlag Berlin, Heidelberg.

Hasenhüttl, C., Kraljić, M., Sachsenhofer, R.F., Jelen, B. & Rieger, R. 2001: Source rocks and hydrocarbon generation in Slovenia (Mura Depression, Pannonian Basin). Marine and Petroleum Geology, 18/1: 115–132

Horváth, F., Bada, G., Szafián, P., Tari, G., Ádám, A., Cloetingh, S., 2006. Formation and deformation of the Pannonian basin: Constraints from observational data. In: Gee, D.G., Stephenson, R.A. (Eds.), European Lithosphere Dynamics, Geol. Soc., London, Mem. 32, pp. 191–206.

Horváth, F., Musitz, B., Balázs, A., Vegh, A., Uhrin A., Nador, A., Koroknai, B., Pap, N., Toth, T. & Worum, G. 2015: Evolution of the Pannonian basin and its geothermal resources. Geothermics, 53: 328–352

Jelen, B. & Rifelj, H 2005a: On the dynamics of the Paratethys Sedimentary Area in Slovenia. -7thWorkshop on Alpine geological Studies, Abstract Book, 45-46, Croatian Geological Society, Zagreb.

Jelen, B. & Rifelj, H. 2001: Ali so se globalne klimatske in tektonske spremembe odrazile na karpatijski in badenijski mikroforaminiferni favni v Sloveniji. –In: A. Horvat(ed.), 15. Posvetovanje slovenskih geologov, povzetki referatov, Geološki zbornik, 16, 38-41, Ljubljana

Jelen, B. & Rifelj, H. 2002: Stratigraphic structure of the B1 Tertiary tectonostratigraphic unit in eastern Slovenia. Geologija, 45, 1, 115-138, Ljubljana.

Jelen, B. & Rifelj, H. 2003. The Karpatian in Slovenia. In: R. Brzobohatý, I. Cicha, M. Kovac & F. Rögl (eds.), The Karpatian. A Lower Miocene Stage of the central Paratethys. 133-139, Masaryk University Brno unit in eastern Slovenia. Geologija, 45, 1, 115-138, Ljubljana.

Jelen, B. & Rifelj, H. 2004: Stratigrafska raziskava, Raziskava današnje geodinamike in njenega vpliva na geološki sistem Slovenije

Jelen, B. & Rifelj, H. 2005b: Patterns and Processes in the Neogene of the Mediterranean region, 12th Congress R.C.M.N.S., Abstract Book, 116-118, Wien

Jelen, B. & Rifelj, H. 2005C: The Haloze formation. In: Project team, Overview of geological data or deep repository for radioactive waste in argillaceous formations in Slovenia, 66-68, rokopis, arhiv Geološkega zavoda Slovenije, Ljubljana.

Jelen, B. & Rifelj, H., BAVEC, M. & RAJVER, D. 2006: Opredelitev dosedanjega konceptualnega geološkega modela Murske depresije. Ljubljana: Geološki zavod Slovenije.
Kurevija, T. & Vulin, D. 2011: High Enthalpy Geothermal Potential of the Deep Gas Fields in Central Drava Basin, Croatia. Water Resources Management, 25/12: 3041–3052

Lenkey, L., Dövényi, P., Horváth, F., Cloetingh, S.A.P.L., 2002. Geothermics of the Pannonian basin and its bearing on the neotectonics. EGU Stephan Mueller Special Publication Series 3, 1–12.

Limberger, J., Calcagno, P., Manzella, A., Trumpy, E., Boxem, T., Pluymaekers, M. P. D., van Wees1, J.-D., 2014. Assessing the prospective resource base for enhanced geothermal systems in Europe, Geoth. Energ. Sci., 2, 55–71

Lučić, D., Saftić, B., Krizmanić, K., Prelgović, E., Britvić, V., Mesić, I. & Tadej, J. 2001: The Neogene evolution and hydrocarbon potential of the Pannonian Basin in Croatia. Marine and Petroleum Geology, 18/1: 133–147

Markič, M. 2013: Zakaj nastopata zemeljski plin in nafta ravno na območju Lendave = Why do earth gas and oil occur in Lendava (in Slovenian). In: Senegačnik, A. (ed.): Mineralne surovine v letu 2013, GeoZS, Ljubljana: 122–138.

Markič, M., Lapanje, A., Rajver, D., Rman, N., Šram, D., Kumelj, Š. 2016: Geological evaluation of potential unconventional oil and gas resources in Euorope. H2020 call, B.2.9.: "Energy Policy support on unconventional gas and oil" from the European Commission, by JRC-IET, service contract no. 11411 between The European Union and GEUS.

Márton, E., Fodor, L., 2003: Tertiary paleomagnetic results and structural analysis from the Transdanubian Range (Hungary); sign for rotational disintegration of the Alcapa unit. Tectonophysics 363, 201-224.

Márton, E., Fodor, L., Jelen, B., Márton, P., Rifelj, H. & Kevric, R. 2002: Miocene to Quaternary deformation in NE Slovenia: complex paleomagnetic and structural study. Journal of Geodynamics, 34, 627-651

Márton, E., Tischler, M., Csontos, L., Fügenschuh, B., Schmid, S.M., 2007. The con- tact zone between the ALCAPA and Tisza-Dacia megatectonic units of Northern Romania in the light of new paleomagnetic data. Swiss Journal of Geosciences 100, 109–124..

Massari, F., Grandesso, P., Stefani, C. & Jobstraibizer, P. G. 1986. A small polyhistory foreland basin evolving in a context of oblique convergence: the Venetian basin (Chattian to Recent, Southern Alps, Italy). Spec. Publ. Ass. Sediment., 8, 141-168.

Matenco, L., Radivojevic, D., 2012. On the formation and evolution of the Pan- nonian Basin: constraints derived from the structure of the junction area between the Carpathians and Dinarides. Tectonics 31.

Mioč, P. & Žnidarčič, M. 1996: Geological characteristics of the oil fields in the Slovenian part of the Panonian Basin. Geologica Croatica, 49/2: 271–275.

Peters, K. E. (1986). Guidelines for evaluating petroleum source rocks using programmed pyrolysis. American Association of Petroleum Geologists Bulletin, 70, 318±329.

Peters, K. E., Clifford, C. W., Moldowan, J., M., 2007. The Biomarker Guide, Volume 2: Bimarkers and Isotopes in Petroleum Exploration and Earth History. Cambridge University Press, Cambridge.

Petroleum Development Consultants (PDC): 2011: Petišovci Gas Field, Slovenia. Comercial Report, issued by Ascent Slovenia Ltd.

Pleničar, M. 1968: Osnovna geološka karta SFRJ = Basic Geological Map of SFRJ 1:100.000 L 33-45 (List = Sheet Goričko) (in Slovenian). Zvezni geološki zavod, Beograd.

Prosser, S., 1993. Rift related depositional system and their seismic expression. Tec- tonics and Seismic Sequence Stratigraphy. In: Williams, G.D. Dobb, A. (Eds.), Geol. Soc. Spec. Publ., 71, 35-66.

Rman, N., Kumelj, S., Tullner, T., Orosz, L., Palotás, K. 2011. Joint three-lingual geothermal database within the framework of T-Jam project. GeoZS, Ljubljana, MAFI, Budapest.

Sachsenhofer, R. F. (1994). Petroleum generation and migration in the Styrian Basin (Pannonian Basin system, Austria): An integrated geochemical and numeric modelling study. Marine and Petroleum Geology, 11, 684-701.

Sachsenhofer, R. F., Dunkl, I., HasenhuÈttl, Ch., & Jelen, B. (1998). Miocene thermal history of the southwestern margin of the Styrian Basin: coali®cation and ®ssion track data from the Pohorje/Kozjak area (Slovenia). Tectonophysics, 297, 11-29.

Sachsenhofer, R.F., Jelen, B., Hasenhüttl, C., Dunkl, I. & Rainer, T. 2001: Thermal history of Tertiary basins in Slovenia (Alpine-Dinaride- Pannonian junction). Tectonophysics, 334: 77– 99

Sandikar, J.M. 1993: Raziskave za podzemno skladiščenje plina v Sloveniji. -Rudarsko-Metalurški zbornik, 40, 1/2, 150-167, Ljubljana.

Scharf, A., Handy, M.R., Favaro, S., Schmid, S.M., Bertrand, A., 2013. Modes of orogen-parallel stretching and extensional exhumation in response to microplate indentation and roll-back subduction (Tauern Window, Eastern Alps). Int. J. Earth Sci..

Schlumberger, 2015. Interactive Petrel © Guru: Convergent interpolation algorithm.

Schmid, S.M., Bernoulli, D., Fügenschuh, B., Matenco, L., Schefer, S., Schuster, R.,Tischler, M., Ustaszewski, K., 2008. The Alpine-Carpathian-Dinaridic oro- genic system: correlation and evolution of tectonic units. Swiss J. Geosci. 101, 139–183.

Šram, D., Rman, N., Riznar, I., Lapanje, A. 2015: The three-dimensional regional geological model of the Mura-Zala Basin, northeastern Slovenia. GEOLOGIJA, 58/2: 139-154

Stampfli, G.M., Borel, G.D., 2002. A plate tectonic model for the Paleozoic and Mesozoic onstrained by dynamic plate boundaries and restored synthetic oceanic isochrons. Earth Planet. Sci. Lett. 196, 17–33.

Tomljenovic, B., Csontos, L., Márton, E., Márton, P., 2008. Tectonic evolution of the northwestern Internal Dinarides as constrained by structures and rotation of Medvednica Mountains, North Croatia. Geological Society, London Special Pub- lications 298, pp. 145–167.

Toth, T., Tari, G. 2014: Structural Inversions in Western Hungary and Eastern Slovenia: Their Impact on Hydrocarbon Trapping and Reservoir Quality. Adapted from oral presentation given at AAPG International Conference & Exhibition, Istanbul, Turkey, September 14-17, 2014

Uhrin, A., Magyari, I., Sztanó, O. 2009: Az aljzatdeformáció hatása a pannóniai üledékképz_dés menetére a Zalai-medencében. — Földtani Közlöny 139, 3, 273–282.

Ustaszewski, K., Kounov, A., Schmid, S.M., Schaltegger, U., Krenn, E., Frank, W., Fügen-schuh, B., 2010. Evolution of the Adria-Europe plate boundary in the northern Dinarides: from continent-continent collision to back-arc extension. Tectonics 29, TC6017.

Ustaszewski, K., Schmid, S.M., Fügenschuh, B., Tischler, M., Kissling, E., Spak- man, W., 2008. A map-view restoration of the Alpine-Carpathian-Dinaridic system for the Early Miocene. Swiss J. Geosci. 101 (Suppl. 1), 273–294.

Van Hinsbergen, D.J.J., Dupont-Nivet, G., Nakov, R., Oud, K., Panaiotu, C., 2008. No significant post-Eocene rotation of the Moesian Platform and Rhodope (Bul- garia): implications for the kinematic evolution of the Carpathian and Aegean arcs. Earth Planet. Sci. Lett. 273, 345–358.

Wygrala, B. P., 1989. Integrated study of an oil field in the southern Po Basin, Northern Italy. PhD thesis, University of Cologne, Germany.